JYU DISSERTATIONS 377

Margarita Bulatova

Noncovalent Interactions as a Tool for Supramolecular Self-Assembly of Metallopolymers

UNIVERSITY OF JYVÄSKYLÄ
FACULTY OF MATHEMATICS
AND SCIENCE

JYU DISSERTATIONS 377

Margarita Bulatova

Noncovalent Interactions as a Tool for Supramolecular Self-Assembly of Metallopolymers

Esitetään Jyväskylän yliopiston matemaattis-luonnontieteellisen tiedekunnan suostumuksella
julkisesti tarkastettavaksi toukokuun 4. päivänä 2021 kello 12.

Academic dissertation to be publicly discussed, by permission of
the Faculty of Mathematics and Science of the University of Jyväskylä,
on May 4, 2021 at 12 o'clock noon.

JYVÄSKYLÄN YLIOPISTO
UNIVERSITY OF JYVÄSKYLÄ

JYVÄSKYLÄ 2021

Editors
Matti Haukka
Department of Chemistry, University of Jyväskylä
Ville Korkiakangas
Open Science Centre, University of Jyväskylä

Permanent link to this publication: http://urn.fi/URN:ISBN:978-951-39-8630-8

ISBN 978-951-39-8630-8 (PDF)
URN:ISBN:978-951-39-8630-8
ISSN 2489-9003

ABSTRACT

Bulatova, Margarita
Noncovalent interactions as a tool for supramolecular self-assembly of metallopolymers
Jyväskylä: University of Jyväskylä, 2021, 62 p. (+included articles)
(JYU Dissertations
ISSN 2489-9003; 377)
ISBN 978-951-39-8630-8 (PDF)

This thesis shows the successful application of noncovalent interactions (NCIs) in crystal engineering. Various NCIs were applied to obtain 10 novel self-assembled metallopolymeric structures: $[PtI_2COD] \cdot CHI_3$, $[PtI_2COD] \cdot 0.5I_2$, $[PtBr_2COD] \cdot 0.5I_2$, $[PtCl_2COD] \cdot I_2$, $[PtI_2COD] \cdot 1.5FIB$, $[PtBr_2COD] \cdot 2FIB$, $[PtCl_2COD] \cdot 2FIB$, *trans*-$[PdI_2(CNXyl)_2] \cdot I_2$, *trans*-$[PtI_2(CNXyl)_2] \cdot I_2$, and $KI \cdot$ 1,1'-bis(pyridin-4-ylmethyl)-2,2'-biimidazole. Several polymer geometries such as 0D, 1D, 2D, and 3D were achieved by fine-tuning the NCIs within the structures. Dependence of the structural organization on the relative strength of the NCI was considered, as well as the impact of the cooperative effect of multiple NCIs. Single crystal X-ray diffraction was used to study NCIs in the solid-state structures experimentally. Modern computational techniques were used to further study the NCIs and their influence on the structure including analysis of electrostatic surface potential (ESP), NCIplot, quantum theory of atoms in molecules (QTAIM), and ESP/electron density (ED) minima analysis.

This thesis is divided into 3 parts. The first part provides a brief introduction to crystal engineering, noncovalent interactions, and applications of crystal engineering to the synthesis of metallopolymers. The second part briefly explains the specific methods and techniques used to study NCI. The last part summarizes the contribution of the author's work in the field of NCIs.

This thesis shows the close relation of the dimensionality of a self-assembled metallopolymer with the strongest noncovalent interaction and that it is also influenced by the cooperativity effect of weaker interactions.

Keywords: crystal engineering, noncovalent interactions, halogen bonding, bifurcated bonding, metal-involved noncovalent interactions, platinum(II) complex, palladium(II) complex, ESP, ELF, NCIplot, supramolecular metallopolymers.

TIIVISTELMÄ (ABSTRACT IN FINNISH)

Bulatova, Margarita
Ei-kovalenttiset vuorovaikutukset työkaluna metallopolymeerien supramolekulaariseen itsekokoonpanoon
Jyväskylä: Jyväskylän yliopisto, 2021, 62 s. (+ sisällytetyt julkaisut)
(JYU Dissertations
ISSN 2489-9003; 377)
ISBN 978-951-39-8630-8 (PDF)

Tässä väitöskirjassa tarkastellaan ei-kovalenttisten vuorovaikutusten (EKV) hyödyntämistä kiteisten materiaalien rakenteiden hallitussa kasvatuksessa. Käyttämällä erilaisia ei-kovalenttisia vuorovaikutuksia pystyttiin rakentamaan kaikkiaan 10 uutta itse-rakentuvaa metallipolymeerirakennetta: $[PtI_2COD] \cdot CHI_3$, $[PtI_2COD] \cdot 0.5I_2$, $[PtBr_2COD] \cdot 0.5I_2$, $[PtCl_2COD] \cdot I_2$, $[PtI_2COD] \cdot 1.5FIB$, $[PtBr_2COD] \cdot 2FIB$, $[PtCl_2COD] \cdot 2FIB$, *trans*-$[PdI_2(CNXyl)_2] \cdot I_2$, *trans*-$[PtI_2(CNXyl)_2] \cdot I_2$, ja KI · 1,1'-bis (pyridin-4-yylimetyyli)-2,2'-biimidatsoli. Eri yhdisteiden yksityiskohtaisia rakenteita voitiin hienosäätää valitsemalla ja vahvistamalla ei-kovalenttisia kontakteja. Tällä tavoin voitiin saavuttaa 0D, 1D, 2D ja 3D järjestelmiä. Työssä analysoitiin eri ei-kovalenttisten vuorovaikutusten roolia, vaikutusta ja yhteisvaikutusta rakenteiden muodostumisessa. Kiinteän tilan analytiikassa hyödynnettiin erityisesti yksi-kide röntgendiffraktiota kiderakenteiden kokeellisessa määrityksessä. Laskennallisia menetelmiä Yksityiskohtaisempaa informaatiota vuorovaikutuksista haettiin käyttämällä laskennallisen kemian menetelmiä, mm. sähköstaattisen pintapotentiaalin (ESP) analysointia, NCIplot-analyysiä, molekyylien ja atomien kvanttiteoriaa (QTAIM), ESP:n ja elektronitiheysminimien analyysiä.

Väitöskirja jakautuu kaikkiaan kolmeen osaan. Ensimmäisessä osassa käydään läpi tutkimuksen taustaa ja tarkasteltavia ei-kovalenttisia vuorovaikutuksia. Edelleen taustoitetaan metallopolymeerien syntetiikkaa. Toisessa osiossa tarkastellaan lyhyesti käytettyjä ei-kovalenttisten vuorovaikutusten tutkimusmenetelmiä. Kolmannessa osassa esitellään varsinainen tekijän kokeellinen ja laskennallinen työ.

Tämä opinnäytetyö osoittaa, että itse-järjestäytyvien metallopolymeerien muodostumisessa ei-kovalenttisilla vuorovaikutuksilla on voimakas ohjaava rooli. Usein prosessia hallitsee voimakkaimmin jokin tietty vuorovaikutus, mutta lopputuloksen kannalta kaikki vuorovaikutukset ja niiden yhteisvaikutus on lopulta huomioitava.

Asiasanat: kidetekniikka, ei-kovalenttiset vuorovaikutukset, halogeenisidos, kaksisuuntainen sidos, metalliin liittyvät ei-kovalenttiset vuorovaikutukset, platina(II)kompleksi, palladium(II)kompleksi, ESP, ELF, NCIplot, supramolekyyliset metallopolymeerit.

Author

Margarita Bulatova
Department of Chemistry
P.O. Box 35
FI-40014 University of Jyväskylä
Jyväskylä, Finland
mminzar@gmail.com
ORCID 0000-0002-1904-5394

Supervisors

Professor Matti Haukka
Department of Chemistry
University of Jyväskylä
Jyväskylä, Finland

Reviewers

Dr. Maximilian N Kopylovich
Centro de Química Estrutural
Instituto Superior Técnico
University of Lisbon
Lisbon, Portugal

Adjunct Professor Anssi Peuronen
Department of Chemistry
University of Turku
Turku, Finland

Opponent

Professor Catharine Esterhuysen
Department of Chemistry and Polymer Science
Stellenbosch University
Stellenbosch, South Africa

PREFACE

This part is usually written to express gratitude, but before that, I would like to explain what my Ph.D. studies meant to me. I came to Matti's group as a scared master's degree student thinking I know nothing about science yet and hoping the situation would change in the future (fool!). I felt like a little monkey who was pressing buttons without much understanding, but somehow things were working. Step by step I started to understand what Matti was saying to me and what information a certain method could provide. I wasn't afraid to try something new anymore, to ask for help, and I started to think I understood something about science and that soon everything will "click". It did (sometimes). Most of the time I was challenged by some new unpredicted results and struggled to get what I was aiming for. However, these moments were the reason to dig a little deeper. Now after writing my thesis I am almost like Jon Snow, I know nothing, compared to all the data available on the topic. However, I definitely enjoyed the challenges and search for the answers that the research was bringing me and trying to solve one puzzle after another. To me, science is about learning something new every day, understanding something a bit deeper. Of course, apart from amazing colors, crystals, ~~explosions,~~ and luminescent substances.

And now back to the tradition. I am thankful to my supervisor, Matti Haukka, for giving me the freedom of research, needed support, and, most important, inspiration in times when science was showing me its stubborn character. I am thankful as well to our EMS research group (including Elmeri, Elina L., Janne, Joona, Kalle, Rahul, Maria, Alex, Matti Tuikka, Lauri, Esa, and Xin) for our group meetings, where I could not stop showing tons of stupid memes and where we all enjoyed kahvi ja pulla hetki.

Of course, I'm very grateful to my colleagues from SPSU. Particularly, V. Yu. Kukushkin, who welcomed me into his amazing research team and gave so much nice advice, D. Ivanov, who inspired me a lot during publications I and II and whose friendship I really appreciate, and M. Kinzhalov, for guiding and helping me in the lab.

A special thanks to my colleagues from the department of chemistry. Miko, for his patient computational chemistry consultations and collaboration, Khai, for his help and consultations about sXRD studies, Manu, for the PXRD studies, Elina S. and Esa, for their help with the NMR studies, Elina K., for the MS studies, Elina H., for her help with general things, and EA. Kari Rissanen, for introducing me to a ~~smelly~~ charming world of organic chemistry during my master's studies. Additional thanks to all faculty members, especially Maritta, Leena, Tuula, Teija, Päivi, Tiina, Kirsi, for finding time to help me with bureaucratic questions.

I would like to thank NSC team of friends Ewa, Karo, Ville, and Nisha for making me smile and getting me drunk when needed. My friend Tonya, who helped me to through my motherhood 101 studies and kept an eye on Evelina when I was working late.

My mom, for believing in me and supporting me no matter what. For her hugs and wise words.

Last, but not least, a very special thanks to Evgeny, my personal scientific consultant, my team, my soulmate, the love of my life. You are the best person I have ever met, and I thank the universe for every moment spent together with you. I love every atom of yours and, of course, I'm grateful to you for our little Evelina, who is giving me extra energy with her smiles and hugs and for our little Martin, who I am excited to meet in June.

Guys, you are all breathtaking and I will always remember the time of my Ph.D. studies! Hugging all of you,

Margarita Bulatova
Jyväskylä 20.02.2021

LIST OF ORIGINAL PUBLICATIONS

I Bulatova M., Ivanov D., and Haukka M., Classics Meet Classics: Theoretical and Experimental Studies of Halogen Bonding in Adducts of Platinum(II) 1,5-Cyclooctadiene Halide Complexes with Diiodine, Iodoform, and 1,4-Diiodotetrafluorobenzene, *Cryst. Growth Des.*, **2021**, *21* (2), 974–987.

II Bulatova M., Ivanov D., Rautiainen J. M., Kinzhalov M.A., Truong K.-N., Lahtinen M., and Haukka M., Uncommon I–I···(I–M) Metal-involving Noncovalent Interaction Supported by Classical Halogen Bond in Palladium(II) and Platinum(II) Isocyanide Cocrystals, *submitted manuscript*.

III Bulatova M., Tatikonda R., Hirva P., Bulatov E., Sievänen E., and Haukka M., Controlling the crystal growth of potassium iodide with a 1,1′-bis(pyridin-4-ylmethyl)-2,2′-biimidazole ligand (L) – formation of a linear $[K_4I_4L_4]_n$ polymer with cubic $[K_4I_4]$ core units, *CrystEngComm*, **2018**, *20* (26), 3631-3633.

Author's contribution

The author of this dissertation performed all syntheses, crystallization experiments, NMR characterizations, X-ray crystallography, and computational studies (except the ELF+QTAIM and ED/ESP minima studies) presented in publication **I**. In publication **II**, the author performed the synthesis, crystallizations, parts of the SCXRD studies and wavefunction calculations, NCIplot analysis, and ESP visualizations. In publication **III**, the author performed the synthetic and crystallization experiments along with part of NMR characterizations. The author wrote the drafts and final manuscripts of publications **I – III**.

Other related publications by the author:

IV Bulatova M., Melekhova A. A., Novikov A. S., Ivanov D. M., and Bokach N. A., Redox reactive (RNC)Cu^{II} species stabilized in the solid state via halogen bond with I_2, *Z. Kristallogr. Cryst. Mater.*, **2018**, *233* (6), 371–377.

V Chernysheva M. V., Bulatova M., Ding X., and Haukka M., Influence of substituents in aromatic ring on the strength of halogen bonding in iodobenzene derivatives. *Cryst. Growth Des.*, **2020**, *20* (11), 7197–7210.

CONTENTS

ABBREVIATIONS

1,3,5-FIB	1,3,5-triiodotrifluorobenzene;
acac	acetylacetonate;
BCP	bond critical point;
BZ	C6H4;
COD	1,5-cyclooctadiene;
CP	critical point;
ED	electron density;
ELF	electron localization function;
ESP	electrostatic potential;
FIB	1,4-diiodotetrafluorobenzene;
HA	hydrogen bond acceptor;
HB	hydrogen bond;
HBD	hydrogen bond donor;
L	1,1'-bis(pyridin-4-ylmethyl)-2,2'-biimidazole;
NCI	noncovalent interaction;
QTAIM	quantum theory of atoms in molecules;
RCP	ring critical point;
RDG	reduced density gradient;
RT	room temperature;
SCXRD	single crystal X-Ray diffraction;
vdW	van der Waals;
XBA	halogen bond acceptor;
XBD	halogen bond donor;
Xyl	2,6-dimethylphenyl.

1 INTRODUCTION

Since the 1987's Nobel Prize in chemistry awarded to Pedersen, Lehn, and Cram, the field of supramolecular chemistry has attracted a lot of attention in the scientific community. It drove the idea to develop the use of noncovalent interactions (NCIs) in combination with crystal engineering. NCIs have found broad applications in synthesis, biomedicine, catalysis, and metallopolymers.[1,2] Metallopolymers consist of coordination complex units that are connected either covalently or noncovalently via a linker compound that creates a polymeric structure.[3]

The aim of this chapter is to introduce the reader to crystal engineering by discussing basic concepts and methods applied in the field. Main definitions and short explanations of the key concepts are presented.

1.1 Crystal engineering

The term crystal engineering was introduced by Schmidt in 1971.[4] It is a relatively young interdisciplinary area that combines crystallography, chemistry, and material sciences. It utilizes intermolecular interactions for the synthesis of novel solid-state materials.[5,6] A thorough understanding of such interactions helps in fine-tuning the desired physical and chemical properties, such as non-linear optics, luminescence, pharmacological and catalytic activity, gas storage, ion capturing, and many more.

There are two keywords in the phrase "crystal engineering". The first, crystal describes a material in which atoms, molecules, or ions are packed in a repeating three-dimensional periodic pattern. This pattern, or molecular arrangement, is closely related to the properties of the material. The second word, "engineering" means the control of the arrangement via various inter- and intramolecular interactions, including hydrogen, halogen, chalcogen, pnictogen bonding, dipole-dipole, various π-interactions, and metallophilic interactions.

The ability to control the structure is closely related to control over the material property.

Molecules are the main building blocks in the crystal that can be assembled into organized structures. Pre-design of a building block is an important step in crystal engineering because this is the stage that determines the physical/chemical properties of the final material. Final adjustments and fine-tuning over the desired system are accomplished via various design strategies.

1.2 Design strategies

There are two types of crystal design strategies. One relies on the desired properties of the final crystal and the other relies on the desired topology.

"From simple to complicated" or "from a molecule to a crystal" is the first of the design strategies. The simplest design sequence is molecule → functional group → synthon → crystal (FIGURE 1).[7] It is essential to choose the key molecule in crystal design. That is, a molecule with certain physical and chemical properties along with the desired intermolecular interaction sites. There can be several key molecules, but the variety affects the ability to control the structure. These molecules or molecular building blocks are assembled into organized structures via intermolecular interactions. Therefore, it is essential to consider the strength, directionality, and possibilities for multiple intermolecular interactions. However, it is more complicated to predict the final crystal structure with more possibilities for intermolecular interactions between molecules.

Topological design is a retrosynthetic strategy that is based on the preferred geometry of the final product.[8] In a retrosynthetic strategy, the target crystal's structure is divided into simpler fragments that can be assembled via synthetic procedures to give the desired product. Topological design is associated with coordination compounds and has been applied in the synthesis of inorganic-organic hybrid systems where the organic molecules cross-link coordination compounds (metal complexes) creating zero-, one-, two-, or three-dimensional networks (FIGURE 2). Here, the main properties of the material arise from the metal complex. However, geometry modification of the organic molecules (ligands) can add extra functions to the material, for example, gas storage or ion capturing.

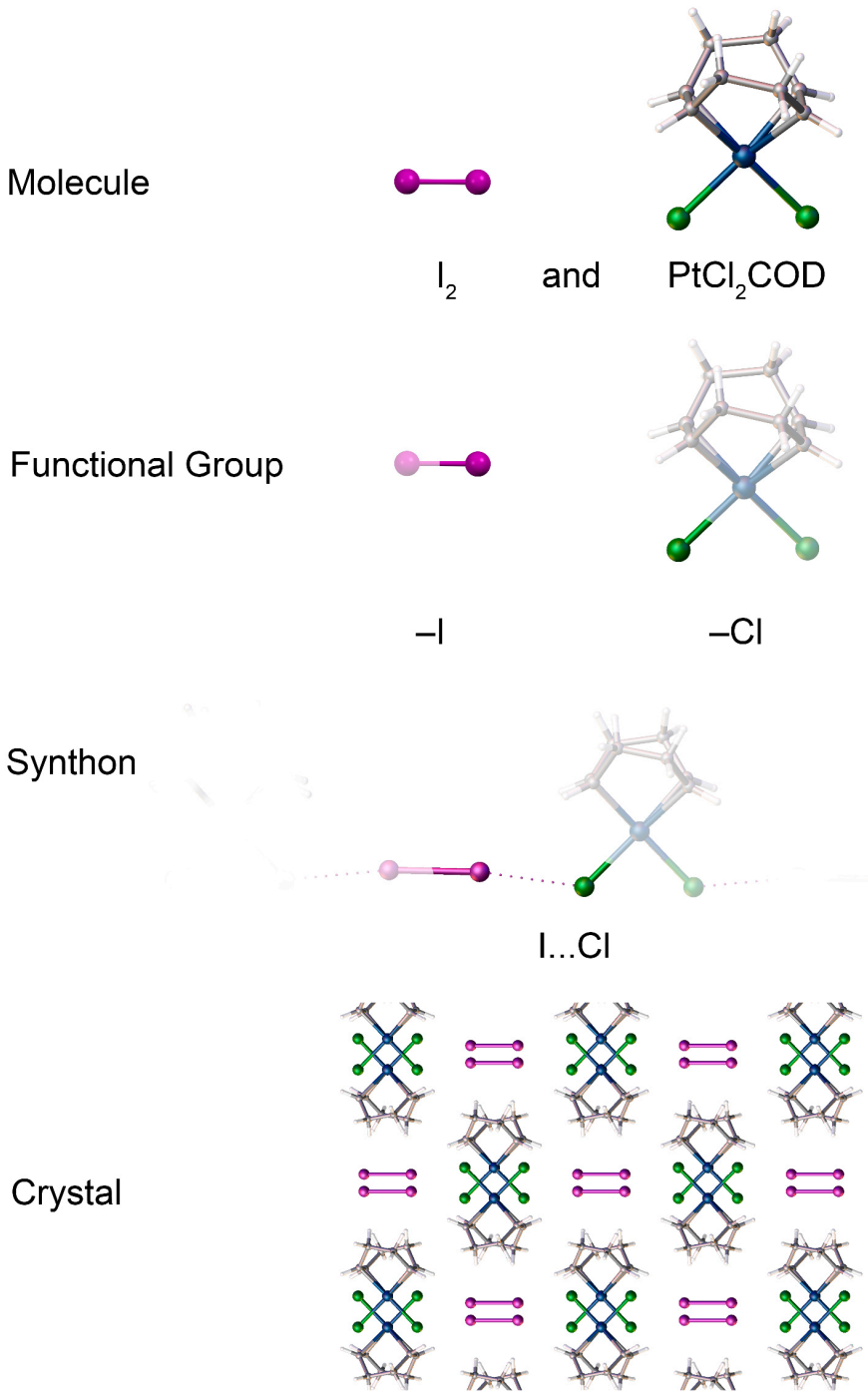

FIGURE 1 Self-assembly via halogen bonding.

Despite the differences, both self-assembly and intermolecular interactions play an important role in both of the aforementioned strategies.

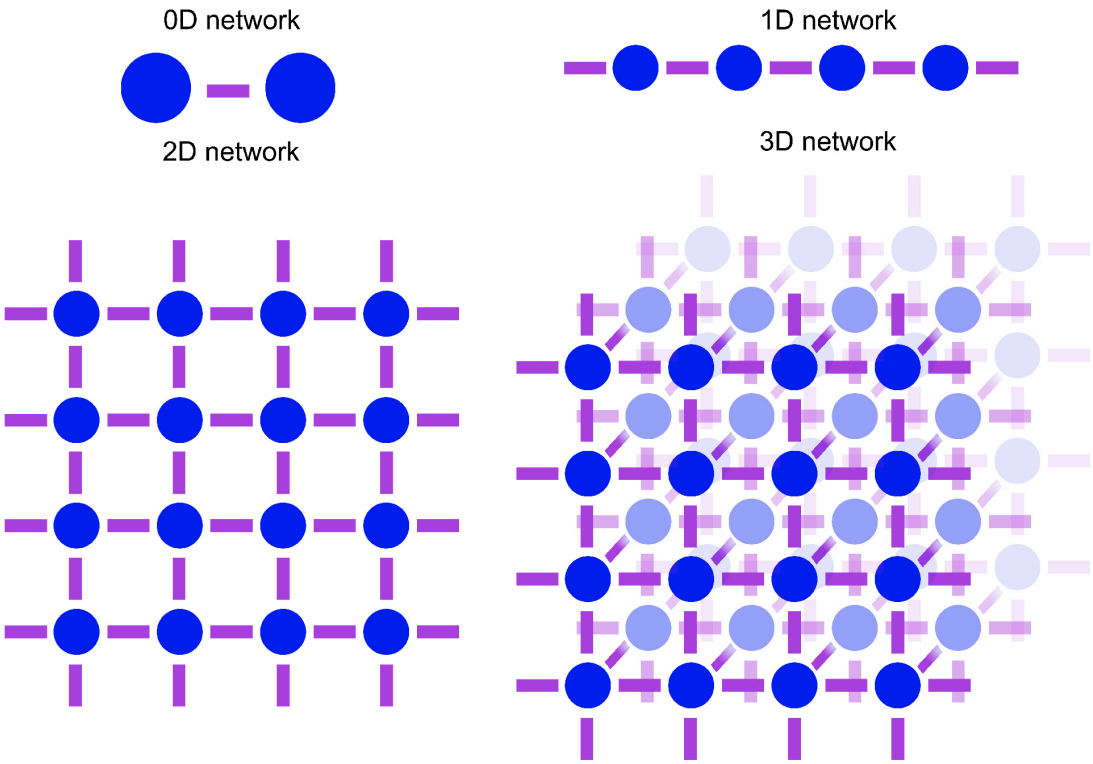

FIGURE 2 Schematic representation of cross-link coordination compounds creating 0D, 1D, 2D, and 3D networks.

1.3 Noncovalent Interactions

In this chapter, the difference between covalent and noncovalent interactions as well as the key noncovalent interactions applied in this thesis will be briefly discussed.

1.3.1 What is an interaction? Covalent vs noncovalent

In introductory chemistry classes in high school, students are taught that there are ionic, metallic, polar, and nonpolar covalent bonds. The definitions are quite strict and one would think it would always be possible to assign an interaction between two atoms to a certain bond type. However, then hydrogen bond is defined as an intramolecular force, which makes things more complicated because a hydrogen bond can be as strong as a covalent by energy.[9] So, is it covalent then? In undergraduate chemistry even more intermolecular interactions are defined as part of the term "noncovalent".

A covalent bond is typically defined as the sharing of an electron pair between two nuclei. On the other hand, a noncovalent interaction is based on the electrostatics, charge transfer, and/or dispersive interaction. If a covalent

interaction leads to the formation of a molecule, a noncovalent interaction leads to the formation of a molecular cluster.

Although the nature of the interaction is a highly discussed subject, in the end, the main question is "what is a bond (interaction) between two atoms"? According to the IUPAC Golden Book:

> When forces acting between two atoms or groups of atoms lead to the formation of a stable **independent molecular entity**, a chemical bond is considered to exist between these atoms or groups.[10]

Simply, if an interaction has physical consequences it does exist.

Although IUPAC has clear definitions for ionic and covalent bonds, instead of assigning an interaction as purely ionic, covalent, or noncovalent, it is preferable to consider the contribution of a certain character of an interaction to a bond. The character of the interaction can be described by some measurable parameters and in the case of bonding these parameters are the energy and distance of the interaction.

The interaction energy scale ranges from hundreds to just a few kJ/mol. The distance scale ranges from a short interaction of less than 2 Å to a long-distance interaction of 2-5 Å. While short-range high-energy interactions are typically assigned to ionic and covalent bonds, the entirety of noncovalent interactions starts at high energy short-range hydrogen bonds and ends at low energy dispersive interactions that approach or even exceed the sum of the van der Waals (vdW) radii. In the end, the strength of interaction must be strong enough to create a stable molecular entity and therefore, although noncovalent interactions are sometimes called "weak", they are strong enough to create new materials.

1.3.2 Halogen bond

Halogen bonding has brought a lot of attention to the scientific community during recent decades as a powerful self-assembly tool.[1,11] According to the IUPAC definition:

> A halogen bond occurs when there is evidence of a net attractive interaction between an electrophilic region associated with a halogen atom in a molecular entity and a nucleophilic region in another, or the same, molecular entity.[12]

A halogen bond can be schematically represented as R–X···Y (FIGURE 3), where R–X is a halogen bond donor (XBD) and Y is a halogen bond acceptor (XBA). XBD consists of a group, R, covalently bonded to any halogen atom with an electrophilic region (X). In XBA, Y is an entity with a nucleophilic region. The d(X···Y) distance between X and Y is usually less than the sum of the vdW radii in halogen bonded systems.

The electrophilic region on the halogen atom is called a σ-hole. Clark et al.[13] have proposed the σ-hole concept, which is a region of a positive electrostatic

potential on the elongation of the R–X σ-bond. More details of the σ-hole concept can be found in section 2.2.1 (ESP).

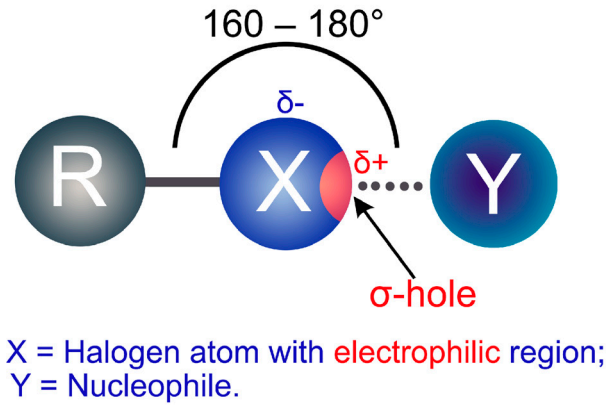

FIGURE 3 Schematic representation of a halogen bond.

The nature of a halogen bond is still debated among scientists. The question of what component of the binding energy dominates is the central issue. As Politzer and Clark suggested, all the components such as dispersion, charge-transfer, polarization, and electrostatics contribute to the interaction. However, the only physical observable is the binding energy.[14]

The main properties of a halogen bond, which include the directionality[15] and tunability,[16] are closely related to σ-hole properties, such as the size and magnitude. The halogen bond is a directional interaction with an angle ∠(R–X···Y) normally between 160° and 180°.[17]

An advantage of halogen bonding is the tunability. The halogen bond strength increases as the electronegativity of halide (X) decreases (F < Cl < Br < I), and as the electron-withdrawing ability of R decreases. Therefore, the strength of a halogen bond can be adjusted by varying the halide or the R group. For example, fluorine can act as a XBD if R is a very strong electron-withdrawing group.[18]

The existence of a halogen bond can be confirmed experimentally, theoretically, or preferably with a combination of techniques. The experimental methods include SCXRD, NMR, IR, Raman, XPS, and UV-vis spectroscopies. Theoretical confirmation can be done via QTAIM, NCIplot, DORI (density overlap region indicator), ESP, ELF analyses. Some of these methods are discussed in chapter 2.

1.3.3 Hydrogen bonding and π–interactions

There are many noncovalent interactions, such as hydrogen bonds (HBs), metallophilic and π-interactions, triel, tetrel, pnictogen, chalcogen, halogen, and aerogen bonds.[19] All of them are actively applied in crystal engineering. In the scope of this work, hydrogen bonding and π-interactions need to be briefly mentioned.

The hydrogen bond can be notated as D–H···A. It can be described primarily via an electrostatic attraction between the positively charged end of a

dipole, D–H, (hydrogen bond donor, HD) and the negatively charged entity, A, (hydrogen bond acceptor, usually bearing a lone electron pair, HA). It can also include some covalent and dispersion contributions.[20] The electronegativity of a D group has to be higher than the electronegativity of a hydrogen atom to sufficiently polarize the D–H bond. Both D and A can be represented by C, N, O, F, P, S, Cl, Se, Br, and I. However, A can also be a double or triple bond as well as any kind of a π-system. HBs can be divided into two groups; symmetrical and asymmetrical (FIGURE 4.1.a and 4.1.b). The strongest hydrogen bonds are known to be short and symmetrical[21] and involve charged species.[22] The HB energies range from 2 (weak) to 40 (strong) kcal mol^{-1}.[22]

The nature of π-interactions is usually explained via the Hunter–Sanders model,[23] where due to the quadrupole moment in the aromatic system, stacking of aromatic fragments is arranged to minimize the electrostatic repulsion between π–systems and maximize attraction between sigma skeleton. This model works well in describing the energetically favorable dispersion-dominating π–interactions, such as face-to-edge, parallel displaced, and reversed polarity face-to-face arrangements of the benzene rings as shown in FIGURE 4.2.b–4.2.d, respectively. In contrast, cation–π and anion–π interactions are mainly determined by electrostatic and induction contributions as shown in FIGURE 4.2.g and 4.2.h, respectively.[24] A more general way to classify these interactions is to subdivide them to neutral (FIGURE 4.2.a–4.2.f) and charged interactions (FIGURE 4.2.g and 4.2.h). The range of energies of π–interactions is quite broad, starting from 1 kcal/mol for dispersion dominated interactions to stronger than 30 kcal mol^{-1} for pancake bonding (parallel π-stacking interaction).[25,26]

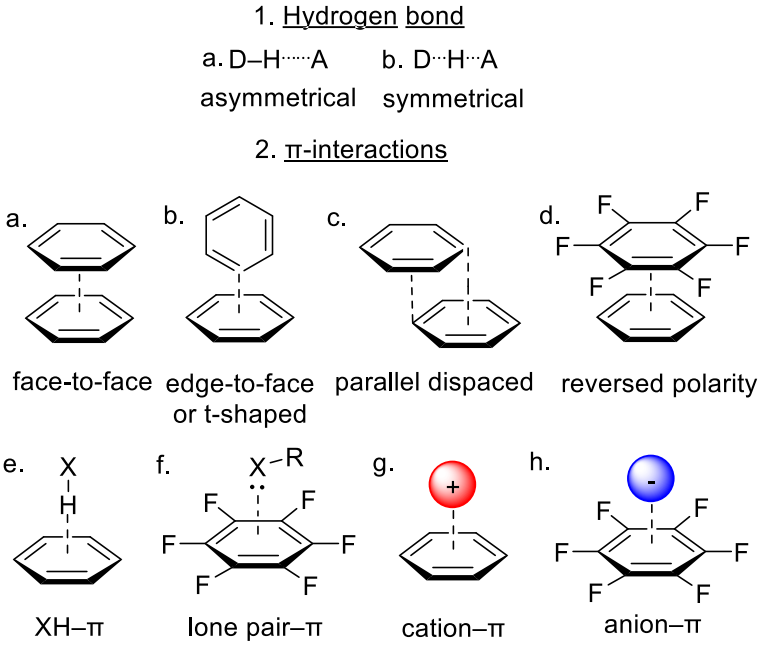

FIGURE 4 Types of hydrogen bonds and π–interactions: 1a) asymmetrical HB; 1b) symmetrical HB; 2) various π–interactions.

1.3.4 Metal-involved noncovalent interactions

In the context of this thesis, the nature of metal-involved noncovalent interactions can be divided into polar, with clear electro- or nucleophilic roles assigned to interacting atoms, and nonpolar, with undefined electro- or nucleophilic roles. Examples of polar interactions include NCIs involving σ-holes (as in hydrogen, halogen, chalcogen, etc.),[27,28] electron belts (as in semicoordination),[29] and π–clouds (as in cation–π).[30,31] In addition, some of the metallophilic interactions in heterometallic complexes such as weak electrostatic attractive interactions between low-valent closed shell (d^{10}, s^2) and pseudo-closed shell (d^8) metal ions can be classified as polar.[32,33] Nonpolar interactions include some halogen bonds of intermediate metal-halogen type[34] and metallophilic interactions known for d-block transition metal complexes (FIGURE 5).[35]

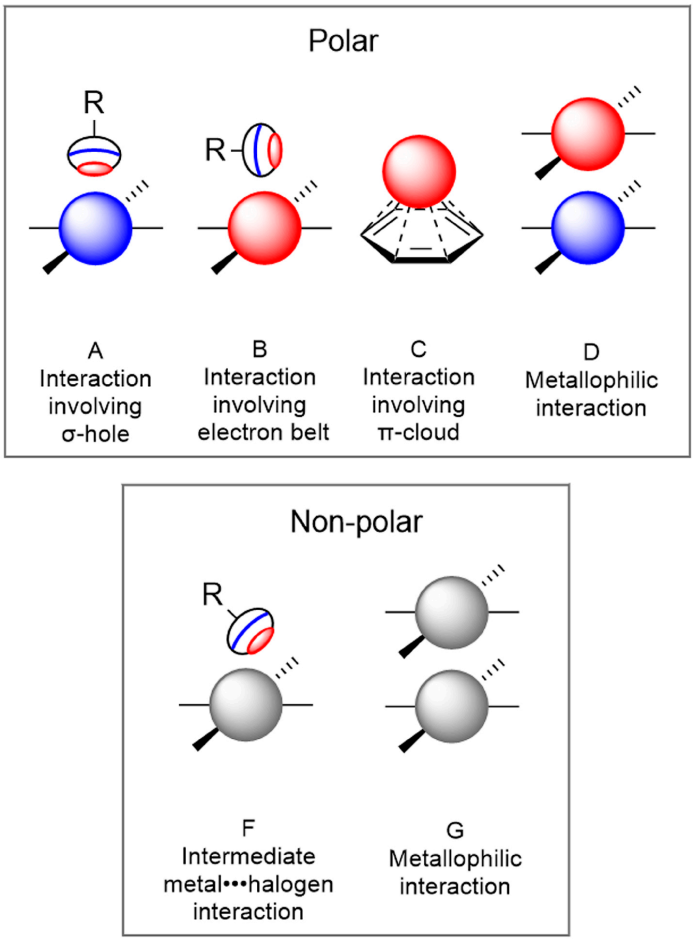

FIGURE 5 Types of noncovalent interactions involving metal centers and halogen atoms. The neutral regions are colored gray, electrophilic regions are colored red, nucleophilic ones are blue.

Although each interaction has its own nature and properties, it is important to remember that frequently several NCIs contribute to the arrangement of the structure. This effect is called **cooperative** and it means that various NCIs are strengthening or weakening each other.[36,37] Cooperative effects are especially

important in metal-involved NCIs that are usually accompanied by stronger types of NCI. For example, cooperation of π–π and metallophilic interactions are necessary to stabilize extended chain structures in neutral [Pt(II)/Pd(II)(CNC_6H_4-*p*-CH_3)$_2Cl_2$] aryl isocyanide complexes (FIGURE 6).[38]

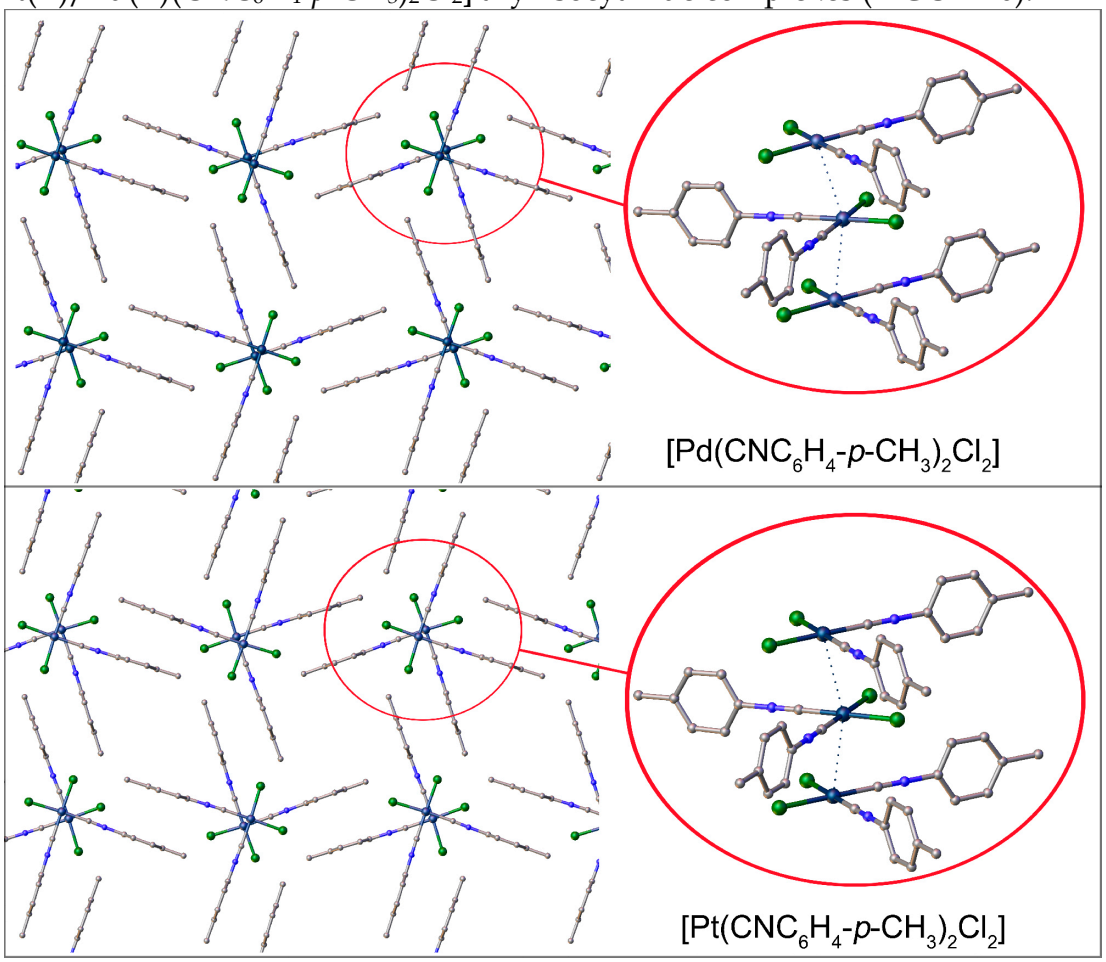

FIGURE 6 Cooperative effect of π–π interactions and metallophilic contacts that stabilizes extended chains of [Pt(II)/Pd(II)(CNC_6H_4-*p*-CH_3)$_2Cl_2$] complexes. Hydrogens are omitted for clarity.[38]

It is possible to achieve various metal-involved contacts by modifying the interlinking molecule even within the same metal complex. A prime illustration of this are I_2 and 1,3,5-triiodotrifluorobenzene (1,3,5-FIB) cocrystals of nitrosoguanidinate Ni(II) complexes [Ni{NH=C(NMe_2)NN(O)}$_2$]. In the case of an I_2 cocrystal, a semi-coordination Ni···I contact is formed. In the 1,3,5-FIB cocrystal, an intermediate type of Ni···I contact was observed[34] and in the 1,4-diiodotetrafluorobenzene cocrystal, no Ni···I contact was observed (FIGURE 7).[39]

Another way to control the metal-involving contacts is to modify the metal center without changing any other variables. For example, in the case of the cocrystals of [M(acac)$_2$] (M = Pd, Pt, acac = acetylacetonate) with 1,3,5-FIB, the XB pattern is dependent on the metal center.[40] Due to the difference in d_z^2-nucleophilicity of the Pt(II) center compared to the Pd(II) center, it is possible to turn the M···I interaction on or off.

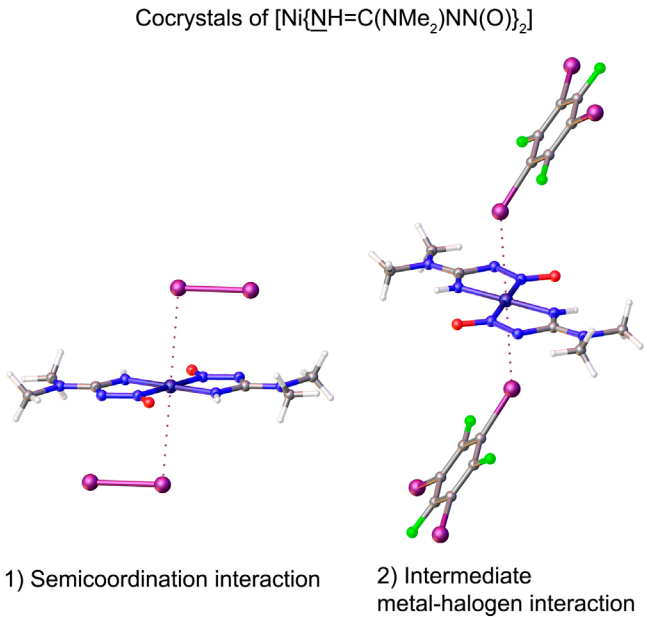

FIGURE 7 Influence of XBD on the NCIs involved on the metal centers of [Ni{NH=C(NMe$_2$)NN(O)}$_2$]: 1) Ni···I semi-coordination contact in an I_2 cocrystal and 2) an intermediate type of Ni···I contact in a 1,3,5-FIB cocrystal.[34] Only metal-involved NCIs are presented in the picture.

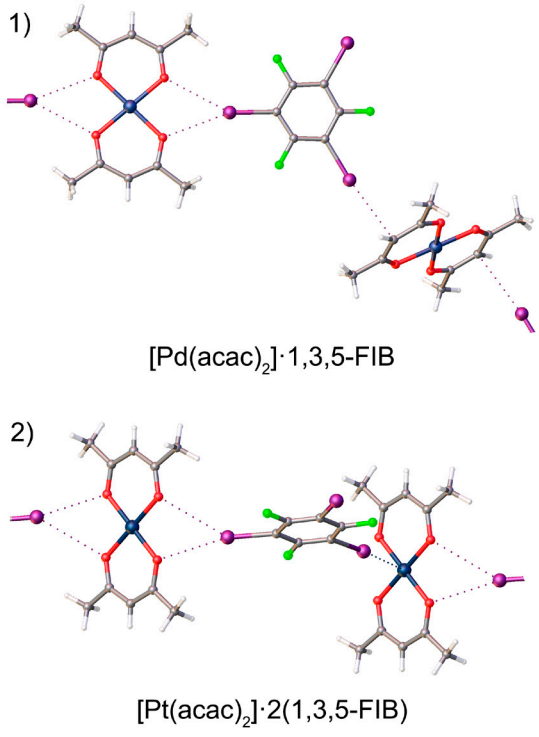

FIGURE 8 Halogen bonding patterns in cocrystals of [M(acac)$_2$] (M = Pd, Pt; acac = acetylacetonate) with 1,3,5-FIB: 1) No M···I contact of 1,3,5-FIB with a Pd(II) center and 2) M···I contact of 1,3,5-FIB with a Pt(II) center.[40]

2 METHODS

This chapter briefly introduces specific methods to study noncovalent interactions used in this thesis. General methods, as well as specific methods not used in these studies, are not discussed.

2.1 Experimental studies

2.1.1 Single crystal X-Ray diffraction (SCXRD)

One of the most common methods for analyzing the molecular structure is single crystal X-ray diffraction (SCXRD). The difficulty with this method is obtaining a single crystal perfect enough to gain publishable data. However, it is able to obtain valuable information on the arrangement of the atoms in space and geometrical parameters, such as bond lengths and angles.

Experimentally obtained distances between non-covalently interacting atoms are usually shorter than the sum of the corresponding vdW radii in NCIs.[41] Bondi's vdW radii are commonly used for NCIs.[42] Thus, the distance reduction ratio (R_{IX}) is a common parameter for estimating and comparing the NCIs relative strengths. For example, a shorter contact means a stronger NCI. R_{IX} can be calculated as $R_{IX} = d(I\cdots X)/(R^{I}_{vdW} + R^{X}_{vdW})$, where I is atom with the electron-deficient area (e.g. iodine), X is an atom with the electron-rich area, $d(I\cdots X)$ is the distance between I and X, and R^{I}_{vdW} and R^{X}_{vdW} are the corresponding vdW radii of I and X.

TABLE 1 Selected data on Bondi's vdW radii.[42]

Atom	Bondi vdW, Å	Atom	Bondi vdW, Å
H	1.20	I	1.98
Cl	1.75	Pd	1.75
Br	1.85	Pt	1.63

2.1.2 ^{15}N, ^{195}Pt NMR spectroscopy

Another useful experimental technique for the study of NCIs is ^{15}N NMR spectroscopy.[43,44] It is able to distinguish various isomers, tautomeric forms, rotamers, and noncovalent interactions.[45,46] Although the ^{15}N nucleus (with I=1/2) has lower natural abundance (0.3%) than ^{13}C (1%), it is advantageous for isotopic labeling because the labeled location is easily identified from the more abundant isotope, ^{14}N. It is also ideal because it has a range of chemical shifts of about 900 pm. This enables investigation of a wide selection of compounds. The main disadvantages of ^{15}N NMR spectroscopy are its low gyromagnetic ratio, which is a factor of 10 lower than ^{1}H, and its low signal-to-noise ratio. It is important to use a reference compound in liquid state ^{15}N NMR studies.

The ^{15}N nucleus is used in solid-state NMR (SSNMR) spectroscopy that is especially valuable for solid-state studies of bulk material, solvent sensitive, and polymeric compounds. The sensitivity of the ^{15}N nucleus appears as a shift of the ^{15}N signal for coordinative or noncovalent interaction.[46,47]

Although ^{195}Pt NMR is one of the oldest NMR methods,[48] it is utilized less in studies of Pt complexes compared to more common methods, such as ^{1}H or ^{13}C NMR. However, ^{195}Pt NMR is an important non-destructive characterization tool.

The ^{195}Pt nucleus has nuclear spin quantum number of I=1/2, a natural abundancy of 33.7% and a $9.94x10^{-3}$ receptivity relative to ^{1}H.[49] Due to the short relaxation times signal accumulates quickly, which makes taking direct 1D ^{195}Pt spectra a routine measurement. An advantage of this method is the unique signal for certain types of Pt centers. Chemical shifts are very sensitive to the environment of the complex in the ^{195}Pt spectra. The method can distinguish between oxidation states, conformations, and ligands in the coordination sphere (donor atoms) of Pt.[50]

^{195}Pt NMR resonances must be compared to a reference compound for the chemical shift (δ(Pt), in ppm). A D_2O solution of $Na_2[PtCl_6]$ is a common reference (δ(Pt) = 0 ppm) because of its good solubility, commercial availability, affordable price, and relative stability. The chemical shifts of ^{195}Pt are dependent on the temperature of spectrum measurement, the concentration of the sample, and solvent effects.[50] The reported error of this method is up to ±5 ppm. However, considering the wide resonance window of 15000 ppm, it is relatively small. It is important to choose the correct window, otherwise, a problem of folded peaks can arise due to the limited working window of the spectrometer.[51]

Although this method is sensitive to the coordination environment of the complex, it is not widely used to investigate noncovalent interactions. The reasons for this are the small differences in chemical shifts of the original complex and the complex with NCIs, stability of the interaction in solution, and solubility of the sample. Great care must be taken when setting the experimental parameters.

In 2020, I···Pt XB was investigated with ^{195}Pt-NMR by Katlenok et al.[52] In this study, I···Pt XB was studied by titrating half-lantern Pt complexes with XBD (XBD = 1,4-diiodotetrafluorobenzene and 1,1'-diiodoperfluorodiphenyl).

Titrations of a 1:1 ratio led to a slight change in the ^{195}Pt chemical shifts. Therefore, the titrations were continued up to a 1:20 molar ratio, where changes in the chemical shifts became noticeable (up to 64 ppm).
To summarize, important features of ^{195}Pt NMR in the context of this thesis are:

- The oxidation state of the metal influences the chemical shifts (FIGURE 9.1).
- Going down in group 17 of the periodic table makes the chemical shifts more negative (FIGURE 9.2).
- Isomerization of square planar Pt complexes influences the chemical shifts (FIGURE 9.3).

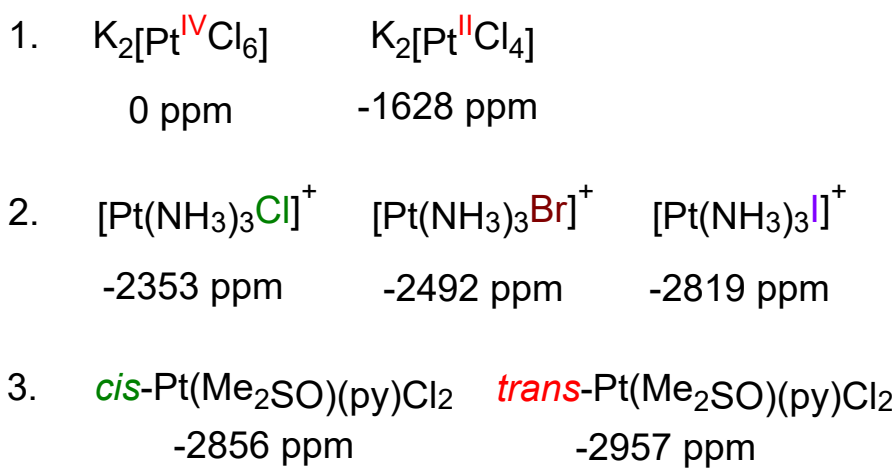

FIGURE 9 Examples of the resolution ability of the ^{195}Pt NMR method. 1) Distinguishing between various oxidation forms, 2) resolving different halides, and 3) resolving *cis*-and *trans*-isomers.

2.2 Theoretical studies

It is not always possible to look deep into the interaction experimentally. Instead, theoretical modeling can provide scientists with this opportunity. In this chapter, we will look into some well-established and modern theoretical techniques used in this thesis. Electrostatic surface potential analysis gives clues to the best nucleophile/electrophile pairing in molecules. QTAIM justifies the pairs and gives estimates the covalency of the interaction. The NCI method visualizes noncovalent interactions in real space and is able to distinguish interactions by the strength and attractive/repulsive nature. A combination of ELF and QTAIM is applied to understand the donor-acceptor nature of the interaction. Analysis of ED and ESP minima profiles reveals the philicity of NCI. Together these methods improve our understanding of the nature of NCIs and give the ability to predict possible structures of systems of interest.

2.2.1 Electrostatic Surface Potential (ESP)

An elegant way to predict the possible direction and strength of a noncovalent interaction suggested by Politzer et al. is the analysis of the electrostatic potential (ESP) surface.[53] ESP is a measurable value that can be obtained both theoretically and experimentally by diffraction techniques.[54,55] It should be calculated at the 0.001 a.u. contour of the molecule's surface because it illustrates 96% of the electronic charge of a molecule as recommended by Bader et al.[56]

Anisotropic charge distribution on the surface of the molecule results in the localized positive or negative potential regions. The positive potential region, called a σ-hole as it is located on the covalent σ-bond, has several important features. This includes the σ-hole magnitude, $V_{S,max}$, the most positive electrostatic potential at the isosurface, and size of a σ-hole, which is the area of the positive ESP. The magnitude determines the strength of the interaction while the size of the σ-hole influences the directionality of the interaction. These features can be influenced by varying the electron-withdrawing or donating groups. Strength of the NCI is correlated with $V_{S,max}$ and increases for the pnictogen group as N < P < As < Sb, for the chalcogen group as O < S < Se < Te, and for the halogen group as F < Cl < Br < I. The common trend in these groups is that the less electronegative and more polarizable atom leads to a bigger $V_{S,max}$. An illustration of this phenomenon is the trifluoromethane halides, where the σ-hole features are enhanced by the strong electron-withdrawing properties of the CF_3 group (FIGURE 10).

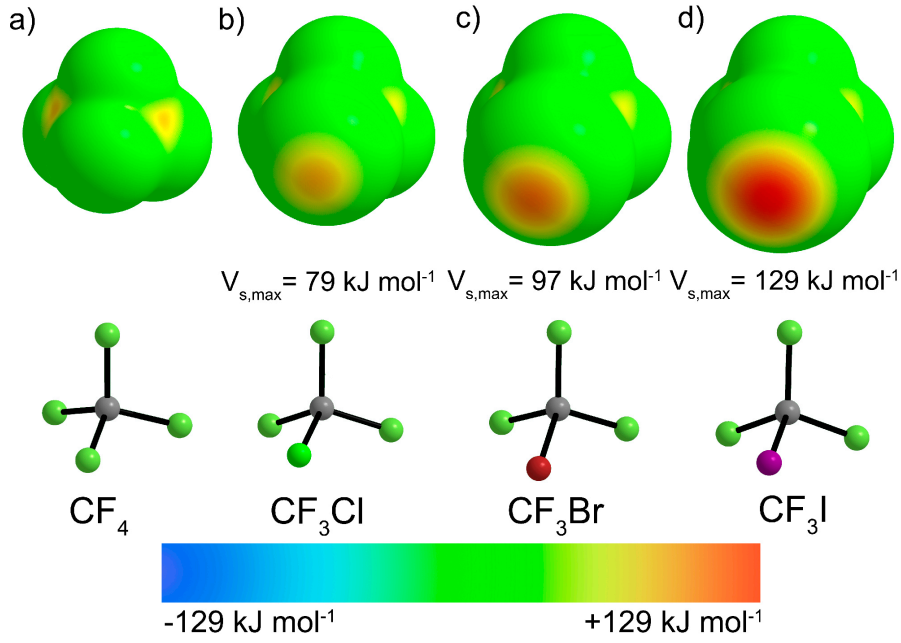

FIGURE 10 Electrostatic potential surface calculated at the PBE0/def2-TZVP level on the 0.001 au molecular surfaces of trifluoromethane halides of a) CF_4, b) CF_3Cl, c) CF_3Br, and d) CF_3I.

2.2.2 Quantum Theory of Atoms in Molecules (QTAIM)

Bader's QTAIM[57] identifies covalent and noncovalent interactions differently by analysis of the topology of the electron density ρ(r), where ρ is the electron density (ED) and r is a spatial variable. The distribution of the ED is affected by electron-nuclear force, with the maximum at the nuclear sites that decays when moving away from the nucleus. Lines of density maximum connecting neighboring atomic regions are called bond paths. Topological analysis of the ρ(r) via the first (gradient, $\nabla\rho(r)$) and second (Laplacian, $\nabla^2\rho(r)$) derivatives provides useful structural information, such as a measure of the strength of an interaction between two molecular systems and of the degree of covalency.

The first derivative of the ED describes the maxima, minima, or saddle points in space (EQUATION 1). It vanishes at certain extremum points called critical points (CPs) where $\nabla\rho(r_{cp}) = 0$. The second derivative, $\nabla^2\rho(r_{cp})$, describes the characteristics of the CPs, such as the local charge concentration or diminution. The symmetric (3×3) matrix of the partial second derivatives is called the Hessian of ρ ($\nabla\nabla^T\rho(r_{cp})$). It is used to explore $\nabla^2\rho(r_{cp})$ and is given in EQUATION 2. Diagonalization of the Hessian matrix allows one to obtain three eigenvalues, λ_1, λ_2, and λ_3, and these represent the principal axes of curvature (EQUATION 3).

Eigenvalues define the rank (number of non-zero eigenvalues) and the signature (the algebraic sum of the signs of eigenvalues) of a CP (rank, signature)). Topologically stable CPs always have a rank of three that gives four possible combinations such as (3, −3), (3, −1), (3, +1), and (3, +3). At (3, −3) CP, all curvatures are negative and ρ is a local maximum. At (3, −1) CP or the **bond critical point (BCP)**, two curvatures are negative, one is positive, and ρ is a maximum in one plane and a minimum perpendicular to that plane. At (3, +1) CP, or the **ring critical point (RCP)**, two curvatures are positive, one negative, and ρ is a minimum in one plane and a maximum perpendicular to that plane. At (3, +3) CP or a **cage critical point**, all curvatures are positive and ρ is a local minimum.

EQUATION 1. $$\nabla\rho(r_{cp}) = \mathrm{i}\frac{\partial\rho}{\partial x} + j\frac{\partial\rho}{\partial y} + k\frac{\partial\rho}{\partial z}$$

EQUATION 2. $$\nabla\nabla^{\mathrm{T}}\rho(r_{cp}) = \begin{pmatrix} \frac{\partial^2\rho}{\partial x^2} & \frac{\partial^2\rho}{\partial x\partial y} & \frac{\partial^2\rho}{\partial x\partial z} \\ \frac{\partial^2\rho}{\partial y\partial x} & \frac{\partial^2\rho}{\partial y^2} & \frac{\partial^2\rho}{\partial y\partial z} \\ \frac{\partial^2\rho}{\partial z\partial x} & \frac{\partial^2\rho}{\partial z\partial y} & \frac{\partial^2\rho}{\partial z^2} \end{pmatrix}$$

EQUATION 3 $$\nabla^2\rho(r_{cp}) = \frac{\partial^2\rho}{\partial x^2} + \frac{\partial^2\rho}{\partial y^2} + \frac{\partial^2\rho}{\partial z^2} = \lambda_1 + \lambda_2 + \lambda_3 \text{, where } \lambda_1 < \lambda_2 < \lambda_3$$

The relationship between the energetic topological parameters and $\nabla^2\rho(r_{cp})$ via the local form of the virial theorem allows one to obtain the total electron energy density, $H(r_{cp})$, the potential electron energy density, $V(r_{cp})$, and the

kinetic energy density, $G(r_{cp})$. Here, $G(r_{cp})$ and $V(r_{cp})$ are positive and negative quantities, respectively (EQUATIONS 4−5).[58]

EQUATION 4. $$\frac{1}{4}\nabla^2\rho(r_{cp}) = 2G(r_{cp}) + V(r_{cp})$$

EQUATION 5 $$H(r_{cp}) = G(r_{cp}) + V(r_{cp})$$

The covalency of the interaction can be studied through the relationship between $V(r_{cp})$ and $G(r_{cp})$. When $|V(r_{cp})| > G(r_{cp})$, then $\nabla^2\rho < 0$ in the internuclear region and indicates a shared interatomic interaction, i.e., covalent or polar bonding. If the magnitude of $G(r_{cp})$ dominates over the interaction, then $\nabla^2\rho(r_{cp}) > 0$, which means closed-shell interactions or ionic bonds and NCIs. Here, $\rho(r_{cp})$ quickly increases away from the BCP.

It is also possible to estimate covalency with the delocalization index, $\delta(i,j)$, which describes the number of electrons shared between atomic basins Ω_i and Ω_j. High localization indices are associated with covalent bonding while low indices indicate ionic or NCIs.[59]

For the description of various NCIs, the QTAIM method became an invaluable tool. For example, topological analysis of the electron density is included in the IUPAC definition of XB. When XB takes place there is a bond path and a (3, –1) critical point between two neighboring atomic basins.[12] Although QTAIM is widely used in the study of NCIs, visual representation of NCIs through BCPs and bond paths is not very intuitive.

2.2.3 Noncovalent Interactions plot (NCIplot)

Developed by Johnson and coworkers in 2010, the NCIplot program has been used in studies of NCIs.[60] This program is a powerful computational tool for real space visualization and estimating the relative strength of NCIs.

The essential quantity in the NCI method is the reduced electron density gradient (s or RDG), which describes a deviation from a homogeneous electron distribution. It is closely related to the quantum-chemical electron density, ρ (EQUATION 6), which is a quantity that allows one to deduce various chemical properties. Thus, s depends on local density inhomogeneities that depend on the chemical region of the molecule. For example, in the event of bonding, the s value approaches zero.

EQUATION 6 $$s(\mathrm{r}) = \frac{1}{3(2\pi^2)^{\frac{1}{3}}}\frac{|\nabla\rho(\mathrm{r})|}{\rho(\mathrm{r})^{\frac{4}{3}}}$$

Another important parameter in the NCI method is the sign of the second eigenvalue ($\mathrm{sign}(\lambda_2)$) of $\nabla^2\rho$ (EQUATION 3). When $\nabla^2\rho = 0$, evaluating the eigenvalues allows to determine the type of interaction: all eigenvalues are negative at nuclei (maxima of ρ), positive at the minima of ρ, and at the remaining points of space have $\lambda_1 < 0$ and $\lambda_3 > 0$, while λ_2 can be both positive and negative. If $\lambda_2 > 0$, the interaction is assigned as repulsive but if $\lambda_2 < 0$, the interaction is

assigned as attractive. This feature is used by the NCI method to characterize the NCIs.

To analyze noncovalent interactions in the system, *s* has to be plotted against the sign(λ_2)ρ. In the resulted 2D graph interactions are represented by spikes. Attractive, dispersive, and repulsive interactions can be assigned through the sign(λ_2)ρ value. Attractive interactions are located in [–0.05, –0.005] sign(λ_2)ρ range. Dispersive interactions associated with low-density values are located in [–0.005, 0.005] sign(λ_2)ρ range. Finally, repulsive interactions are located in [0.005, 0.05] sign(λ_2)ρ range.[60] In 3D visualizations based on 2D plot data NCIs are represented by reduced density gradient isosurfaces. The color of the isosurface represents the interaction strength. Isosurfaces are colored in the red-green-blue (RGB) scheme, where red indicates strong destabilizing interactions, green indicates delocalized medium to weak interactions, and blue indicates strong stabilizing interactions.

The main advantage of the NCI method is its insensitivity to the choice of computational method (the same densities are obtained with different methods). Another advantage is the possibility to compare the relative strength of interactions between a series of compounds. For example, in the case of the 4-halobenzonitriles series (ClBzCN, BrBzCN, and IBzCN; Bz = C_6H_4),[61] the N-XBD distances were found 3.31 Å for ClBzCN, 3.27 Å for BrBzCN, and 3.18 Å for IBzCN. The corresponding R_{IX} values are 1.00 for ClBzCN, 0.96 for BrBzCN, and 0.90 for IBzCN, suggesting that the strength of XB is increases in the row ClBzCN, BrBzCN, and IBzCN. The NCIplot method gives the same trend with the corresponding sign(λ_2)ρ values of –0.005 for ClBzCN, –0.008 for BrBzCN, and –0.013 for IBzCN (FIGURE 11).

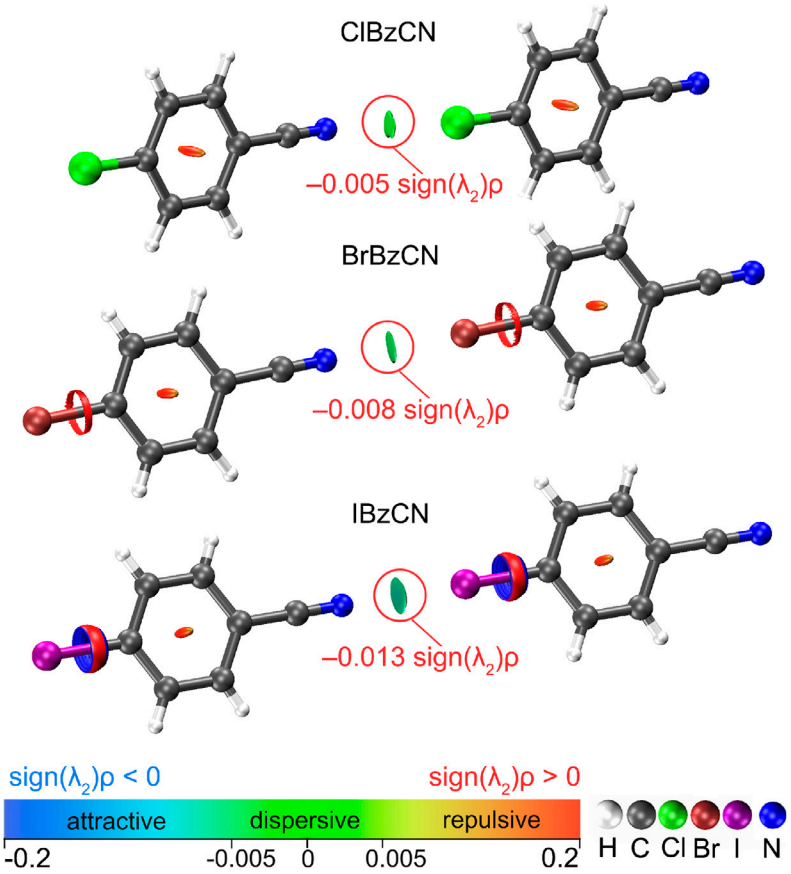

FIGURE 11 Isosurfaces representing NCIs in the 4-halobenzonitrile series (ClBzCN, BrBzCN, and IBzCN)[61] calculated on the PBE0-D3/def2-TZVP level. N···Hal halogen bonds represented as green isosurfaces with the corresponding sign(λ_2)ρ values in red.

2.2.4 Electron Localization Function (ELF)

As a derivative of the electron density, the ELF allows one to locate areas of shared and unshared electron pairs and describe the bonding (both covalent and noncovalent).[62] Just as in NCI method, an advantage of the ELF is its independence from the calculation method or the basis set used. Visualization of the ELF provides an intuitive understanding of interactions that involve electron pairs. The scale is defined as $0 \leq ELF \leq 1$, where 1 corresponds to areas of high localization of electrons, i.e., lone electron pairs, chemical bonds, and atomic shells. A combination of the ELF and QTAIM analyses shows bond paths at the interaction areas to give an additional view on the donor-acceptor nature of the interacting species. This combination has been applied in the investigations of XBs and other NCIs.[63–70]

The power of combining ELF and QTAIM can be demonstrated by visualizing the halogen bonding (I1A···X) in the $[PtX_2COD] \cdot nI_2$ (X = I, Br, Cl; n = 0.5 or 1) cocrystals (FIGURE 12). In the I1A···X XB bond path, a (3, –1) critical point passes through the region of higher electron localization (lone pairs) on the

halide ligands and there is lower electron localization (σ-hole) on I1A atoms in I_2. This confirms the electrophilic nature of I_2 and the nucleophilic nature of the halide atom in a halogen bond. Moreover, the decreasing ELF values for halide ligands of Cl > Br > I predicts the strongest XB interaction with [$PtCl_2COD$], which is confirmed via other methods in sections 2.2.5 and 3.3.1.

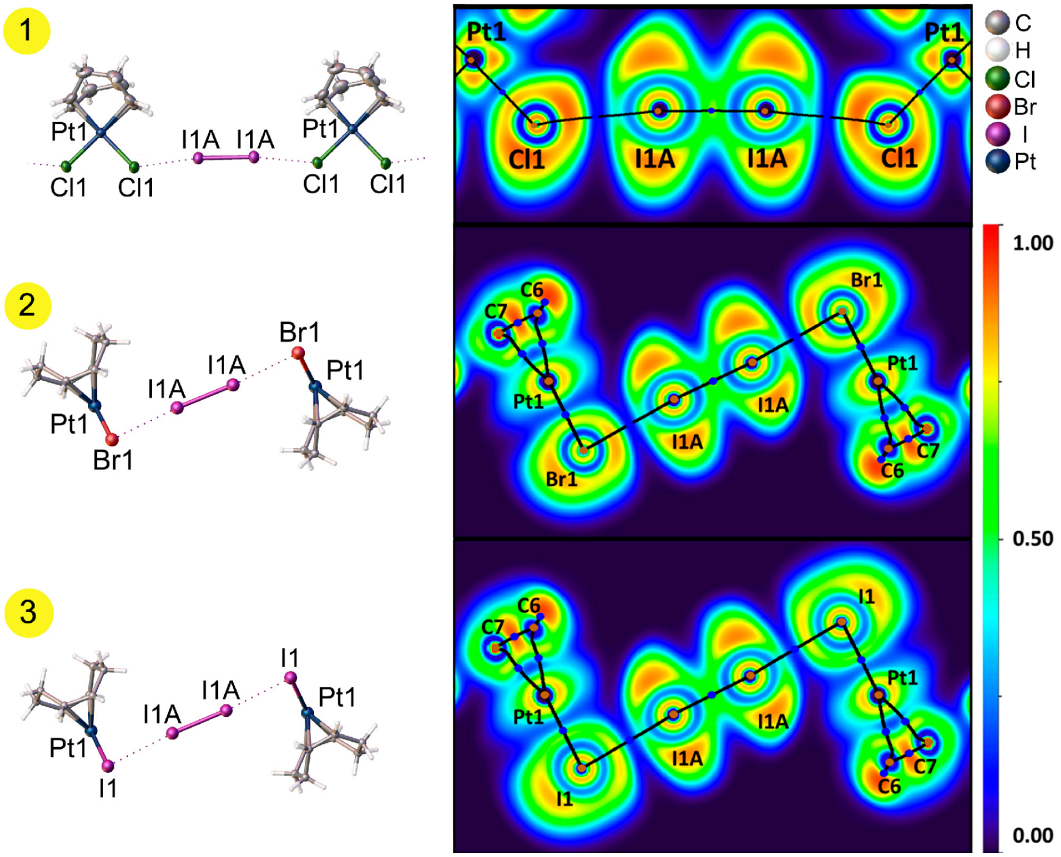

FIGURE 12 Halogen bonds I1A···X in cocrystals of [$PtCl_2COD$] · I_2 (1), [$PtBr_2COD$] · 0.5I_2 (2), and [PtI_2COD] · 0.5I_2 (3) and the corresponding ELF projections together with bond paths (black lines), BCPs (blue dots), nuclear critical points (NCPs, brown dots), and RCPs (orange dots).

2.2.5 Electron Density (ED) and ESP (ED/ESP) minima studies

Analysis of the ED and ESP minima profiles along the bond path allows one to determine the philicity of interacting atoms in NCIs.[67–69,71–74] This method is based on the superposition of gradient fields of the electrostatic potential φ(**r**) and electron density ρ(**r**). Boundaries of ρ-basins and φ-basins of the bonded atoms can be determined at zero-flux conditions $\nabla\rho(\mathbf{r})\cdot\mathbf{n}(\mathbf{r})=0$ and $\nabla\varphi(\mathbf{r})\cdot\mathbf{n}(\mathbf{r})=0$. Here, **n**(**r**) is a unit vector normal to the surface of atomic φ-basin. This method allows one to deduce the electrostatic forces involved in the interaction and determine the nucleophilic/electrophilic nature of the interacting atoms in combination with the QTAIM BCPs and bond paths. In the 1D profiles of the ρ(**r**) and φ(**r**) functions along the bond path between interacting atoms, the minimum of

φ(**r**) is shifted towards the nucleophilic atom while the ρ(**r**) minimum is shifted towards the electrophilic atom.

This can be illustrated with the $[PtX_2COD] \cdot nI_2$ (X = I, Br, Cl; n = 0.5 or 1) cocrystals that contain halogen bonds, where the nucleophilic nature of the $[PtX_2COD]$ halide and electrophilic nature of the iodine atoms of I_2 is confirmed via ESP and ELF analyses (see sections 2.2.4 and 3.3.1). Analysis of the ED/ESP minima shows a clear shift of ESP minimum towards the $[PtX_2COD]$ nucleophilic halide whereas the ED minimum shifts towards the electrophilic I1A atom in all cocrystals (FIGURE 13).

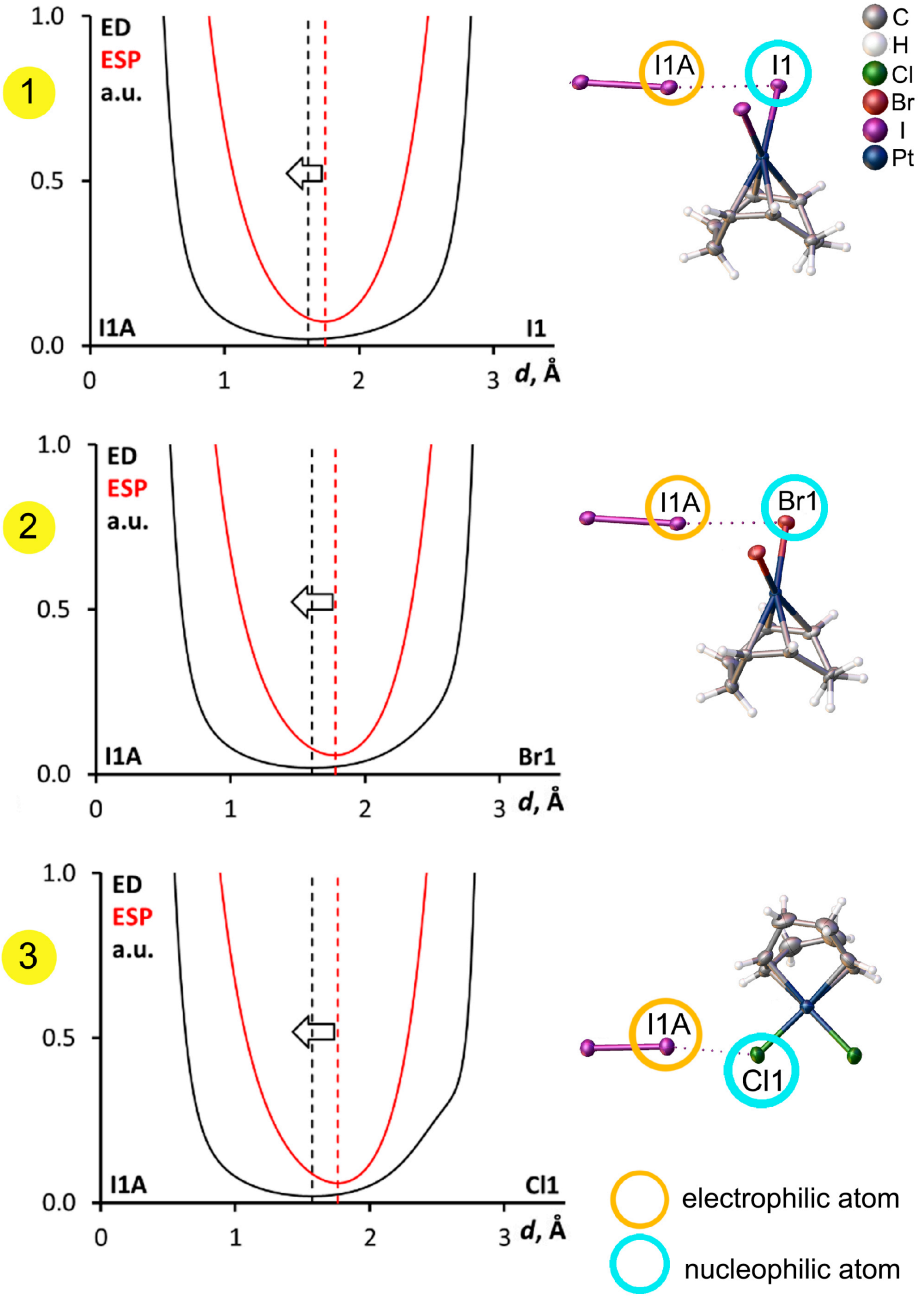

FIGURE 13 1D profiles of the ED (black) and ESP (red) functions along the I1A···X1 (X = I, Br, Cl) bond paths and the corresponding structures in $[PtI_2COD] \cdot 0.5I_2$ (1), $[PtBr_2COD] \cdot 0.5I_2$ (2), and $[PtCl_2COD] \cdot I_2$ (3) cocrystals.

3 RESULTS AND DISCUSSION

This chapter establishes the main direction of the research in this thesis. It starts with the choice of the systems, the aims of the study, and continues with the influence of various NCIs on the structure of metallopolymers. Synthetic procedures along with experimental and computational details can be found in publications I-III and the corresponding supplementary information files.

3.1 Choice of systems studied

As the general idea of our research was the application of NCIs for the creation of noncovalently bonded metallopolymers, the systems of the study had to be metal complexes with some interlinking units. Out of many metal complexes, Pt and Pd complexes were of particular interest to us because they have been widely applied in synthesis, catalysis, and medicine.[75–77] Tunability of the halogen bond was utilized to create different metallopolymers based on [PtX_2COD] (X = I, Br, Cl; COD = 1,5-cyclooctadiene) and *trans*-[$MI_2(CNXyl)_2$] (M = Pd or Pt; CNXyl = 2,6-dimethylphenyl isocyanide) complexes. [PtX_2COD] complexes are known as a great starting material for the synthesis of square planar Pt(II) complexes.[78–80] It was expected that axial Pt-X XBs would be obstructed due to the bulkiness of the COD ligand, which simplified the study of XB by limiting the amount of the additional interactions. In the case of *trans*-[$MI_2(CNXyl)_2$], relatively simple synthetic routes and availability of the d_z^2 orbital on the metallocentre made these square planar complexes perfect candidates for the study of metal-involved interactions. In addition, the similar atomic radii of Pd (1.4 Å) and Pt (1.35 Å)[81] enable us to obtain isomorphic Pd and Pt complexes to analyze similarities and differences in the isomorphic I_2 cocrystals, in particular, the influence of the metal center on the metal-involved NCI.

Three molecules were chosen as XBDs. These were I_2, 1,4-diiodotetrafluorobenzene (FIB), and CHI_3. These XBDs can be called "classic" as they were discussed in the IUPAC definition of a XB[12] and even in Hassel's Nobel

speech.[82] Furthermore, various geometries of the target metallopolymer can be achieved as I_2 and FIB have two possible directions for XB and CHI_3 has three. Additionally, FIB is capable of π-interactions and CHI_3 is a known hydrogen bond donor. Overall, tuning the geometry of the desired metallopolymer can be accomplished in two directions: by varying the halide (X) of the complex and by varying the XBD molecule.

In the case of systems of paper III, the original idea was to create a covalently bonded Pt metallopolymer. However, instead of coordinating to Pt, L was formed a noncovalently bonded 1D polymeric structure with KI. There were several attempts to control crystal growth of the ionic salt, out of which two general methods can be distinguished. The first was mechanical by limiting growth space, e.g., in single-walled carbon nanotube.[83] The second was chemical by directing crystal growth with coordination compounds that limit the growth.[84–86] We were focused on the second method, and have chosen 1,1´-bis(pyridin-4-ylmethyl)-2,2´-biimidazole (L) as a modifier molecule. N-heterocyclic-based ligands, including L, have the ability to form HBs and XBs as shown by Aakeröy et al.[87,88] The 1D polymeric structure obtained was a perfect example of NCIs application in KI crystal growth control by chemical modifier.

The molecules described here can be divided into two categories, electrophiles and nucleophiles (FIGURE 14). Molecules with electrophilic centers interacted with molecules with nucleophilic centers to yield 10 new cocrystals self-assembled via NCIs. They are $[PtI_2COD] \cdot CHI_3$, $[PtI_2COD] \cdot 0.5I_2$, $[PtBr_2COD] \cdot 0.5I_2$, $[PtCl_2COD] \cdot I_2$, $[PtI_2COD] \cdot 1.5FIB$, $[PtBr_2COD] \cdot 2FIB$, $[PtCl_2COD] \cdot 2FIB$, *trans*-$[PdI_2(CNXyl)_2] \cdot I_2$, *trans*-$[PtI_2(CNXyl)_2] \cdot I_2$, and $KI \cdot L$. The influence of the NCIs on the structural organization in those cocrystals will be discussed further.

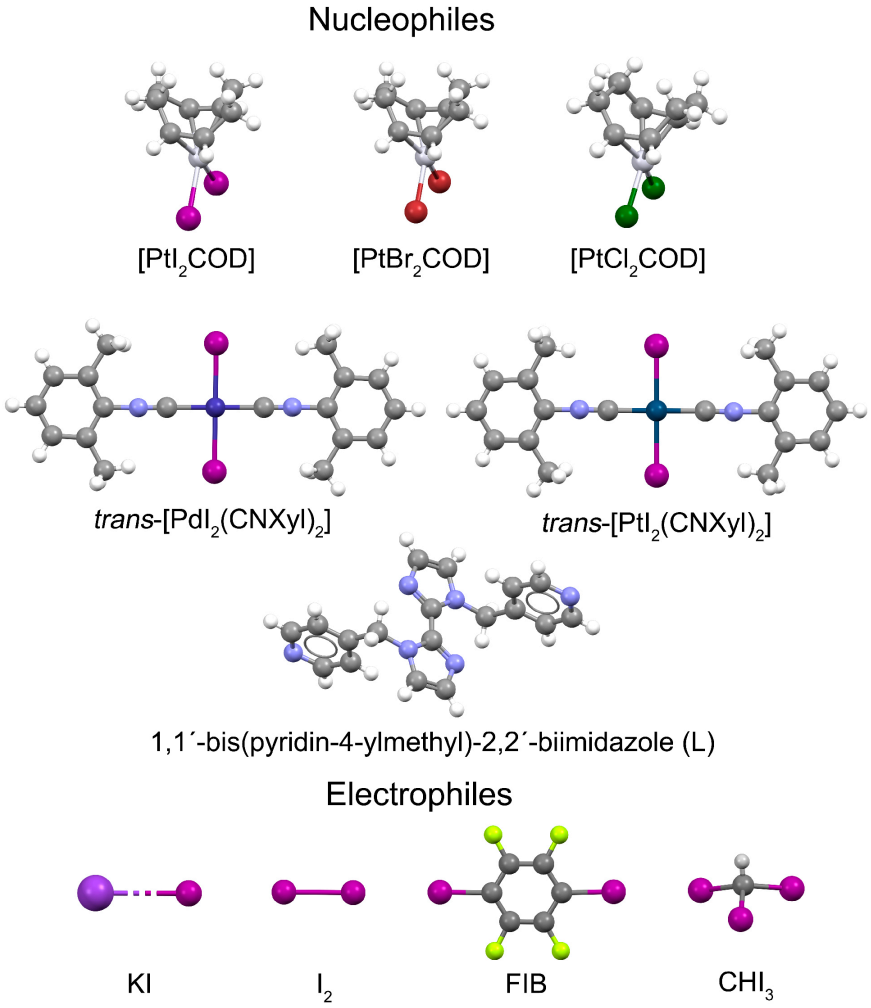

FIGURE 14 Nucleophilic ([PtX_2COD], *trans*-[$MI_2(CNXyl)_2$], and L) and electrophilic (KI, I_2, CHI_3, FIB) molecules utilized in the creation of metallopolymeric structures.

3.2 Aims of the study

The heroes of this thesis are noncovalent interactions, which are called weak in some sources compared to covalent or ionic bonds. However, the cooperative effect of several NCIs may enhance the stability of the final material. A general aim of this thesis was to utilize NCIs to design novel noncovalently bonded metallopolymers. A more ambitious aim was to use a combination of approaches to deepen our understanding of intermolecular interactions. NCIs can be more precisely used in crystal engineering with a greater level of understanding of noncovalent bonding. The main experimental analysis used to study NCIs here was single crystal X-ray diffraction, which was accompanied by various computational methods. The combination of these answered questions about the nature of the NCIs.

This thesis is based on 3 publications that used the approach "molecule → noncovalent interaction → metallopolymer". The major goal was to create novel metallopolymers bonded by NCIs. The additional subgoals were:

1) Study the influence of various halogen bond donors in the self-assembly of metallopolymers and utilize halogen bonds to control the geometry and length of the final product (publications I and II).
2) Investigate the role of metal-involved interactions in various metallopolymeric cocrystals (publications I–III).
3) Consider the influence of cooperative effects of NCI on the structure of the obtained cocrystals (publications I–III).

3.3 Noncovalent interactions in self-assembled metallopolymers

3.3.1 Halogen bonding as a tool for self-assembly of metallopolymers[I,II]

Halogen bonding was the key instrument to interlink [PtX_2COD] and *trans*-[$MI_2(CNXyl)_2$] (M = Pd or Pt) complexes into metallopolymers. However, in the case of the Pd/Pt isocyanide complexes, the focus was to study metal-involved interactions (see section 3.3.2).

Analysis of anisotropic charge distribution was applied to XBDs to determine the directionality of possible NCIs. CHI_3 molecule has four electron deficient areas available for NCIs, and $V_{s,max}$ value of the HB site area is higher than $V_{s,max}$ values of the XB sites (FIGURE 15). Even higher $V_{s,max}$ values (TABLE 2) were found for I_2 and FIB molecules that have two electron deficient areas each. Therefore, the strength of XBs is expected to be higher for I_2 and FIB XBDs compared to CHI_3.

TABLE 2 Maximum ESP ($V_{s,max}$) of selected halogenated molecules (calculated at the PBE0-D3/def2-TZVP level).

Molecule	Atom	$V_{s,max}$, kJ mol^{-1}
CHI_3	I	110
	H	129
I_2	I	137
FIB	I	139

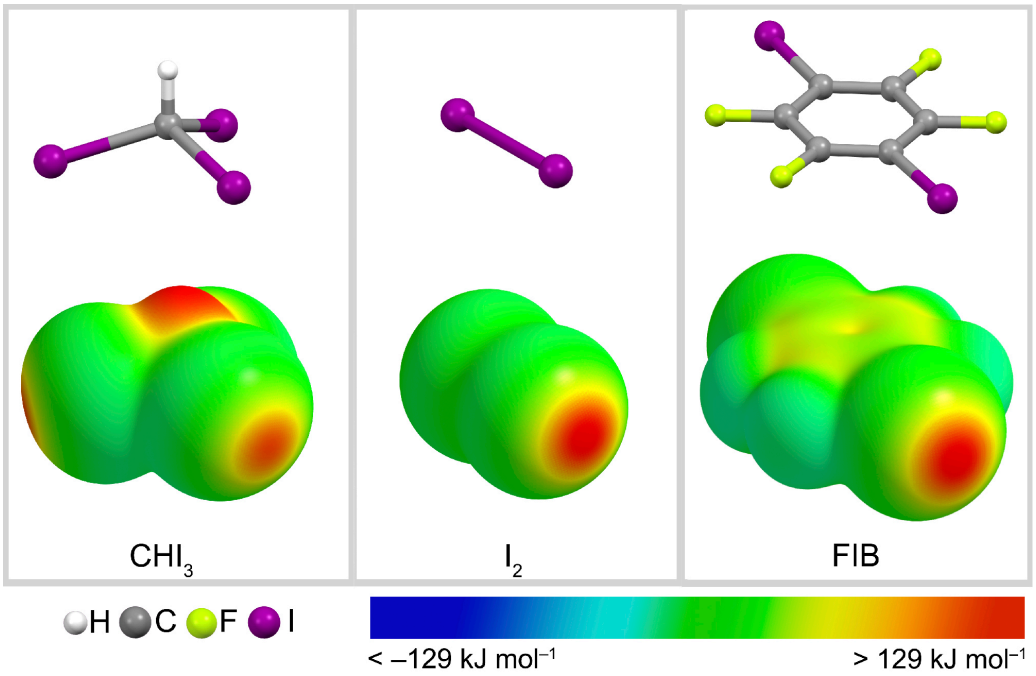

FIGURE 15 Electrostatic potential surface of CHI_3, I_2, and FIB calculated at the PBE0-D3/def2-TZVP level on the 0.001 au molecular surfaces.[I]

Four types of geometries were achieved with the halogen bonding applied. These include 0D, 1D, 2D, and 3D. Both 0D and 1D geometries were obtained for $[PtX_2COD] \cdot nI_2$ cocrystals (FIGURE 16). Geometries of the 0D network were found for $[PtBr_2COD] \cdot 0.5I_2$ and $[PtI_2COD] \cdot 0.5I_2$ isostructural cocrystals, which represent heterotrimeric clusters, i.e., clusters containing three subunits where one differs from the other two. The $[PtCl_2COD] \cdot I_2$ cocrystal represents a 1D network. ^{195}Pt NMR studies confirmed that in cocrystallizations with I_2 neither substitution of the halide in the $[PtX_2COD]$ complex nor Pt(II) oxidation happens. For $CDCl_3$ solutions of $[PtX_2COD] \cdot I_2$ samples, only one ^{195}Pt peak was found with no significant shift compared to the sample of $[PtX_2COD]$ in $CDCl_3$. This allowed us to build supramolecular systems that contained Pt(II) centers based on these cocrystals. Moreover, fine-tuning of the complex composition, such as changing the halide, gave the possibility to switch from an isolated cluster to a polymeric structure.

Measured geometrical parameters of the cocrystal confirms "classical" halogen bonding with the ∠(I–I···I) angles close to 180° (TABLE 3). The R_{IX}

parameter is higher for heterotrimers, which means a slightly stronger XB in the case of $[PtCl_2COD] \cdot I_2$ cocrystal.

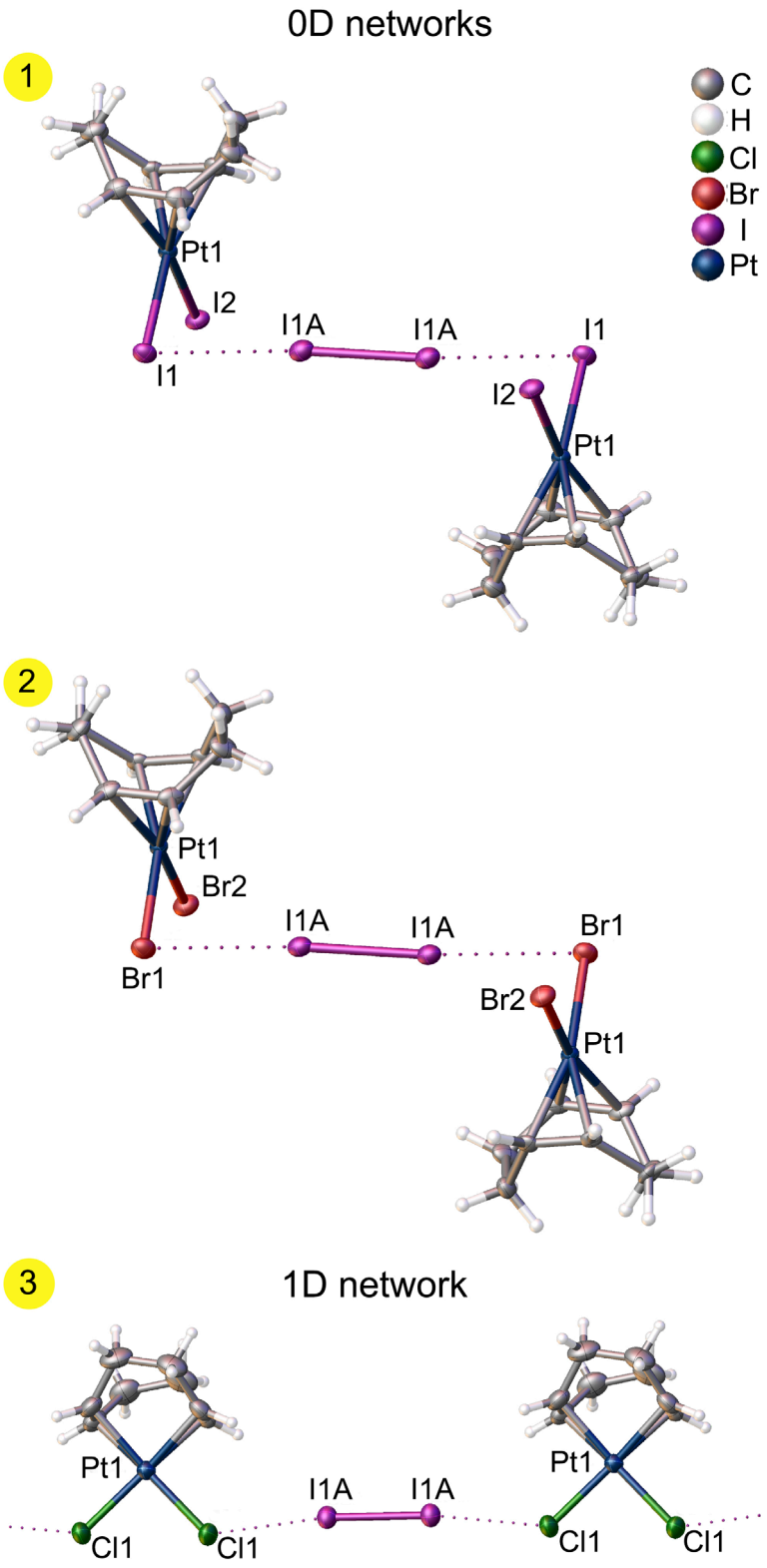

FIGURE 16 Halogen bonding in the 0D networks (heterotrimers) of $[PtI_2COD] \cdot 0.5I_2$ (1) and $[PtBr_2COD] \cdot 0.5I_2$ (2) along with the 1D network of $[PtCl_2COD] \cdot I_2$ (3).

TABLE 3 Characteristic parameters of the I–I···X–Pt (X = I, Br, Cl)) halogen bonds in the 0D networks of $[PtI_2COD] \cdot 0.5I_2$ and $[PtBr_2COD] \cdot 0.5I_2$ cocrystals along with the 1D network of $[PtCl_2COD]\ I_2$.

Cluster	d(I···X), Å	∠(I–I···X), °	∠(I···X–Pt), °	R_{IX}
$[PtI_2COD] \cdot 0.5I_2$	3.4107(5)	175.779(17)	86.130(11)	0.86
$[PtBr_2COD] \cdot 0.5I_2$	3.2850(7)	175.75(2)	87.276(19)	0.86
$[PtCl_2COD] \cdot I_2$	3.1465(14)	173.11(3)	127.01(6)	0.84

2D network geometries were found for $[PtI_2COD] \cdot CHI_3$ cocrystal. The first dimension is created by XB and the second by HB. In addition, a 2D network was found in *trans*-$[MI_2(CNXyl)_2] \cdot I_2$ cocrystals where the first dimension is created by XB and the second by π-stacking (FIGURE 17). Cocrystal of $[PtI_2COD] \cdot CHI_3$ represents the first known example of a transition metal iodide complex with CHI_3. However, the strength of XBs in CHI_3 cocrystal is the weakest of all the studied systems (TABLE 4) based on the R_{IX} parameter. The cocrystal was also the most unstable of all systems studied, most likely due to the light sensitivity of the iodoform itself.[89]

TABLE 4 Characteristic parameters of the Y–I···I–M (Y = CHI_2 or I and M = Pd or Pt) halogen bond in the 2D network of $[PtI_2COD] \cdot CHI_3$ and *trans*-$[MI_2(CNXyl)_2] \cdot I_2$ cocrystals.

Cluster	Y–I···I–M	d(I···I), Å	∠(I–I···I), °	∠(I···I–M), °	R_{IX}
$[PtI_2COD] \cdot CHI_3$	I_2HC–I1A···I1–Pt1	3.6359(5)	167.79(14)	124.032(14)	0.92
	I_2HC–I2A···I1–Pt1	3.6815(5)	172.83(14)	110.322(13)	0.93
	I_2HC–I3A···I1–Pt1	3.7723(5)	164.41(15)	92.385(11)	0.95
trans-$[PdI_2(CNXyl)_2] \cdot I_2$	I3–I4···I1–Pd1	3.4986(11)	173.07(3)	65.82(2)	0.88
	I4–I3···I2–Pd2	3.5034(11)	173.10(3)	65.74(2)	0.88
trans-$[PtI_2(CNXyl)_2] \cdot I_2$	I3–I4···I1–Pt1	3.5195(9)	172.13(3)	66.875(17)	0.89
	I4–I3···I2–Pt2	3.5206(9)	172.31(3)	66.751(17)	0.89

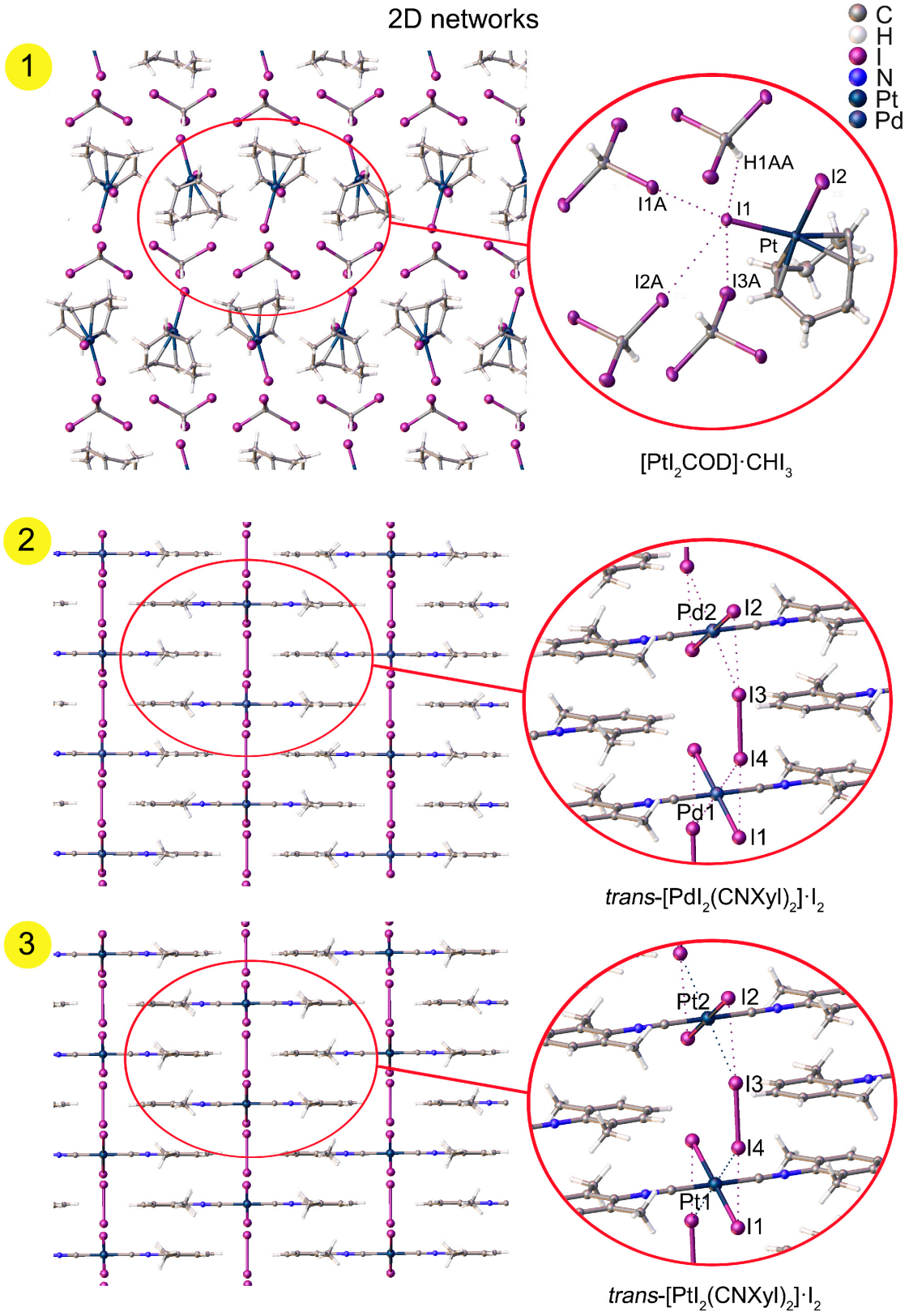

FIGURE 17 Halogen bonding in the 2D networks of $[PtI_2COD] \cdot CHI_3$ (1), *trans*-$[PdI_2(CNXyl)_2] \cdot I_2$ (2), and *trans*-$[PtI_2(CNXyl)_2] \cdot I_2$ (3) cocrystals.

An uncommon bifurcated I–I···(I–M) contact was found in *trans*-$[MI_2(CNXyl)_2] \cdot I_2$ (M = Pd or Pt) cocrystals that could be divided into two contacts as I···I and M···I. The relative strengths of the I···I interactions are fairly similar in both cocrystals according to R_{IX} parameter with 0.88 and 0.89 for Pd and Pt cocrystals, respectively (TABLE 4). The M···I contact strength estimated by the R_{IX} value is weaker than of the I···I contact in both cocrystals, which suggests I···I XB is the determining factor for the interaction between the complex and I_2 molecule.

3D geometries where 2 dimensions are created by XB and the third is added by π–stacking were obtained for $[PtX_2COD] \cdot n$FIB cocrystals (FIGURE 18). The $[PtI_2COD] \cdot 1.5$FIB cocrystal contains two nonequivalent Pt(II) complex units. In the first unit, complex of Pt(II) forms four XBs with four FIB molecules (orange circles in FIGURE 18.1); in the second, complex of Pt(II) forms two XBs with two FIB molecules (red circles in FIGURE 18.1). The $[PtBr_2COD] \cdot 2$FIB and $[PtCl_2COD] \cdot 2$FIB cocrystals have isomorphic structures (FIGURE 18.2 and 18.3) and in both structures the Pt(II) complex forms four XBs with four FIB molecules (red circles in FIGURE 18.2 and 18.3). The XB is averagely stronger in the isomorphic cocrystals than in $[PtI_2COD] \cdot 1.5$FIB according to the R_{IX} values (TABLE 5).

TABLE 5 Characteristic parameters of the C–I···X–Pt (X = I, Br or Cl) halogen bond in the 3D networks of $[PtI_2COD] \cdot 1.5$FIB, $[PtBr_2COD] \cdot 2$FIB and $[PtCl_2COD] \cdot 2$FIB cocrystals.

Cluster	C–I···X–Pt	d(I···X), Å	∠(C–I···X), °	∠(I···X–Pt), °	R_{IX}[a]
$[PtI_2COD] \cdot 1.5$FIB	C–I1A···I2–Pt1	3.7054(6)	175.71(18)	71.518(13)	0.94
	C–I3A···I1–Pt1	3.5928(5)	175.12(15)	106.504(17)	0.91
	C–I2A···I4–Pt2	3.7371(6)	177.50(18)	71.250(13)	0.94
	C–I4A···I3–Pt2	3.6081(5)	171.80(18)	78.371(13)	0.91
	C–I5A···I3–Pt2	3.5870(6)	177.21(16)	121.312(15)	0.91
	C–I6A···I4–Pt2	3.8068(5)	168.46(17)	93.962(12)	0.96
$[PtBr_2COD] \cdot 2$FIB	C–I1A···Br1–Pt1	3.4635(15)	176.5(3)	83.00(4)	0.90
	C–I2A···Br1–Pt1	3.3296(16)	171.1(3)	116.40(5)	0.87
$[PtCl_2COD] \cdot 2$FIB	C–I1A···Cl1–Pt1	3.396(2)	175.99(19)	83.06(6)	0.91
	C–I2A···Cl1–Pt1	3.214(2)	172.56(19)	119.55(8)	0.86

[a] $R_{IX} = d(I\cdots X)/(R^I_{vdW} + R^X_{vdW})$, where R_{IX} is distance reduction ratio, I is a donor atom, X is an acceptor atom, d(I···X) is the distance between I and X in Å; R^I_{vdW} and R^X_{vdW} are the vdW radii of I and X correspondingly determined by Bondi.[42]

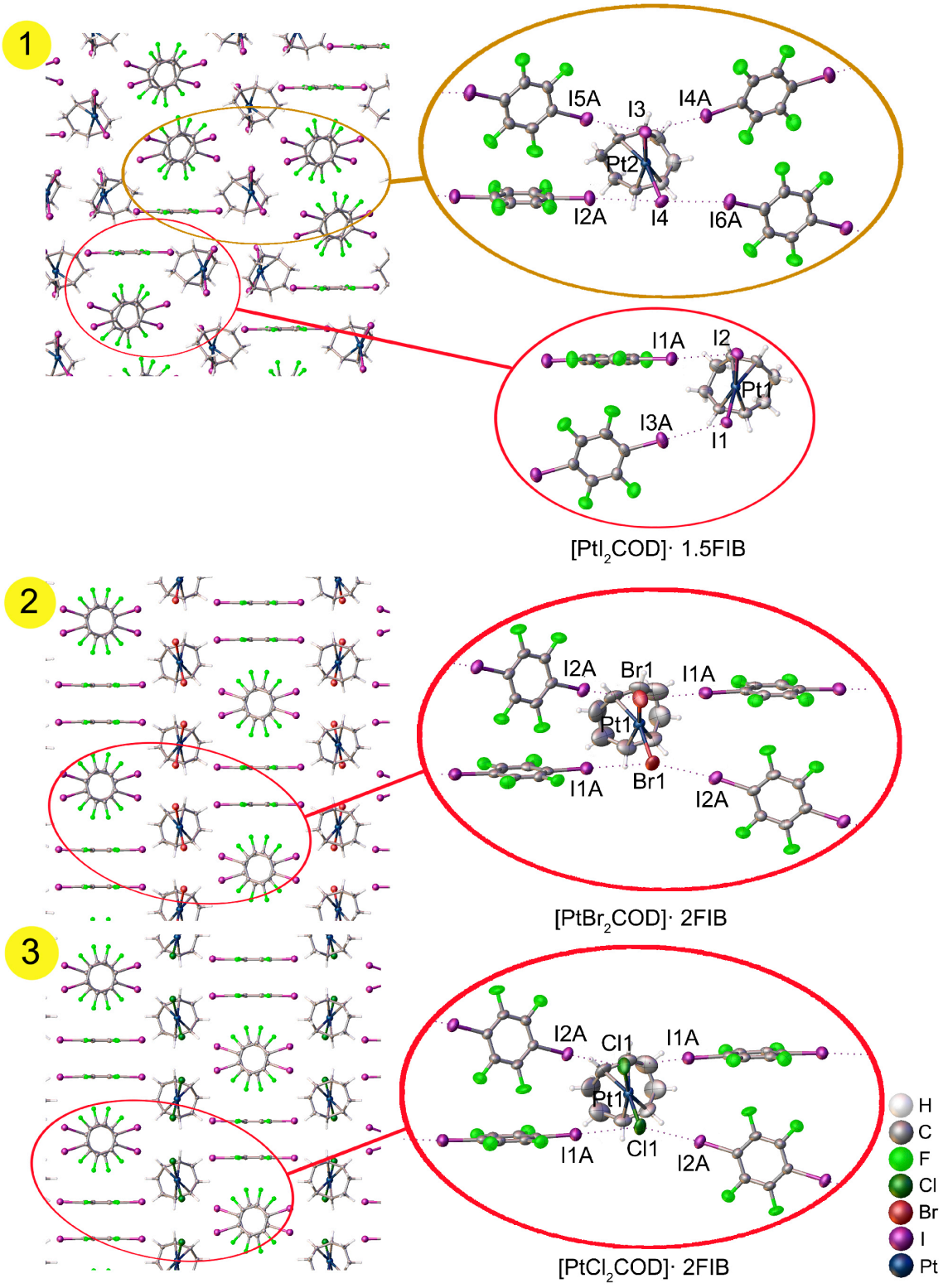

FIGURE 18 Halogen bonding in the 3D networks of $[PtI_2COD] \cdot 1.5FIB$ (with two independent $[PtI_2COD]$ units) (1), $[PtBr_2COD] \cdot 2FIB$ (2), and $[PtCl_2COD] \cdot 2FIB$ (3) cocrystals.

Among the CHI_3, I_2, and FIB cocrystals the average R_{IX} parameter indicates that strength of XB increases in the row CHI_3 ($\overline{\boldsymbol{R_{IX}}} = 0.93$), FIB ($\overline{\boldsymbol{R_{IX}}} = 0.91$), and I_2

($\overline{\boldsymbol{R_{IX}}}$ = 0.87). Comparing this trend with the $V_{s,max}$ values, both the highest R_{IX} and lowest $V_{s,max}$ values reflect the weakest XB of the systems studied, which was for CHI_3 molecule. However, FIB and I_2 systems had similar $V_{s,max}$ values but noticeably different R_{IX} values, which raised the question of the strength of the XB.

The NCI method allowed us to compare the relative strength of XBs in these systems and visualize the interaction patterns in real space. This demonstrated the directionality of the interaction. Comparison of the relative strengths of XB through the peak sign(λ_2)ρ values is presented in TABLE 6 in the order of strongest to weakest interaction. The strongest XBs were found for the I_2 cocrystals (FIGURE 19), the FIB cocrystals had medium XB strength (FIGURE 20.1-20.3), and in the CHI_3 cocrystal were the weakest XBs we considered (FIGURE 20.4). Interestingly, there was no correlation between the strength of the XB and the variation of the halide (I, Br, or Cl) or the metal center (Pt or Pd) in the discussed systems. The strongest XBs were found in the linear I_2 cocrystals (heterotrimers or 1D polymer). The presence of additional interactions, either M···I or HB or π–interactions, weakens the halogen bond in the case of 2D and 3D systems. The relative strength of XB is dependent on XBD and increases in the order of CHI_3 < FIB < I_2 according to the NCI analysis.

TABLE 6 Sign(λ_2)ρ data on noncovalent interactions in various halogen bonded clusters.

Cluster	Interaction	sign(λ_2)ρ
$([PtI_2COD])_2 \cdot I_2$	I1A···I1–Pt1	–0.0198[a]
$([PtCl_2COD])_2 \cdot I_2$	I1A···Cl1–Pt1	–0.0198[a]
$([PtBr_2COD])_2 \cdot I_2$	I1A···Br1–Pt1	–0.0191[a]
(*trans*-$PdI_2(CNXyl)_2])_4 \cdot I_2$	I4···I1–Pd1 & I3···I2–Pd1	–0.0167[b]
(*trans*-$[PtI_2(CNXyl)_2])_4 \cdot I_2$	I4···I1–Pt1 & I3···I2–Pt1	–0.0164[b]
$[PtCl_2COD] \cdot (FIB)_{10}$	I2A···Cl1–Pt1	–0.0163[a]
	I1A···Cl1–Pt1	–0.0118[a]
$[PtBr_2COD] \cdot (FIB)_{10}$	I2A···Br1–Pt1	–0.0161[a]
	I1A···Br1–Pt1	–0.0129[a]
$([PtI_2COD])_2 \cdot (FIB)_{10}$	I1A···I2–Pt1	–0.0138[a]
	I3A···I1–Pt1	–0.0113[a]
	I5A···I3–Pt2 &	–0.0131[a]
	I4A···I3–Pt2	–0.0131[a]
	I2A···I4–Pt2	–0.0104[a]
	I6A···I4–Pt2	–0.0094[a]
$[PtI_2COD] \cdot (CHI_3)_4$	I1A···I1–Pt1 & I2A···I1–Pt1	–0.0123[a]
		–0.0123[a]
	I3A···I1–Pt1	–0.0102[a]
	H1AA···I1–Pt1	–0.0097[a]

[a]Peak sign(λ_2)ρ values of NCIs calculated for the single point structures at the PBE0-D3/def2-TZVP level. [b]Peak sign(λ_2)ρ values of NCIs calculated for the single point structures at the M06L/def2TZVP/def2TZV level.

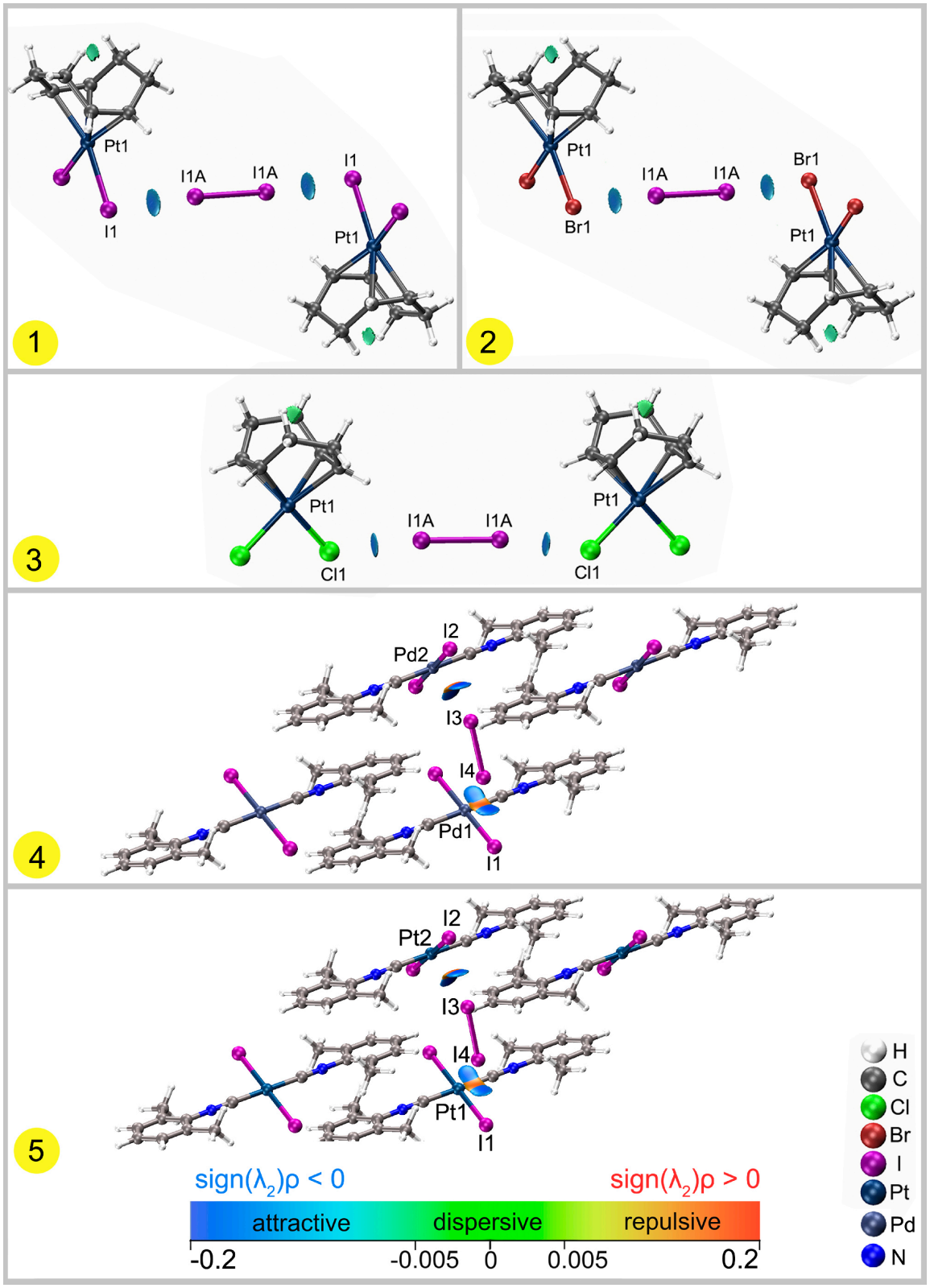

FIGURE 19 Isosurfaces representing the strongest halogen bonding in the clusters of 1) $([PtI_2COD])_2 \cdot I_2$, 2) $([PtBr_2COD])_2 \cdot I_2$, 3) $([PtCl_2COD])_2 \cdot I_2$, 4) (*trans*-$PdI_2(CNXyl)_2])_4 \cdot I_2$, and 5) (*trans*-$[PtI_2(CNXyl)_2])_4 \cdot I_2$.

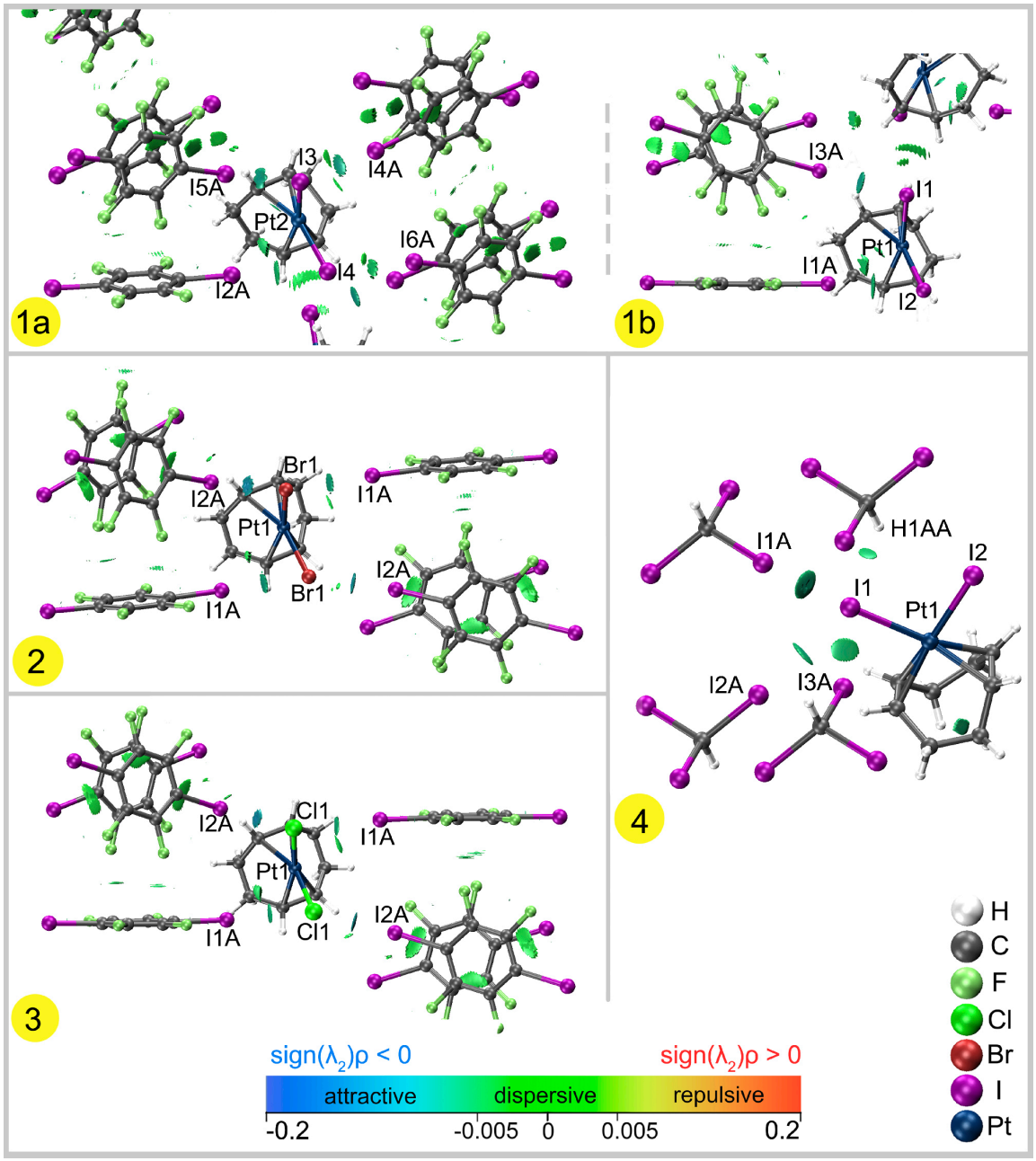

FIGURE 20 Isosurfaces representing the moderate to weakest halogen bonding in 1) clusters of $([PtI_2COD])_2 \cdot (FIB)_{10}$ with two independent $[PtI_2COD]$ units (a and b), 2) $[PtBr_2COD] \cdot (FIB)_{10}$, 3) $[PtCl_2COD] \cdot (FIB)_{10}$, and 4) $[PtI_2COD] \cdot (CHI_3)_4$.

To conclude, XB was successfully used to create various supramolecular systems as presented in publications I and II. It is possible to modify the strength of interaction and size of a cluster by varying XBD. Changing the halide in the complex allowed us to synthesize systems of various geometries.

Isostructural cocrystals were obtained in publications I and II. In publication I, this was achieved by varying the Pt(II) complex halide and in publication II by varying the metal center of the complex. In the series of $[PtX_2COD] \cdot nXBD$ cocrystals, one pair of isomorphs was formed. They were $[PtBr_2COD]/[PtI_2COD]$ cocrystals with I_2 and $[PtCl_2COD]/[PtBr_2COD]$

cocrystals with FIB. The [$PtBr_2COD$] cocrystals were always an isomorphic pair, which demonstrates the intermediate nature of Br in the Cl–Br–I row.

An essential role of XB in crystal engineering of the systems under study was justified through SCXRD and computational studies. The halogen bonds allow building novel self-assembled polymers as the strongest noncovalent stabilizing interaction with the possibility of fine-tuning.

3.3.2 The role of metal-involved NCIs in the stabilization of metallopolymers[I–III]

During SCXRD and NCI method structural analysis metal-involving I···M contacts were found in addition to halogen bonding in [PtX_2COD] · nFIB and *trans*-[$MI_2(CNXyl)_2$] · I_2 (M = Pd or Pt) cocrystals (FIGURE 21). The strongest interactions based on R_{IX} and sign(λ_2)ρ values were found in *trans*-[$MI_2(CNXyl)_2$]$_4$ ·I_2 (TABLE 7). The R_{IX} values were 0.94 for I···Pd and 0.93 for I···Pt and the sign(λ_2)ρ values were –0.0159 for I···Pd and –0.0160 for I···Pt. In addition, there is only a small difference in these values between I···M and I···I interactions (TABLE 4 and TABLE 6). Therefore, the I···M interaction can be interpreted as fairly strong. The I···Pt interactions of the [PtX_2COD] · nFIB cocrystals are at the border of existence based on the R_{IX} values (R_{IX} > 1) and much weaker than the I···I XB in the same cocrystal based on the sign(λ_2)ρ values (TABLE 6 and TABLE 7). The I···Pt interactions with the lowest R_{IX} and sign(λ_2)ρ values were selected for further studies and these include C1A–I1A···Pt1 and C4A–I2A···Pt2.

The I···M interactions were further studied with the ELF, QTAIM, and ED/ESP minima analyses to estimate the impact and donor-acceptor nature of the I···M contact on the structural stabilization in the cocrystal.

TABLE 7 Characteristic sign(λ_2)ρ and geometric parameters of the metal-involved X–I···M–I (X = C or I; M = Pd or Pt) interactions in of cocrystals of the 0–3D networks.

Cluster	X–I···M–I	d(I···M), Å	∠(X–I···M), °	R_{IX}[a]	sign(λ_2)ρ
([PtI_2COD])$_2$ ·(FIB)$_{10}$	C1A–I1A···Pt1	3.7990(6)	142.14(18)	1.02	–0.0089[a]
	C4A–I2A···Pt2	3.8127(4)	141.13(17)	1.02	–0.0087[a]
	C10A–I4A···Pt2	4.0089(5)	148.38(18)	1.07	–0.0066[a]
[$PtBr_2COD$] ·(FIB)$_{10}$	C2A–I1A···Pt1	3.9821(8)	143.8(3)	1.06	–0.0065[a]
[$PtCl_2COD$] ·(FIB)$_{10}$	C3A–I1A···Pt1	3.8732(6)	143.02(18)	1.03	–0.0075[a]
(*trans*-[$PdI_2(CNXyl)_2$])$_4$ ·I_2	I3–I4···Pd1	3.4038(8)	128.58(3)	0.94	–0.0159[b]
	I4–I3···Pd2	3.4038(8)	128.64(3)	0.94	–0.0159[b]
(*trans*-[$PtI_2(CNXyl)_2$])$_4$ ·I_2	I3–I4···Pt1	3.4648(6)	128.10(3)	0.93	–0.0160[b]
	I4–I3···Pt2	3.4601(6)	128.27(3)	0.93	–0.0160[b]

[a]Peak sign(λ_2)ρ values of NCIs calculated for the single point structures at the PBE0-D3/def2-TZVP level.

[b]Peak sign(λ_2)ρ values of NCIs calculated for the single point structures at the M06L/def2TZVP/def2TZV level.

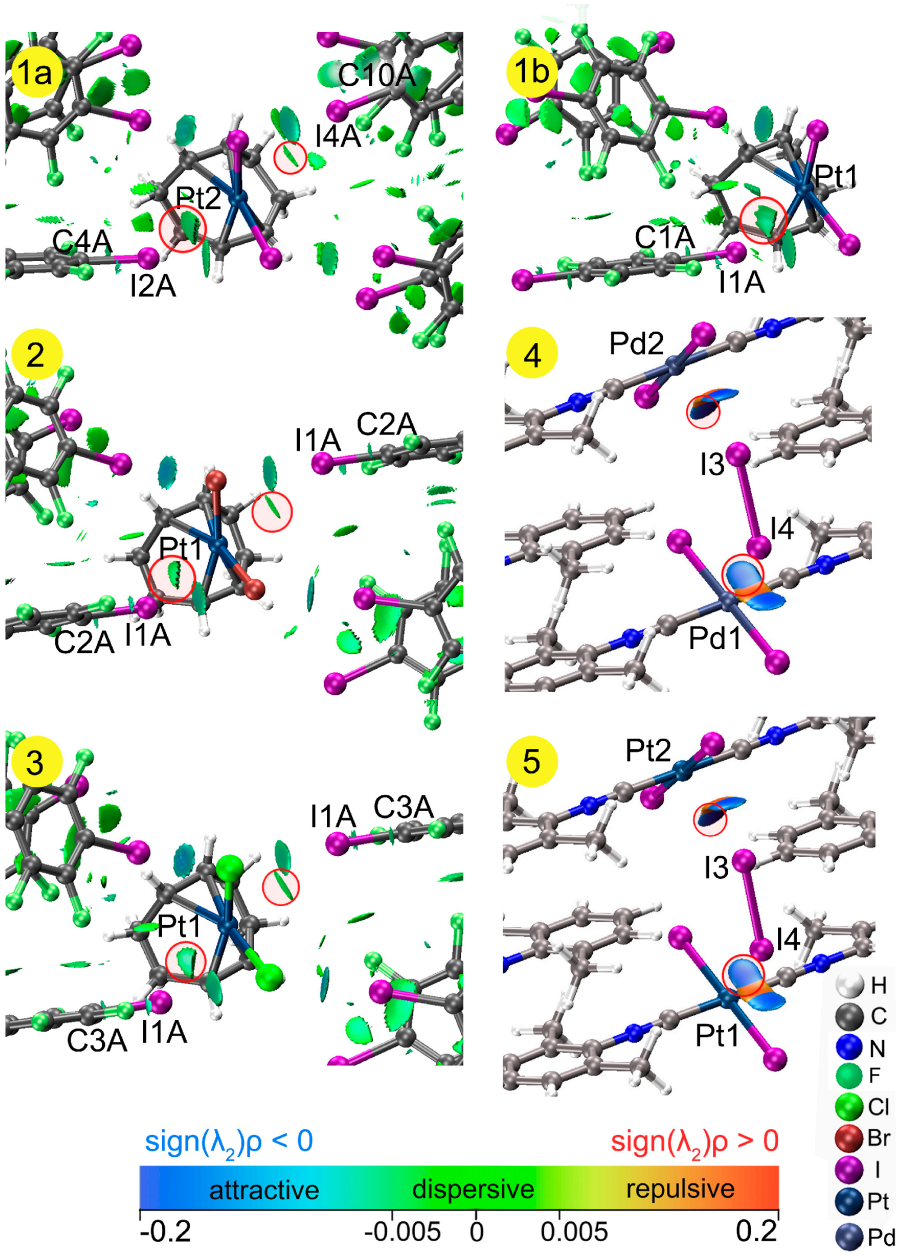

FIGURE 21 Isosurfaces representing the metal-involving interactions (red circles) in the clusters of 1) $([PtI_2COD])_2 \cdot (FIB)_{10}$ with two independent $[PtI_2COD]$ units (a and b), 2) $[PtBr_2COD] \cdot (FIB)_{10}$, 3) $[PtCl_2COD] \cdot (FIB)_{10}$, 4) (*trans*-$[PdI_2(CNXyl)_2])_4 \cdot I_2$, and 5) (*trans*-$[PtI_2(CNXyl)_2])_4 \cdot I_2$.

Combined ELF and QTAIM analyses confirmed the existence of I···M interactions in the *trans*-$[MI_2(CNXyl)_2]_4 \cdot I_2$ clusters for the I3–I4···M1 and I4–I3···M2 contacts (FIGURE 22.1 and 22.2) and the $([PtI_2COD])_2 \cdot (FIB)_{10}$ cluster for C1A–I1A···Pt1 and C4A–I2A···Pt2 contacts (FIGURE 22.3 and 22.4). Appropriate (3, -1) BCPs and bond paths connecting the I and M centers were found for these contacts. The filled d_{z^2} orbitals were identified by the increasing ELF areas around the Pd and Pt atoms above and below the bond paths connecting metal centers and iodide ligands (cyan color in FIGURE 22). The I···M bond paths pass exactly through the d_{z^2} orbitals.

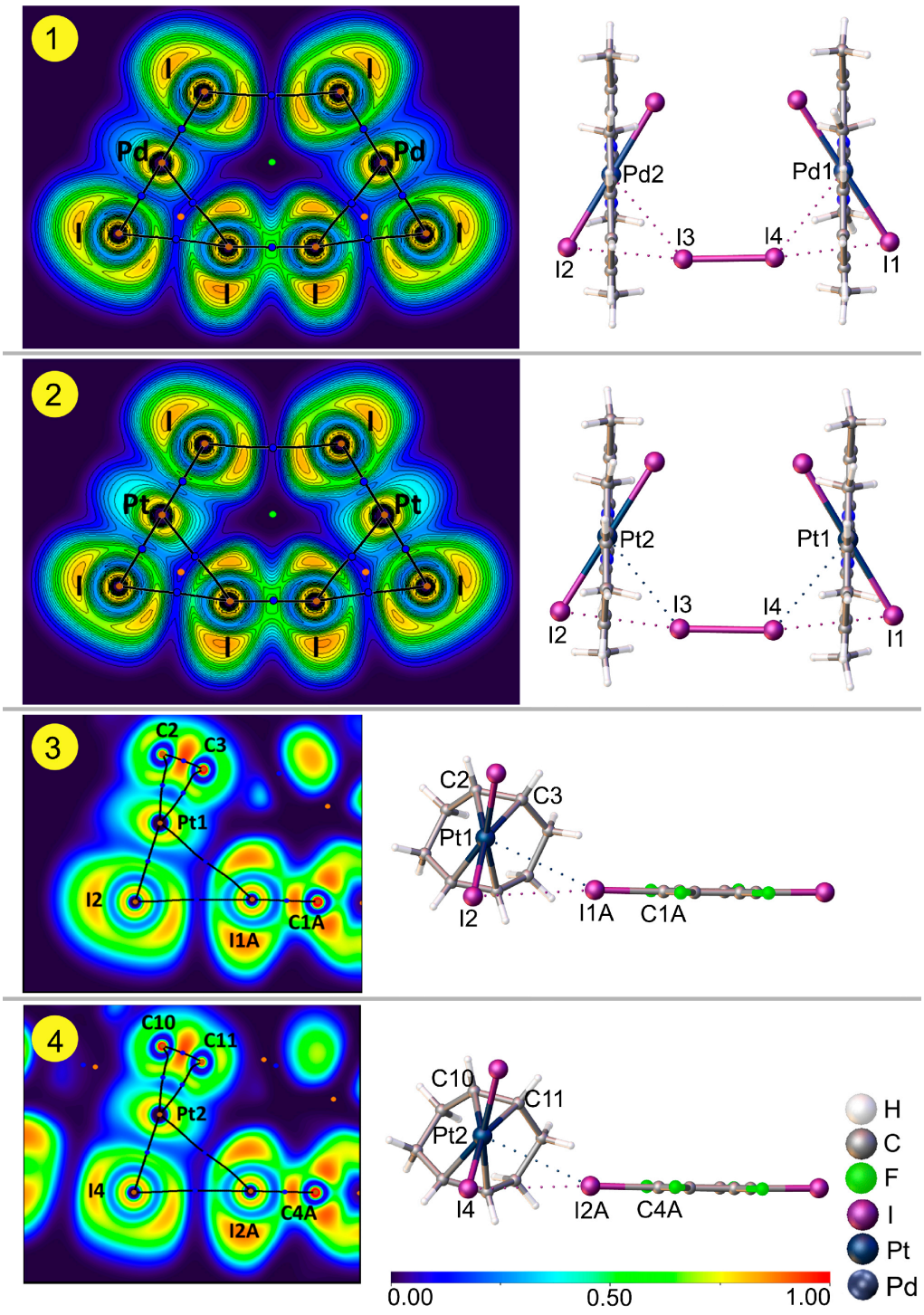

FIGURE 22 The ELF projection and QTAIM bond paths (black lines), BCPs (blue dots), nuclear critical points (brown dots), cage critical points (green dots), and ring critical points (orange dots) for the X–I···I and X–I···M interactions (X = I or Cl; M = Pd or Pt) in the clusters of 1) (*trans*-$[PdI_2(CNXyl)_2]$)$_4 \cdot I_2$, 2) (*trans*-$[PtI_2(CNXyl)_2]$)$_4 \cdot I_2$, and 3–4) two independent $[PtI_2COD]$ units of the $([PtI_2COD])_2 \cdot (FIB)_{10}$ cluster.

Relatively low concentrations of electron pairs in the d_z^2 orbitals areas outside the I–M–I plane in the *trans*-[$MI_2(CNXyl)_2$] · I_2 cocrystals may indicate the weak nucleophilic nature of the metal centers (FIGURE 22). On the other hand, I···M bond paths go through the areas of intermediate electron pair concentration of the iodine atoms in I_2. Thus, the I···M interaction may be weakly polar or nonpolar.

Bond paths connecting noncovalently interacting I and Pt centers in the ([PtI_2COD])$_2$ ·(FIB)$_{10}$ cluster pass between maximum and minimum ELF areas on the I atoms. This makes the philicity of the interacting centers unclear, especially as Pt(II) centers can act as electrophiles[34,90] and nucleophiles.[27,40,91]

Analysis of the order of the ED and ESP minima along the bond path is a way to describe the philicity of interacting atoms in NCIs.[67–69,71–74] In this method, the nucleophilic atom is the one where the minimum ESP is shifted towards it. Alternatively, the electrophilic atom is the one the ED minimum is shifted towards it. The ESP minima is slightly shifted to the Pt ED basins in both ([PtI_2COD])$_2$ · (FIB)$_{10}$ and (*trans*-[$PtI_2(CNXyl)_2$])$_4$ · I_2. This indicates the weak nucleophilic nature of the Pt atoms (FIGURE 24.1 and 24.2). In both cases, the I···Pt interaction can be considered as metal-involved halogen bonding.

The minima of the ED and ESP functions are overlapped in the (*trans*-[$PdI_2(CNXyl)_2$])$_4$ · I_2 cluster (FIGURE 24.3). This indicates the nonpolar nature of the I···Pd interaction with unclear nucleophilic/electrophilic roles. Analogous intermediate interaction between semi-coordination and metal-involving halogen bonding have been described for a Ni(II) complex.[34]

Such nonpolar noncovalent interactions involving metal atoms resembling metallophilic Pd···Pd and Pt···Pt interactions in related palladium and platinum chloride isocyanide complexes have been discussed.[38,92–94] We decided to perform ELF and ED/ESP minima analysis for two systems with confirmed metallophilic nature to compare the similarity of such contacts, namely COYBOI01 and CPICPT12.[93] Two model clusters, (*cis*-[$PdCl_2(CNPh)_2$])$_2$ and (*cis*-[$PtCl_2(CNPh)_2$])$_2$ were created based on the SCXRD data. Combined ELF and QTAIM analysis of the model clusters indicated the existence of nonpolar metallophilic interactions of Pd···Pd and Pt···Pt with an appropriate (3,-1) BCP and a bond path connecting the interacting metals along with a symmetric distribution of lone pairs (FIGURE 23).

Further 1D profiles of the ED and ESP functions along the M···M bond paths in (*cis*-[$MCl_2(CNPh)_2$])$_2$ (M = Pd or Pt) clusters were analyzed. Overlapped ED and ESP functions were observed for the M···M interactions in the clusters of (*cis*-[$PdCl_2(CNPh)_2$])$_2$ and (*cis*-[$PtCl_2(CNPh)_2$])$_2$ analogous to the I···Pd interaction in the (*trans*-[$PdI_2(CNXyl)_2$])$_4$ · I_2 (FIGURE 24.4a and 24.4b, respectively). Additionally, QTAIM analysis revealed that the electron density and Laplacian values of ED in the I···Pd BCPs in (*trans*-[$PdI_2(CNXyl)_2$])$_4$ · I_2 cluster (0.016/0.037–0.038 a.u.) are similar to Pd···Pd (0.012/0.030 a.u.) and Pt···Pt (0.016/0.038 a.u.) BCPs in the (*cis*-[$MCl_2(CNPh)_2$])$_2$ cluster. Both have nonpolarity and similar strength I···Pd contacts to metallophilic interactions and can be considered as a *quasimetallophilic* interactions.

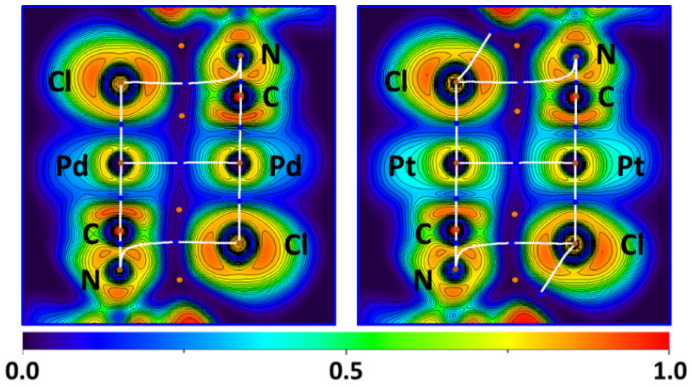

FIGURE 23 The ELF projection and QTAIM bond paths (white lines), BCPs (blue dots), nuclear critical points (brown dots), cage critical points (green dots), and ring critical points (orange dots) for the M···M interactions in (*cis*-$[PdCl_2(CNPh)_2]$)$_2$ (left) and (*cis*-$[PtCl_2(CNPh)_2]$)$_2$ (right) model clusters.

Another example of metal-involving NCIs was found for the system of an inorganic compound (KI) in the environment of organic compound (N-heterocyclic ligand L). In this hybrid material, the cubic motif of potassium iodide remained the same within a coordination polymer of 1D potassium iodide wire wrapped by the organic ligand (FIGURE 25).

Although there are examples of hybrid materials containing KI units in the literature, but in all of the known examples original motif of KI is quite distorted. The one with the least distortion was achieved by limiting the growth of KI in a single-walled carbon nanotube.[83] However, using this growth limitation method disables the opportunities to further modify the structure with chemical modifiers. Previously, chemical modifiers were only allowing to synthesize finite units of KI within hybrid material or infinite units with noticeable distortion from the original cubic KI structure.[84–86,95–97]

To the best of our knowledge, the $[K_4I_4L_4]_n$ synthesized in our group was the first hybrid material containing a 1D-chain of KI with a geometry of the K_4I_4 core closely resembling that of pure KI salt (TABLE 8) with only minor distortion. The K-I-K and I-K-I angles between the neighboring cubes in the polymer are 170.41(2)°, while in pure KI, the corresponding angles are 180°. The distortion is most likely due to the flexibility of the ligand. Interestingly, the ligand bite angle may be crucial for the interaction as a similar ligand, 1,1′-bis(pyridin-3-ylmethyl)-2,2-biimidazole, did not produce a polymeric structure. A strong interaction between KI and the ligand leads to a sum of the vdW bond distances (1.55 + 2.75 = 4.3 Å) much shorter than the of the N–K interaction (2.815(2) and 2.906(2) Å).

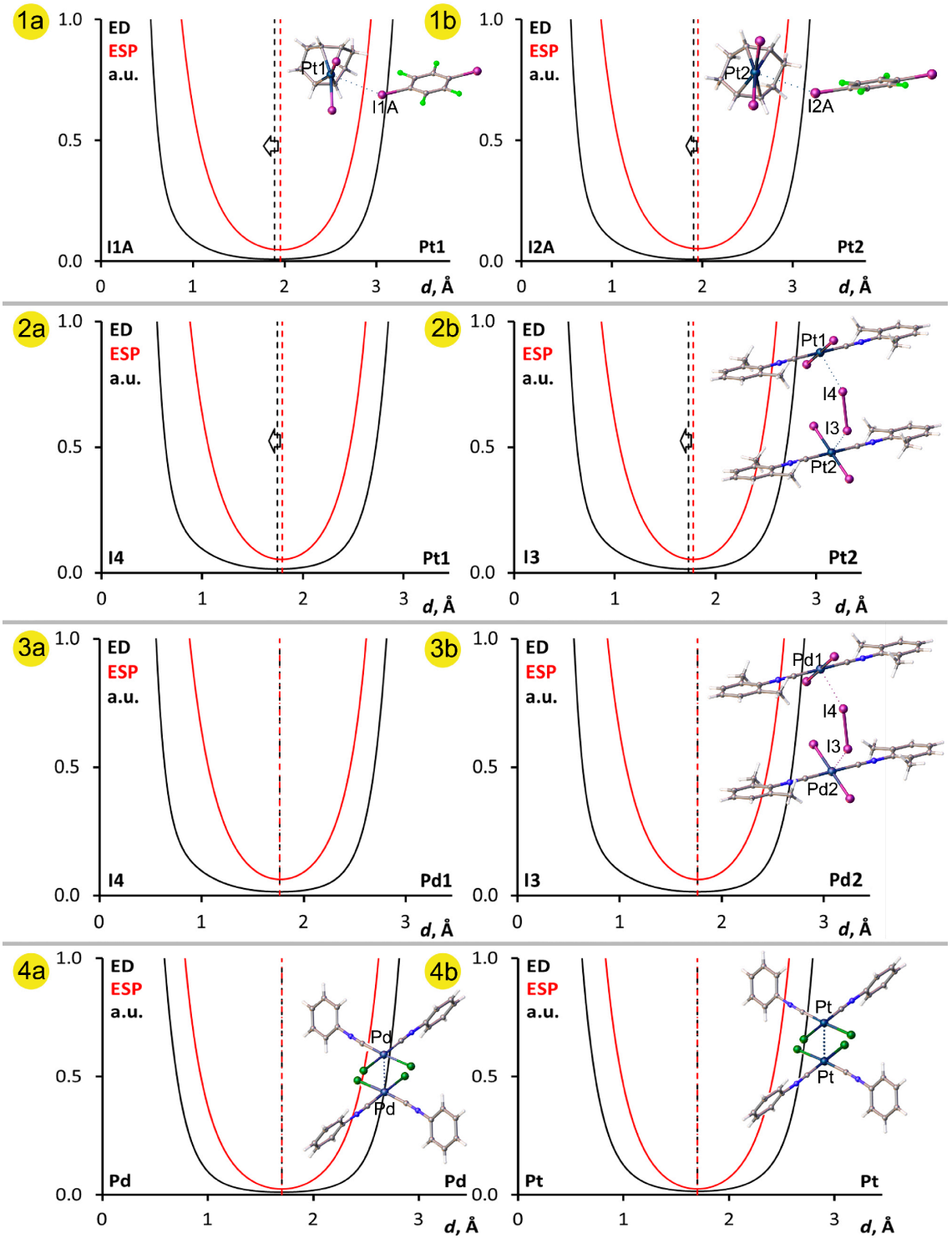

FIGURE 24 1D profiles of the ED (black) and ESP (red) functions along the I···M bond paths in the two independent $[PtI_2COD]$ units of $([PtI_2COD])_2 \cdot (FIB)_{10}$ cluster (1a and 1b), (*trans*-$[PtI_2(CNXyl)_2])_4 \cdot I_2$ (2a and 2b), (*trans*-$[PdI_2(CNXyl)_2])_4 \cdot I_2$ (3a and 3b), and along the M···M bond paths in (*cis*-$[PdCl_2(CNPh)_2])_2$ (4a) and in (*cis*-$[PtCl_2(CNPh)_2])_2$ (4b).

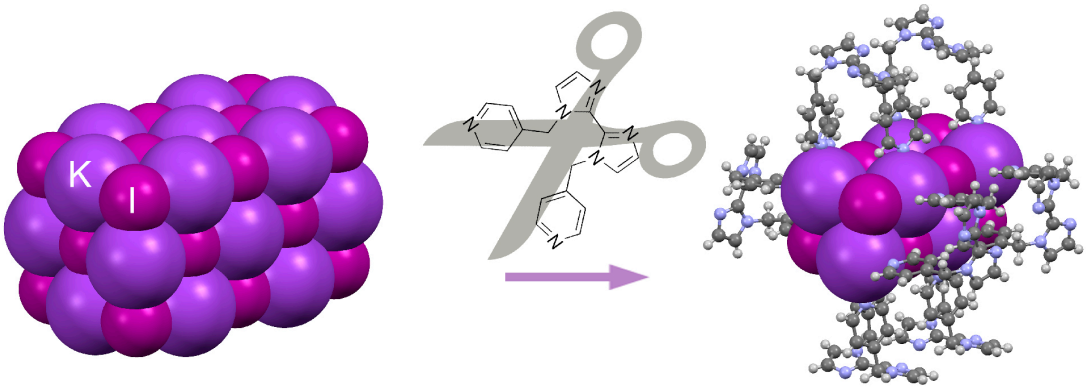

FIGURE 25 Noncovalent scissors: a unique 1D-polymer of KI cut out from 3D KI salt by 1,1′-bis(pyridin-4-ylmethyl)-2,2′-biimidazole ligand (L).

TABLE 8 Comparison of the bond lengths and angles in the 1D-polymer of KI ($[K_4I_4L_4]_n$) and pure KI ($[KI]_n$).

Compound	Distances		Angles	
	d(X–Y)	Å	Angle	°
$[K_4I_4L_4]_n$	K1–I1 = K3–I3	3.5037(5)	∠K-I-K	86.336(13) – 89.198(11)
	K2–I2 = K4–I4 = K1–I3 = K3–I1	3.5674(5)		
	K4–I2 = K2–I4	3.5037(5)	∠I-K-I	90.397(10) – 96.490(13)
	K1–I2 = K2–I1 = K3–I4 = K4–I3	3.4759(4)		
$[KI]_n$	K1–I1	3.5246(4)	∠K-I-K	90

Additional confirmation of the interaction of potassium ions with nitrogen atoms of the ligand in the bulk material was studied by ^{15}N CPMAS (CP = cross polarization, MAS = magic angle spinning) NMR spectroscopy. The solid-state ^{15}N NMR spectrum of a pure ligand was compared to that of the 1D-polymer. Two magnetically nonequivalent nitrogen nuclei corresponding to the pyridine (δ = 251.82 ppm) and biimidazole (δ = 200.09 ppm) nitrogen atoms were detected in the ligand spectrum. However, only one magnetically nonequivalent nitrogen nuclei (δ = 199.09 ppm) peak was observed in the KI polymer, which was assigned to biimidazole nitrogen atoms that are not involved in complexation. The disappearance of pyridine ^{15}N chemical shifts can be caused by quenching of the ^{15}N pyridine signal from coordination of the pyridine nitrogen atoms to KI.

Coordination to KI influences the physical properties of the ligand, e.g., luminescence. The ligand in a pure form is luminescent in the solid-state with two emission maxima at 340 nm and 430 nm with excitations at 315 and 350 nm, respectively. Comparison of the spectra of the pure ligand and the 1D-polymer revealed quenching of the luminescence in the polymer. This is likely due to quenching of the excited states by the heavy K and I atoms.

It is worth mentioning that in liquid state studies, ^{1}H, ^{13}C, and 2D PFG $^{1}H,^{15}N$ HMBC NMR spectra and luminescence, no coordination of the ligand to

KI was detected in a MeOH solution and no signal intensity change compared to the pure ligand was detected.

The nature of the interaction between KI and supporting ligands was analyzed by QTAIM via comparisons of $[K_4I_4]_n$, $[K_4I_4]_n[K_2I_2]_{4n}$, and $[K_4I_4L_4]_n$ model clusters with n = 2 (FIGURE 26), as well as a single KI molecule (TABLE 9). The nature of K···I and I···I interactions is quite similar within the model clusters. It is clearly electrostatic as the potential energy density/kinetic energy density ratio is less than 1 and only minimal electron sharing is involved in the interaction according to the small δ(A,B) delocalization index value. There is no clear influence of the ligand on K···I and I···I interactions in the cluster representing ligand-supported 1D-chain of KI ($[K_4I_4L_4]_2$). However, the K···N interaction (13–16 kJmol^{-1}) is the strongest in the system according to interaction energy values. This raises the question of what makes ligand coordination favorable for this structure.

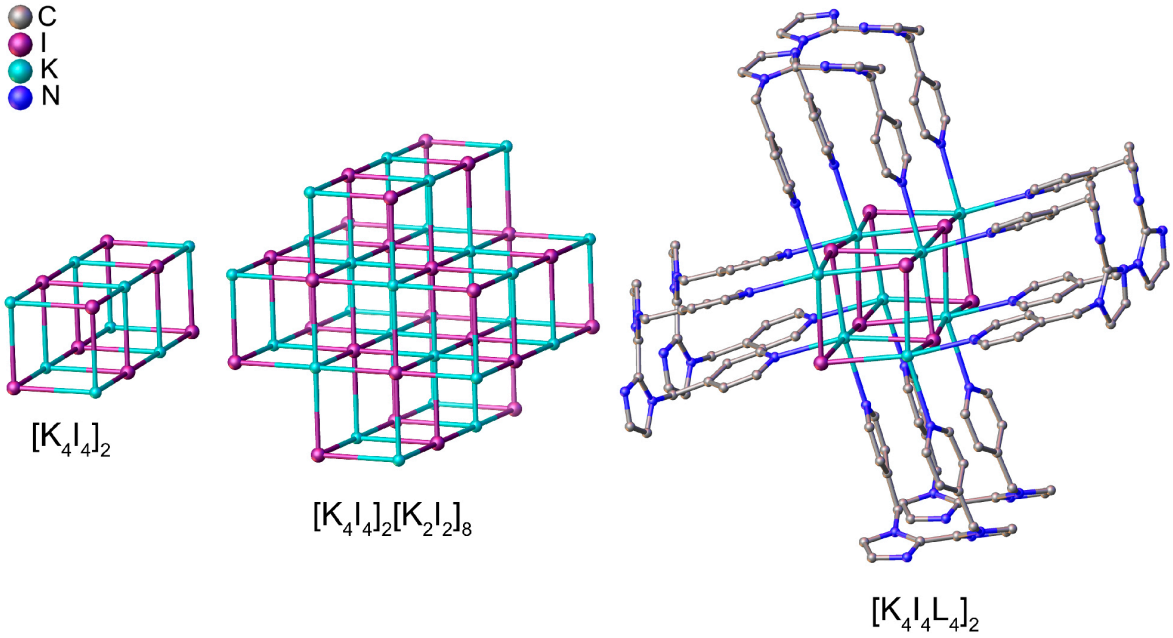

FIGURE 26 Visualization of $[K_4I_4]_2$, $[K_4I_4]_2[K_2I_2]_8$, and $[K_4I_4L_4]_2$ model clusters. Hydrogens of L are omitted for clarity.

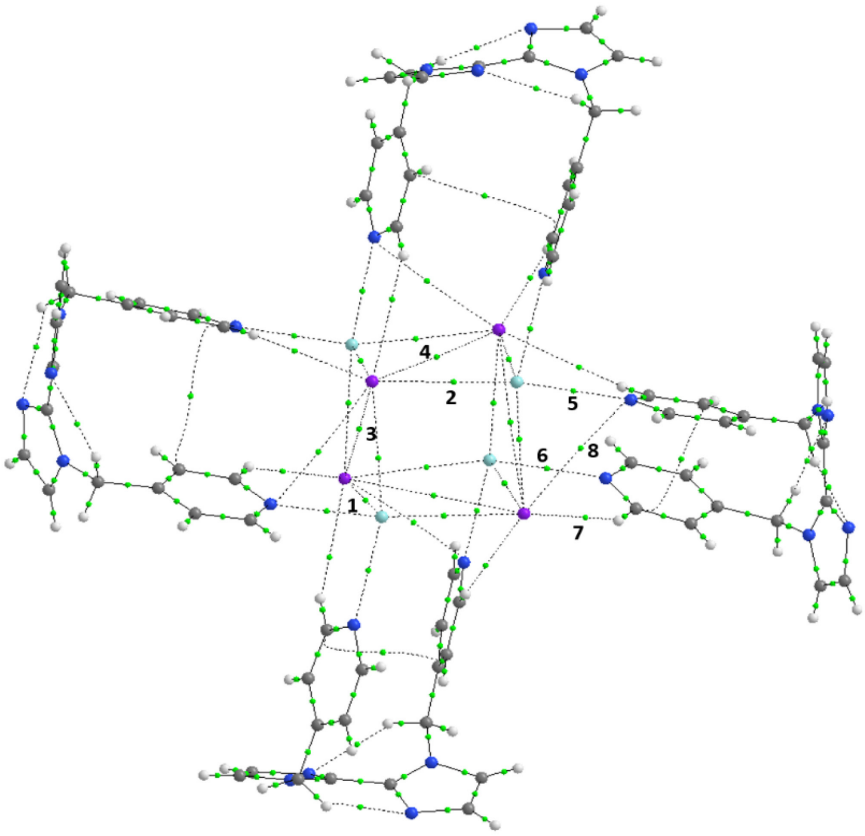

FIGURE 27 $[K_4I_4L_4]$ cluster model including bond paths (lines) and BCPs (green dots). The numbering of the selected BCPs is identical to TABLE 9.

Additional QTAIM studies were performed to understand the effect of the ligand coordination on structural stabilization. Model clusters comprising 1, 2, and 3 units of potassium iodide salt $[K_4I_4]_n[K_2I_2]_{4n}$ and ligand-supported 1D-polymers $[K_4I_4L_4]_n$ were compared. It was shown that a one-dimensional extension of the $[K_4I_4L_4]_n$ chain is energetically more favorable than extension of the $[K_4I_4]_n[K_2I_2]_{4n}$ chain representing pure KI. This indicates the stabilizing role of the ligand (TABLE 10).

To summarize, metal-involved interactions can influence the growth of the crystal. It is important to consider the geometrical parameters of linker molecules as they may have a strong effect on structural self-assembly. For example, the bite angle of the modifier ligand fits the geometry of KI salt better to yield a ligand-supported 1D-KI polymer.

TABLE 9 The QTAIM analysis of the electron density (ρ / $eÅ^{-3}$), the ratio of potential energy density and kinetic energy density (|V|/G), delocalization index between A and B (bonding) atoms (δ (A,B)), and interaction energy between two interacting atoms (E_{INT}) at the selected BCP of the $[K_4I_4]_2$, $[K_4I_4]_2[K_2I_2]_8$, $[K_4I_4L_4]_2$ model clusters, and the single KI molecule. The numbering of the BCPs can be found in FIGURE 27.

BCP#	Type	ρ / $eÅ^{-3}$	|V|/G	δ (A,B)	E_{INT} / $kJmol^{-1}$
			$[K_4I_4]_2$		
1	K···I	0.063	0.81	0.11	-6.8
2	K···I	0.064	0.82	0.10	-7.0
3	I···I	0.018	0.74	0.04	-1.0
4	I···I	0.018	0.73	0.04	-1.0
			$[K_4I_4]_2[K_2I_2]_8$		
1	K···I	0.063	0.82		-6.9
2	K···I	0.062	0.81		-6.7
3	I···I	0.016	0.70		-0.9
4	I···I	0.016	0.70		-0.9
			$[K_4I_4L_4]_2$		
1	K···I	0.070	0.84	0.11	-7.8
2	K···I	0.066	0.84	0.10	-7.4
3	I···I	0.018	0.73	0.03	-1.0
4	I···I	0.018	0.73	0.03	-1.0
5	K···N	0.113	0.85		-16.4
6	K···N	0.095	0.85		-13.2
7	H···I	0.033	0.77		-4.5
8	N···I	0.033	0.85		-3.0
			KI		
1	K···I	0.150	0.98	0.31	-21.7

TABLE 10 Stabilization energies (E^{stab}) in $kJmol^{-1}$ for the ligand supported models of $[K_4I_4]_n[K_2I_2]_{4n}$ and the chain-like models of $[K_4I_4]_n$ depending on the number of units n. The values are referenced to the smallest unit of n = 1.

n	E^{stab} $[K_4I_4]_n[K_2I_2]_{4n}$, $kJmol^{-1}$	E^{stab} $[K_4I_4L_4]_n$, $kJmol^{-1}$	ΔE^{stab} ,$kJmol^{-1}$
1	0	0	0
2	-131	-143	12
3	-265	-293	28

3.3.3 Cooperative effect of various NCIs[I–III]

Similar to other studies, our structural investigations were focused on the application of a certain NCI (either XB or metal-involved interaction). However, it is always a combination of NCIs influencing the structural organization and even the weakest interactions matter. In the aforementioned research, $[PtX_2COD]$ and *trans*-$[MI_2(CNXyl)_2]$ cocrystals along with ligand-supported 1D-polymer of KI, cooperative effects of multiple interactions influenced the structural organization. Metal-involved interactions, hydrogen bonding, and π–interactions directed the final geometry of the cocrystal in addition to the strongest interaction in the system (XB or K···N).

The issue with these cooperative effects is the difficulty in predicting all possible interactions within the system. However, the more that is known about the possible NCIs, the easier it is to predict the product's final geometry. This includes donor/acceptor pairs, directionality, and possible interaction sites. Therefore, one can estimate structural organization in advance by choosing the appropriate linker.

In this thesis, I_2, CHI_3, and FIB were used as XBDs. Iodine molecule was the simplest XBD with two potential interaction sites. Indeed, I_2 acted as a classical XBD via σ-hole and either heterotrimeric or 1D polymer cocrystals with [PtX_2COD] were observed. However, in *trans*-[MI_2(CNXyl)$_2$] cocrystals, a combination of XBs between a complex and I_2 along with intermolecular π-stacking between CNXyl ligands formed a 2D structure. Therefore, it is important to consider not only linker properties but also the interlinking unit properties.

There are four sites available for NCIs in the case of CHI_3, three of which for XBs and one for HB. Availability of hydrogen bonding adds an extra dimension to the halogen bonded 1D-chain. This builds a 2D structure in the [PtI_2COD] · CHI_3 cocrystal. The HB is the weakest NCI in this cocrystal according to NCIplot analysis. However, it is comparable in strength with the weakest XB at sign(λ_2)ρ = –0.0097 compared to sign(λ_2)ρ = –0.0102, respectively.

The FIB molecule has many potential sites for NCI. The iodine atoms can participate in XBs, phenyl ring in π-interactions, fluorine atoms in various intermolecular interactions. Therefore, application of FIB in the design of cocrystals is the most demanding from the prediction point of view, but the most simple from the experimental. This is because structures with FIB are more stable than with I_2 or CHI_3. In [PtX_2COD] · nFIB, the contacts that direct the 2D structural arrangement are the XBs between the iodine atoms of the complex and FIB. The stacking of the FIB molecules adds the last dimension completing the 3D arrangement. The unusual I···Pt, F···π, and I···π noncovalent interactions enhance the structural stabilization of the cocrystal together with classical halogen bonds.

An interplay of strong K···N interactions and weak H···I (E_{INT} =-4.5 kJmol^{-1}) and N···I (E_{INT} =-3.0 kJmol^{-1}) interactions stabilizes the structure of the ligand-supported 1D-polymer of KI. Intramolecular H···N bonds within the ligand has an extra impact on the ligand's rigidity, which also affects the bite angle of the ligand.

Although multiple interaction sites of linker molecules make predicting possible geometries more challenging, in some cases it's advantageous. Cooperativity of multiple NCIs is known to improve structural stabilization, chelation, and regioselectivity in catalysis.[37]

SUMMARY

Although the field of NCIs has blossomed during the last 20 years, there is still much to learn. The simultaneous involvement of several NCIs makes it difficult to predict the geometry of the final product. Scientists are trying to split the problem into smaller parts and first have a good understanding of each NCI's nature. This could improve the predictability of the NCI, which is crucial for the real world applications. The application is always an important task for researchers. This is the reason to accumulate as much fundamental data as possible and that is what I hope my Ph.D. research has contributed to.

The aim of this thesis was to unite three research projects from my Ph.D. studies. Applications of the "molecule → noncovalent interaction → metallopolymer" strategy to these systems allowed us to create polymeric compounds with differing 0-3D dimensional geometries. It was shown that the dimensionality is closely related to the strongest noncovalent interaction with additional cooperating weaker interactions.

Halogen bonding is a powerful tool in the supramolecular self-assembly of metallopolymers. It was clearly the strongest interaction and therefore a driving force for self-assembly in publications I and II. The choice of halogen bond donor influences the strength of the interaction within these systems, which was shown by SCXRD and the NCIplot method. The interaction strength of the XBDs increasease as CHI_3 < FIB < I_2. Therefore, structural optimization can be performed by choosing the appropriate donor-acceptor pairing.

Metal-involved interactions influenced the structural stabilization in the research in publications I–III. Metal-involved type contact was found to be almost two times weaker than halogen bonding in the $[PtI_2COD] \cdot 1.5FIB$ cocrystals, while the M···I interaction in *trans*-$[MI_2(CNXyl)_2] \cdot I_2$ was found to be only a bit weaker than the I···I halogen bond. This played a crucial role in the structural organization. Curiously, the N–K interaction was the strongest in the 1D-KI polymeric structure and had the biggest impact its stabilization according to the QTAIM analysis. Therefore, the N–K interaction is the driving force in the structural organization of this system.

Lastly, the cooperativity of various interactions effected the structural arrangements in the aforementioned systems. These relatively weaker interactions even added one more dimension to the structure in some cases. For example, the H···I hydrogen bond in $[PtI_2COD] \cdot CHI_3$ cocrystal or the π–stacking interactions between CNXyl fragments in *trans*-$[MI_2(CNXyl)_2] \cdot I_2$ cocrystals. A combination of strong N–K interactions and weaker N···I and H···I interactions stabilized the polymer growth in the ligand-supported 1D KI chain.

To conclude, all three research projects from my Ph.D. studies have contributed to fundamental knowledge of noncovalent interactions. All projects illustrate the ability of NCIs to fine-tune the structural organization. The aim of fundamental science is to expand our understanding of the topic so this "know-how" can be applied to generate new functional materials.

REFERENCES

1 Cavallo G., Metrangolo P., Milani R., Pilati T., Priimagi A., Resnati G., Terraneo G., The Halogen Bond. *Chem. Rev.* **2016**, *116* (4), 2478–2601.

2 Lin M., Dai Y., Xia F., Zhang X., Advances in Non-Covalent Crosslinked Polymer Micelles for Biomedical Applications. *Mater. Sci. Eng. C* **2021**, *119*, 111626.

3 Dzhardimalieva G.I., Uflyand I.E., Design and Synthesis of Coordination Polymers with Chelated Units and Their Application in Nanomaterials Science. *RSC Adv.* **2017**, *7* (67), 42242–42288.

4 Schmidt G.M.J., Photodimerization in the Solid State. *Pure Appl. Chem.* **1971**, *27* (4), 647–678.

5 Mahmudov K.T., Kopylovich M.N., Guedes da Silva M.F.C., Pombeiro A.J.L., Non-Covalent Interactions in the Synthesis of Coordination Compounds: Recent Advances. *Coord. Chem. Rev.* **2017**, *345*, 54–72.

6 Maharramov A.M., Mahmudov K.T., Kopylovich M.N., Pombeiro A.J.L.*Non-Covalent Interactions in the Synthesis and Design of New Compounds*; John Wiley & Sons, Ltd, 2016.

7 R. Desiraju G., Crystal Engineering: From Molecule to Crystal. *J. Am. Chem. Soc.* **2013**, *135* (27), 9952–9967.

8 Desiraju G.R., Crystal Engineering. From Molecules to Materials. *J. Mol. Struct.* **2003**, *656* (1), 5–15.

9 Hibbert F., Emsley J., Hydrogen Bonding and Chemical Reactivity; Bethell, D. B. T.-A. in P. O. C., Ed.; Academic Press, 1990; Vol. 26, pp 255–379.

10 Minkin V.I., Glossary of Terms Used in Theoretical Organic Chemistry (IUPAC Recommendations 1999). *Pure Appl. Chem.* **1999**, *71* (10), 1919–1981.

11 Schindler S., Huber S.M., Metrangolo P., Resnati G.*Halogen Bonding II: Impact on Material Chemistry and Life Science*; 2015.

12 Desiraju G.R., Ho P.S., Kloo L., Legon A.C., Marquardt R., Metrangolo P., Politzer P., Resnati G., Rissanen K., Definition of the Halogen Bond (IUPAC Recommendations 2013). *Pure Appl. Chem.* **2013**, *85* (8), 1711–1713.

13 Clark T., Hennemann M., Murray J.S., Politzer P., Halogen Bonding: The σ-Hole. *J. Mol. Model.* **2007**, *13* (2), 291–296.

14 Politzer P., Murray J.S., Clark T., Metrangolo P., Resnati G.*Halogen Bonding I: Impact on Materials Chemistry and Life Science*; 2015.

15 Huber S.M., Scanlon J.D., Jimenez-Izal E., Ugalde J.M., Infante I., On the Directionality of Halogen Bonding. *Phys. Chem. Chem. Phys.* **2013**, *15* (25), 10350–10357.

16 Riley K.E., Murray J.S., Fanfrlík J., Řezáč J., Solá R.J., Concha M.C., Ramos F.M., Politzer P., Halogen Bond Tunability I: The Effects of Aromatic Fluorine Substitution on the Strengths of Halogen-Bonding Interactions Involving Chlorine, Bromine, and Iodine. *J. Mol. Model.* **2011**, *17* (17), 3309–3318.

17 Ramasubbu N., Parthasarathy R., Murray-Rust P., Angular Preferences of Intermolecular Forces around Halogen Centers: Preferred Directions of

Approach of Electrophiles and Nucleophiles around Carbon-Halogen Bond. *J. Am. Chem. Soc.* **1986**, *108* (15), 4308–4314.

18 Metrangolo P., Murray J.S., Pilati T., Politzer P., Resnati G., Terraneo G., Fluorine-Centered Halogen Bonding: A Factor in Recognition Phenomena and Reactivity. *Cryst. Growth Des.* **2011**, *11* (9), 4238–4246.

19 Brammer L., Halogen Bonding, Chalcogen Bonding, Pnictogen Bonding, Tetrel Bonding: Origins, Current Status and Discussion. *Faraday Discuss.* **2017**, *203* (0), 485–507.

20 Jeffrey G.A.*An Introduction to Hydrogen Bonding*; Topics in Physical Chemistry - Oxford University Press; Oxford University Press, 1997.

21 Frey P.A., Review: Strong Hydrogen Bonding in Molecules and Enzymatic Complexes. *Magn. Reson. Chem.* **2001**, *39* (S1), S190–S198.

22 A. Kollman P., C. Allen L., Theory of the Hydrogen Bond. *Chem. Rev.* **2002**, *72* (3), 283–303.

23 Hunter C.A., Sanders J.K.M., The Nature of .Pi.-.Pi. Interactions. *J. Am. Chem. Soc.* **1990**, *112* (14), 5525–5534.

24 David Sherrill C., Energy Component Analysis of π Interactions. *Acc. Chem. Res.* **2012**, *46* (4), 1020–1028.

25 Sinnokrot M.O., Valeev E.F., Sherrill C.D., Estimates of the Ab Initio Limit for π-π Interactions: The Benzene Dimer. *J. Am. Chem. Soc.* **2002**, *124* (36), 10887–10893.

26 Kertesz M., Pancake Bonding: An Unusual Pi-Stacking Interaction. *Chem. – A Eur. J.* **2019**, *25* (2), 400–416.

27 Ivanov D.M., Novikov A.S., Ananyev I. V, Kirina Y. V, Kukushkin V.Y., Halogen Bonding between Metal Centers and Halocarbons. *Chem. Commun.* **2016**, *52* (32), 5565–5568.

28 Brammer L., Metals and Hydrogen Bonds. *Dalton Trans.* **2003**, No. 16, 3145–3157.

29 Zelenkov L.E., Ivanov D.M., Sadykov E.K., Bokach N.A., Galmés B., Frontera A., Kukushkin V.Y., Semicoordination Bond Breaking and Halogen Bond Making Change the Supramolecular Architecture of Metal-Containing Aggregates. *Cryst. Growth Des.* **2020**, *20* (10), 6956–6965.

30 Subha Mahadevi A., Narahari Sastry G., Cation−π Interaction: Its Role and Relevance in Chemistry, Biology, and Material Science. *Chem. Rev.* **2012**, *113* (3), 2100–2138.

31 Demircan Ç.A., Bozkaya U., Transition Metal Cation-π Interactions: Complexes Formed by Fe2+, Co2+, Ni2+, Cu2+, and Zn2+ Binding with Benzene Molecules. *J. Phys. Chem. A* **2017**, *121* (34), 6500–6509.

32 Raju S., Singh H.B., Butcher R.J., Metallophilic Interactions: Observations of the Shortest Metallophilicinteractions between Closed Shell (D10···d10, D10···d8, D8···d8) Metal Ions [M···M′ M = Hg(Ii) and Pd(Ii) and M′ = Cu(i), Ag(i), Au(i), and Pd(Ii)]. *Dalton Trans.* **2020**, *49* (26), 9099–9117.

33 Sculfort S., Braunstein P., Intramolecular D10–D10 Interactions in Heterometallic Clusters of the Transition Metals. *Chem. Soc. Rev.* **2011**, *40* (5), 2741–2760.

34 M. Bikbaeva Z., M. Ivanov D., S. Novikov A., V. Ananyev I., A. Bokach N., Yu. Kukushkin V., Electrophilic–Nucleophilic Dualism of Nickel(II) toward Ni···I Noncovalent Interactions: Semicoordination of Iodine Centers via Electron Belt and Halogen Bonding via σ-Hole. *Inorg. Chem.* **2017**, *56* (21), 13562–13578.

35 Petrović P., Djukic J.-P., Hansen A., Bannwarth C., Grimme S., Non-Covalent Stabilization in Transition Metal Coordination and Organometallic Complexes. *Non-covalent Interactions in the Synthesis and Design of New Compounds*. April 19, 2016, pp 115–143.

36 Saha S., Narahari Sastry G., Cooperative or Anticooperative: How Noncovalent Interactions Influence Each Other. *J. Phys. Chem. B* **2015**, *119* (34), 11121–11135.

37 Subha Mahadevi A., Narahari Sastry G., Cooperativity in Noncovalent Interactions. *Chem. Rev.* **2016**, *116* (5), 2775–2825.

38 M. Sluch I., J. Miranda A., Elbjeirami O., A. Omary M., M. Slaughter L., Interplay of Metallophilic Interactions, π–π Stacking, and Ligand Substituent Effects in the Structures and Luminescence Properties of Neutral PtII and PdII Aryl Isocyanide Complexes. *Inorg. Chem.* **2012**, *51* (20), 10728–10746.

39 Novikov A., Ivanov D.M., Bikbaeva Z.M., Bokach N.A., Kukushkin V.Y., Noncovalent Interactions Involving Iodofluorobenzenes: The Interplay of Halogen Bonding and Weak Lp(O)···π-Holearene Interactions. *Cryst. Growth Des.* **2018**, *18* (12), 7641–7654.

40 Rozhkov A. V, Ivanov D.M., Novikov A.S., Ananyev I. V, Bokach N.A., Kukushkin V.Y., Metal-Involving Halogen Bond Ar–I···[Dz2PtII] in a Platinum Acetylacetonate Complex. *CrystEngComm* **2020**, *22* (3), 554–563.

41 Troff R.W., Mäkelä T., Topić F., Valkonen A., Raatikainen K., Rissanen K., Alternative Motifs for Halogen Bonding. *Eur. J. Org. Chem.* **2013**, *2013*, 1617–1637.

42 Bondi A., Van Der Waals Volumes and Radii. *J. Phys. Chem.* **1964**, *68* (3), 441–451.

43 Szell P.M.J., Bryce D.L., Solid-State NMR Studies of Halogen Bonding BT - Modern Magnetic Resonance; Webb, G. A., Ed.; Springer International Publishing: Cham, 2016; pp 1–18.

44 Hakkert S.B., Gräfenstein J., Erdelyi M., The 15N NMR Chemical Shift in the Characterization of Weak Halogen Bonding in Solution. *Faraday Discuss.* **2017**, *203* (0), 333–346.

45 Witanowski M., Nitrogen n.m.r. Spectroscopy. *Pure Appl. Chem.* **1974**, *37* (1–2), 225–233.

46 Lorente P., Shenderovich I.G., Golubev N.S., Denisov G.S., Buntkowsky G., Limbach H.-H., 1H/15N NMR Chemical Shielding, Dipolar 15N,2H Coupling and Hydrogen Bond Geometry Correlations in a Novel Series of Hydrogen-Bonded Acid–Base Complexes of Collidine with Carboxylic Acids. *Magn. Reson. Chem.* **2001**, *39* (S1), S18–S29.

47 Bouchmella K., Dutremez S.G., Alonso B., Mauri F., Gervais C., 1H, 13C,

and 15N Solid-State NMR Studies of Imidazole- and Morpholine-Based Model Compounds Possessing Halogen and Hydrogen Bonding Capabilities. *Cryst. Growth Des.* **2008**, *8* (11), 3941–3950.

48 Proctor W.G., Yu F.C., On the Nuclear Magnetic Moments of Several Stable Isotopes. *Phys. Rev.* **1951**, *81* (1), 20–30.

49 Pregosin P.S., Platinum-195 Nuclear Magnetic Resonance. *Coord. Chem. Rev.* **1982**, *44* (2), 247–291.

50 Priqueler J.R.L., Butler I.S., Rochon F.D., An Overview of 195Pt Nuclear Magnetic Resonance Spectroscopy. *Appl. Spectrosc. Rev.* **2006**, *41* (3), 185–226.

51 Appleton T.G., NMR Spectroscopy, Heteronuclei, La-Hg; Lindon, J. C., Tranter, G. E., Koppenaal, D. W. B. T.-E. of S. and S. (Third E., Eds.; Academic Press: Oxford, 2017; pp 342–345.

52 Katlenok E.A., Haukka M., Levin O. V, Frontera A., Kukushkin V.Y., Supramolecular Assembly of Metal Complexes by (Aryl)I···d [PtII] Halogen Bonds. *Chem. – A Eur. J.* **2020**, *26* (34), 7692–7701.

53 Brinck T., Murray J.S., Politzer P., Surface Electrostatic Potentials of Halogenated Methanes as Indicators of Directional Intermolecular Interactions. *Int. J. Quantum Chem.* **1992**, *44*, 57–64.

54 Stewart R.F., Valence Structure from X-Ray Diffraction Data: Physical Properties. *J. Chem. Phys.* **1972**, *57* (4), 1664–1668.

55 Naray-Szabo G., G. Ferenczy G., Molecular Electrostatics. *Chem. Rev.* **2002**, *95* (4), 829–847.

56 Bader R.F.W., Carroll M.T., Cheeseman J.R., Chang C., Properties of Atoms in Molecules: Atomic Volumes. *J. Am. Chem. Soc.* **1987**, *109* (26), 7968–7979.

57 Bader R.F.W.*Atoms in Molecules: A Quantum Theory*; Clarendon Press, 1990.

58 Popelier P.L.A., The QTAIM Perspective of Chemical Bonding. In *The Chemical Bond*; Frenking, G., Shaik, S., Eds.; Wiley Online Books; Wiley-VCH Verlag GmbH & Co. KGaA, 2014; pp 271–308.

59 Janusz Grabowski S., What Is the Covalency of Hydrogen Bonding? *Chem. Rev.* **2011**, *111* (4), 2597–2625.

60 R. Johnson E., Keinan S., Mori-Sánchez P., Contreras-García J., J. Cohen A., Yang W., Revealing Noncovalent Interactions. *J. Am. Chem. Soc.* **2010**, *132* (18), 6498–6506.

61 Desiraju G.R., Harlow R.L., Cyano-Halogen Interactions and Their Role in the Crystal Structures of the 4-Halobenzonitriles. *J. Am. Chem. Soc.* **1989**, *111* (17), 6757–6764.

62 Savin A., Becke A.D., Flad J., Nesper R., Preuss H., von Schnering H.G., A New Look at Electron Localization. *Angew. Chem., Int. Ed. Engl.* **1991**, *30* (4), 409–412.

63 Triguero S., Llusar R., Polo V., Fourmigué M., Halogen Bonding Interactions of Sym-Triiodotrifluorobenzene with Halide Anions: A Combined Structural and Theoretical Study. *Cryst. Growth Des.* **2008**, *8* (7), 2241–2247.

64 Cauliez P., Polo V., Roisnel T., Llusar R., Fourmigué M., The Thiocyanate

Anion as a Polydentate Halogen Bond Acceptor. *CrystEngComm* **2010**, *12*, 558–566.

65 Juárez-Pérez E.J., Aragoni M.C., Arca M., Blake A.J., Devillanova F.A., Garau A., Isaia F., Lippolis V., Núñez R., Pintus A., Wilson C., A Unique Case of Oxidative Addition of Interhalogens IX (X=Cl, Br) to Organodiselone Ligands: Nature of the Chemical Bonding in Asymmetric I–Se–X Polarised Hypervalent Systems. *Chem. – A Eur. J.* **2011**, *17* (41), 11497–11514.

66 Xu L., Sang P., Zou J.-W., Xu M.-B., Li X.-M., Yu Q.-S., Evaluation of Nucleotide C–Br···O–P Contacts from ONIOM Calculations: Theoretical Insight into Halogen Bonding in Nucleic Acids. *Chem. Phys. Lett.* **2011**, *509* (4), 175–180.

67 Bartashevich E. V, Matveychuk Y. V, Troitskaya E.A., Tsirelson V.G., Characterizing the Multiple Non-Covalent Interactions in N, S-Heterocycles–Diiodine Complexes with Focus on Halogen Bonding. *Comput. Theor. Chem.* **2014**, *1037*, 53–62.

68 Bartashevich E., Yushina I., Kropotina K., Muhitdinova S., Tsirelson V., Testing the Tools for Revealing and Characterizing the Iodine{--}iodine Halogen Bond in Crystals. *Acta Crystallogr. B* **2017**, *73* (2), 217–226.

69 Dabranskaya U., M. Ivanov D., S. Novikov A., V. Matveychuk Y., A. Bokach N., Yu. Kukushkin V., Metal-Involving Bifurcated Halogen Bonding C–Br···η2(Cl–Pt). *Cryst. Growth Des.* **2018**, *19* (2), 1364–1376.

70 D. Yushina I., A. Kolesov B., Interplay of Intra- and Intermolecular Interactions in Solid Iodine at Low Temperatures: Experimental and Theoretic Spectroscopy Study. *J. Phys. Chem. A* **2019**, *123* (21), 4575–4580.

71 Mata I., Molins E., Alkorta I., Espinosa E., Topological Properties of the Electrostatic Potential in Weak and Moderate N···H Hydrogen Bonds. *J. Phys. Chem. A* **2007**, *111* (28), 6425–6433.

72 Lamberts K., Handels P., Englert U., Aubert E., Espinosa E., Stabilization of Polyiodide Chains via Anion···anion Interactions: Experiment and Theory. *CrystEngComm* **2016**, *18* (21), 3832–3841.

73 Bartashevich E., Mukhitdinova S., Yushina I., Tsirelson V., Electronic Criterion for Categorizing the Chalcogen and Halogen Bonds: Sulfur{--}iodine Interactions in Crystals. *Acta Crystallogr. B* **2019**, *75* (2), 117–126.

74 Bartashevich E., Matveychuk Y., Tsirelson V., Identification of the Tetrel Bonds between Halide Anions and Carbon Atom of Methyl Groups Using Electronic Criterion. *Molecules* **2019**, *24* (6), 1083.

75 Khalil M., Kadja G.T.M., Ilmi M.M., Advanced Nanomaterials for Catalysis: Current Progress in Fine Chemical Synthesis, Hydrocarbon Processing, and Renewable Energy. *J. Ind. Eng. Chem.* **2021**, *93*, 78–100.

76 Bates R.*Organic Synthesis Using Transition Metals: Second Edition*, 2nd ed.; John Wiley & Sons, Ltd., 2012.

77 Sodhi R.K., Paul S., Metal Complexes in Medicine: An Overview and Update from Drug Design Perspective. *CTOIJ* **2019**, *14* (2), 555883.

78 Hildebrand A., Sárosi I., Lönnecke P., Silaghi-Dumitrescu L., Sárosi M.B.,

Silaghi-Dumitrescu I., Hey-Hawkins E., Heteropolytopic Arsanylarylthiolato Ligands: Cis–Trans Isomerism of Nickel(II), Palladium(II), and Platinum(II) Complexes of 1-AsPh2-2-SHC6H4. *Inorg. Chem.* **2012**, *51* (13), 7125–7133.

79 Petz W., Kutschera C., Neumüller B., Reaction of the Carbodiphosphorane Ph3PCPPh3 with Platinum(II) and -(0) Compounds: Platinum Induced Activation of C−H Bonds. *Organometallics* **2005**, *24* (21), 5038–5043.

80 Lachachi M.B., Benabdallah T., Aguiar P.M., Youcef M.H., Whitwood A.C., Lynam J.M., Synthesis of a Series of New Platinum Organometallic Complexes Derived from Bidentate Schiff-Base Ligands and Their Catalytic Activity in the Hydrosilylation and Dehydrosilylation of Styrene. *Dalton Trans.* **2015**, *44* (26), 11919–11928.

81 Slater J.C., Atomic Radii in Crystals. *J. Chem. Phys.* **1964**, *41* (10), 3199–3204.

82 Hassel O., Structural Aspects of Interatomic Charge-Transfer Bonding. *Science (80-.).* **1970**, *170* (3957), 497–502.

83 Sloan J., Novotny M.C., Bailey S.R., Brown G., Xu C., Williams V.C., Friedrichs S., Flahaut E., Callender R.L., York A.P.E., Coleman K.S., Green M.L.H., Dunin-Borkowski R.E., Hutchison J.L., Two Layer 4:4 Co-Ordinated KI Crystals Grown within Single Walled Carbon Nanotubes. *Chem. Phys. Lett.* **2000**, *329* (1–2), 61–65.

84 Kruszynski R., Sieranski T., Bilinska A., Bernat T., Czubacka E., Alkali Metal Halogenides Coordination Compounds with Hexamethylenetetramine. *Struct. Chem.* **2012**, *23* (5), 1643–1656.

85 Amo-Ochoa P., Jiménez-Aparicio R., Perles J., Torres M.R., Gennari M., Zamora F., Structural Diversity in Paddlewheel Dirhodium(II) Compounds through Ionic Interactions: Electronic and Redox Properties. *Cryst. Growth Des.* **2013**, *13* (11), 4977–4985.

86 Liu B., Qiu Y.-C., Peng G., Deng H., In Situ Solvothermal Syntheses of a Heteronuclear Copper(I)-Alkaline Metallic Tetrazole-Based Coordination Polymer. *CrystEngComm* **2010**, *12* (1), 270–276.

87 Aakeröy C.B., Wijethunga T.K., Desper J., Molecular Electrostatic Potential Dependent Selectivity of Hydrogen Bonding. *New J. Chem.* **2015**, *39* (2), 822–828.

88 Aakeröy C.B., Desper J., Tharanga K.W., Practical Crystal Engineering Using Halogen Bonding: A Hierarchy Based on Calculated Molecular Electrostatic Potential Surfaces. *J. Mol. Struct.* **2014**, *1072*, 20–27.

89 Gibson K.E., Iredale T., The Photodecomposition of Iodoform and of the Alkyl and Alkylene Iodides. *Trans. Faraday Soc.* **1936**, *32* (0), 571–576.

90 Stephenson N.C., The Crystal Structure of Di-Iododi-(o-Phenylenebisdimethylarsine) Platinum(II) Pt(C6H4[As(CH3)2]2)2I2. *J. Inorg. Nucl. Chem.* **1962**, *24* (7), 791–795.

91 Baykov S. V., Dabranskaya U., Ivanov D.M., Novikov A.S., Boyarskiy V.P., Pt/PD and I/Br Isostructural Exchange Provides Formation of C−I···PD, C−Br···PT, and C−Br···Pd Metal-Involving Halogen Bonding. *Cryst. Growth Des.* **2018**, *18* (10), 5973–5980.

92 D. Harvey P., D. Truong K., T. Aye K., Drouin M., D. Bandrauk A., Resonance-Enhanced Intraligand and Metal-Metal Raman Modes in Weakly Metal-Metal-Interacting Platinum(II) Complexes and Long-Range Relationship between Metal-Metal Separations and Force Constants. *Inorg. Chem.* **2002**, *33* (11), 2347–2354.

93 Sluch I.M., Miranda A.J., Slaughter L.M., Channeled Polymorphs of Cis-M(CNPh) 2Cl 2 (M=Pt, Pd) with Extended Metallophilic Interactions. *Cryst. Growth Des.* **2009**, *9* (3), 1267–1270.

94 Kinzhalov M.A., Kashina M. V, Mikherdov A.S., Katkova S.A., Suslonov V. V., Synthesis of Platinum(II) Phoshine Isocyanide Complexes and Study of Their Stability in Isomerization and Ligand Disproportionation Reactions. *Russ. J. Gen. Chem.* **2018**, *88* (6), 1180–1187.

95 Buttery J.H.N., Effendy, Mutrofin S., Plackett N.C., Skelton B.W., Whitaker C.R., White A.H., Complexes of Group 1 Salts with N,N'-Aromatic Bidentate Ligands , of 1 : 1 Salt : Base Ratio. *Z. Anorg. Allg. Chem.* **2006**, *6* (LiCl), 1809–1828.

96 Martin A., Mena M., Pérez-Redondo A., Yélamos C., A New Double-Cube Nitride Complex Containing Titanium and Potassium. *Acta Crystallogr. C* **2011**, *67* (5), m157--m159.

97 Tripathi G., Ramanathan G., Crystallographic Studies on Complexes of Potassium Iodide and Copper Perchlorate with N, N′ -Dicyclohexylurea Tethered to a Benzo-12-Crown-4. *J. Mol. Struct.* **2018**, *1156*, 273–279.

ORIGINAL PAPERS

I

CLASSICS MEET CLASSICS: THEORETICAL AND EXPERIMENTAL STUDIES OF HALOGEN BONDING IN ADDUCTS OF 1,5-CYCLOOCTADIENE PLATINUM(II) HALIDE COMPLEXES WITH DIIODINE, IODOFORM AND 1,4-DIIODOTETRAFLUOROBENZENE

by

Margarita Bulatova, Daniil Ivanov & Matti Haukka

Cryst. Growth & Des., **2021**, *21 (2)*, 974–987

DOI: 10.1021/acs.cgd.0c01314

CRYSTAL GROWTH & DESIGN

pubs.acs.org/crystal

Article

Classics Meet Classics: Theoretical and Experimental Studies of Halogen Bonding in Adducts of Platinum(II) 1,5-Cyclooctadiene Halide Complexes with Diiodine, Iodoform, and 1,4-Diiodotetrafluorobenzene

Margarita Bulatova, Daniil M. Ivanov, and Matti Haukka*

Cite This: https://dx.doi.org/10.1021/acs.cgd.0c01314

Read Online

ACCESS | Metrics & More | Article Recommendations | Supporting Information

ABSTRACT: Complexes of PtX_2COD (X = Cl, Br, I; COD = 1,5-cyclooctadiene) were cocrystallized with classical halogen-bond donors (CHI_3, I_2, and 1,4-diiodotetrafluorobenzene (FIB)), resulting in noncovalently bound supramolecular aggregates of various lengths—from heterotrimers to polymers. The influence of halides in the complexes on the geometry and strength of the halogen bond (XB) was studied both experimentally by single-crystal XRD and theoretically by quantum chemical methods such as noncovalent interaction plots (NCI-plot), electrostatic potential (ESP) surface analysis, and a combination of electron localization function (ELF) and quantum theory of atoms in molecules (QTAIM) analyses. It was shown that strength of XB interactions in the adducts increases in the order CHI_3 > FIB > I_2. Although halogen bonding was found to be the main preorganizing force in the structures, in the case of FIB adducts a rare Pt···I interaction was involved in additional stabilization of the structure. Hence, fine-tuning of halogen bonding can influence the length of the polymer, as well as the strength and directionality of interactions in the adduct.

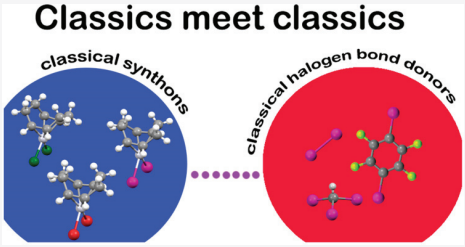

1. INTRODUCTION

Platinum(II) square-planar complexes are actively used in synthesis, catalysis, photochemistry, and supramolecular chemistry.[1,2] In the case of noncovalent interactions Pt(II) complexes with halides as ligands are particularly interesting, due to the ability of both the halide and a Pt(II) center to participate in a halogen bond.[3−5] Platinum(II) halide 1,5-cyclooctadiene (COD) complexes (PtX_2COD, X = Cl, Br, I) are classically used in the synthesis of complexes featuring a square-planar platinum(II) center[6−8] due to the easily replaceable COD ligand. The COD ligand is quite bulky and due to steric hindrance can possibly obstruct the participation of a Pt(II) center in halogen bonding.

Noncovalent interactions, in particular halogen bonds (XBs), are known for their preorganizational abilities in coordination chemistry.[9,10] According to the IUPAC definition[11] of a halogen bond, typical halogen-bond donors (further XBD) include such molecules as I_2, CHI_3, and 1,4-diiodotetrafluorobenzene (FIB). Moreover, I_2 and CHI_3 have played a key role in the understanding of the structural features of halogen bonds in Hassel's Nobel lecture.[12] The use of such classical halogen-bond donors as FIB, I_2, and CHI_3 leads to the formation of strong noncovalent interactions in their adducts.

Due to the tunability, relative strength, and directionality, halogen bonding has been used as a self-assembly tool in crystal engineering:[13−15] for example, in the synthesis of self-assembled polymers.[16−19] To apply halogen bonding as a fine-tuning tool, it is crucial to understand its nature, and for this purpose, several theoretical[20−23] and experimental methods[14] may be used. However, only a combination of methods will give a full picture of the nature of the interactions.

Although the field of halogen-bond-driven self-assembled metallopolymers has vastly progressed in the past decade,[24−27] the topic is still developing and the question how to control the geometry of a polymer and, particularly, the strength of interactions between polymer units is still in the air. To answer this question, simple molecular systems should be explored. In this study classics meet classics: classical halogen-bond donors XBD (such as molecular iodine, iodoform, FIB) and classical synthons PtX_2COD were used to create metallopolymeric adducts. The aim of this research was to study the influence of various halides in the complexes on the supramolecular preorganization of the halogen-bond acceptor (XBA). For this purpose, noncovalent interactions were investigated using modern computational (such as NCI-plot, ELF, and ESP analyses) and structural (single-crystal X-ray diffraction

Received: September 23, 2020
Revised: December 30, 2020

Scheme 1. Synthesis of $PtX_2COD{\cdot}nXBD$ Adducts

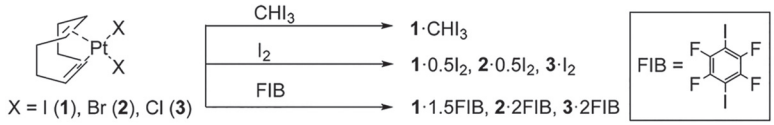

Table 1. Characteristic Parameters of the Y–I···X–Pt Halogen Bonds (Y = C, I; X = I, Br, Cl) in the Crystal Structures of the Obtained Adducts

cluster	Y–I···X–Pt	d(I···X), Å	∠(Y–I···X), deg	∠(I···X–Pt), deg	R_{IX}[a]
1·CHI_3	I_2HC–I1A···I1–Pt1	3.6359(5)	167.79(14)	124.032(14)	0.92
	I_2HC–I2A···I1–Pt1	3.6815(5)	172.83(14)	110.322(13)	0.93
	I_2HC–I3A···I1–Pt1	3.7723(5)	164.41(15)	92.385(11)	0.95
1·0.5I_2	I–I1A···I1–Pt1	3.4107(5)	175.779(17)	86.130(11)	0.86
2·0.5I_2	I–I1A···Br1–Pt1	3.2850(7)	175.75(2)	87.276(19)	0.86
3·I_2	I–I1A···Cl1–Pt1	3.1465(14)	173.11(3)	127.01(6)	0.84
1·1.5FIB	C–I1A···I2–Pt1	3.7054(6)	175.71(18)	71.518(13)	0.94
	C–I3A···I1–Pt1	3.5928(5)	175.12(15)	106.504(17)	0.91
	C–I2A···I4–Pt2	3.7371(6)	177.50(18)	71.250(13)	0.94
	C–I4A···I3–Pt2	3.6081(5)	171.80(18)	78.371(13)	0.91
	C–I5A···I3–Pt2	3.5870(6)	177.21(16)	121.312(15)	0.91
	C–I6A···I4–Pt2	3.8068(5)	168.46(17)	93.962(12)	0.96
2·2FIB	C–I1A···Br1–Pt1	3.4635(15)	176.5(3)	83.00(4)	0.90
	C–I2A···Br1–Pt1	3.3296(16)	171.1(3)	116.40(5)	0.87
3·2FIB	C–I1A···Cl1–Pt1	3.396(2)	175.99(19)	83.06(6)	0.91
	C–I2A···Cl1–Pt1	3.214(2)	172.56(19)	119.55(8)	0.86

[a] $R_{IX} = d(I{\cdots}X)/(R^{I}_{vdW} + R^{X}_{vdW})$, where R_{IX} is a distance reduction ratio, I is a donor atom, X is an acceptor atom, d(I···X) is the distance between I and X in Å, and R^{I}_{vdW} and R^{X}_{vdW} are the van der Waals radii of I and X, respectively, as determined by Bondi.[30]

(SCXRD)) methods, and the results are discussed in the following sections.

2. RESULTS AND DISCUSSION

2.1. Synthesis of PtX_2COD Adducts. PtX_2COD complexes were synthesized according to the procedure reported by Rigamonti et al.[28] with slight modifications such as longer reaction times and an additional recrystallization step. $PtX_2COD{\cdot}nXBD$ adducts (X = I (**1**), Br (**2**), Cl (**3**); XBD = I_2, CHI_3, FIB) were obtained by slow cocrystallization of PtX_2COD and the corresponding XBD, taken in a 1:2 molar ratio, from $CHCl_3$ solutions at room temperature (Scheme 1). No cocrystals with iodoform were obtained for **2** and **3**. Similarly, attempts to cocrystallize PtX_2COD with iodopentafluorobenzene were unsuccessful.

2.2. Analysis of the SCXRD Structures. The relative strengths of halogen bonds or other noncovalent interactions can be estimated by a comparison of the experimentally obtained distance between noncovalently interacting atoms and the sum of the corresponding van der Waals (vdW) radii.[29] The reduction in the distances of noncovalent interaction (in percent) can be calculated as $R_{IX} = d(I{\cdots}X)/(R^{I}_{vdW} + R^{X}_{vdW}) \times 100\%$, where R_{IX} is a distance reduction ratio, I (iodine) is an XBD atom, X is a, XBA atom, d(I···X) is the distance between I and X, and R^{I}_{vdW} and R^{X}_{vdW} are the vdW radii of I and X, respectively, as determined by Bondi.[30] Crystal structures of the obtained adducts were investigated by SCXRD. Characteristic parameters of XB in the Y–I···X–Pt (where Y = C, I; X = I, Br, Cl) interaction can be found in Table 1.

2.2.1. CHI_3 Adduct. In the adduct **1**·CHI_3 PtI_2COD complexes are linked to one another through CHI_3 molecules via halogen bonding, creating a 1D polymeric structure (Figure 1). In the crystal structure only one iodine of the complex (I1, Figure 1) participates in noncovalent interactions. The platinum complex in **1**·CHI_3 is interacting with four CHI_3 molecules, forming one hydrogen bond (see Table S2 in the Supporting Information for the details) and three halogen bonds (Table 1). The donor–acceptor distances in all of the halogen bonds were found to be less of the sum of vdW radii.

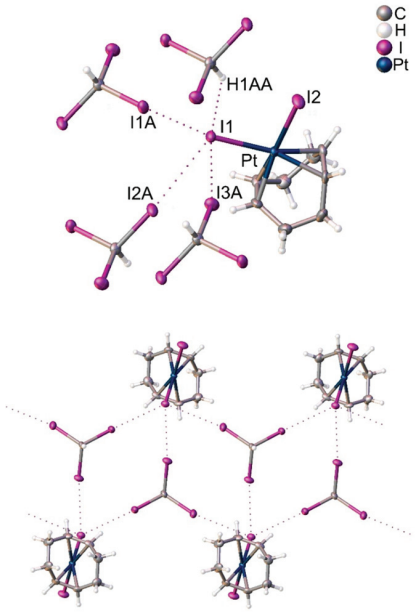

Figure 1. Adduct **1**·CHI_3: noncovalent interactions of the adduct **1**·CHI_3 (top); halogen-bonding-driven $(\mathbf{1}{\cdot}CHI_3)_n$ polymer (bottom).

https://dx.doi.org/10.1021/acs.cgd.0c01314
Cryst. Growth Des. XXXX, XXX, XXX–XXX

Furthermore, geometric parameters of the halogen bonds were found to be typical.

Although there are a few examples of CHI_3 adducts with some transition-metal complexes (*trans*-$[PtX_2(NCNAlk_2)_2]$ (X = Cl, Br)[31] and *trans*-$[MCl_2(NCNMe_2)_2]$ (M = Pt, Pd)[5]) and with an alkali-metal complex ($[Na(DB18C6)(H_2O)_2]I\cdot(THF)_2(CHI_3)$, where DB18C6 = dibenzo-18-crown-6[32]), **1**·CHI_3 is the first example of a CHI_3 adduct with a transition-metal iodide complex.

2.2.2. I_2 Adducts. In the series of PtX_2COD adducts with I_2 (Figure 2) **1**·0.5I_2 and **2**·0.5I_2 form isolated heterotrimers (**1**···I_2···**1** and **2**···I_2···**2**) with isomorphic structures, whereas the adduct **3**·I_2 forms the polymer $[\mathbf{3}\cdot I_2]_n$. On the basis of the experimentally obtained geometrical parameters (Table 1) it is assumed that in all the adducts the I_2 molecule acts as a XBD, while complexes **1**−**3** act as XBAs. Within the series the strengths of the XBs are rather similar: the distance reduction ratio R_{IX} is 0.86 for adducts **1**·0.5I_2 and **2**·0.5I_2 and 0.84 for **3**·I_2, meaning a slightly stronger XB. However, ∠(I···X−Pt) is closer to a 90° angle in the case of adducts **1**·0.5I_2 and **2**·0.5I_2 (86.130(11) and 87.276(19)°, respectively), and in the case of **3**·I_2 the angle is obtuse (127.01(6)°). This can be explained by a difference in the halide charge polarizations[33]—the least polarized chloride is less sensitive to the direction from which XBD I_2 will approach **3**. Further discussion can be found in section 2.3.1.

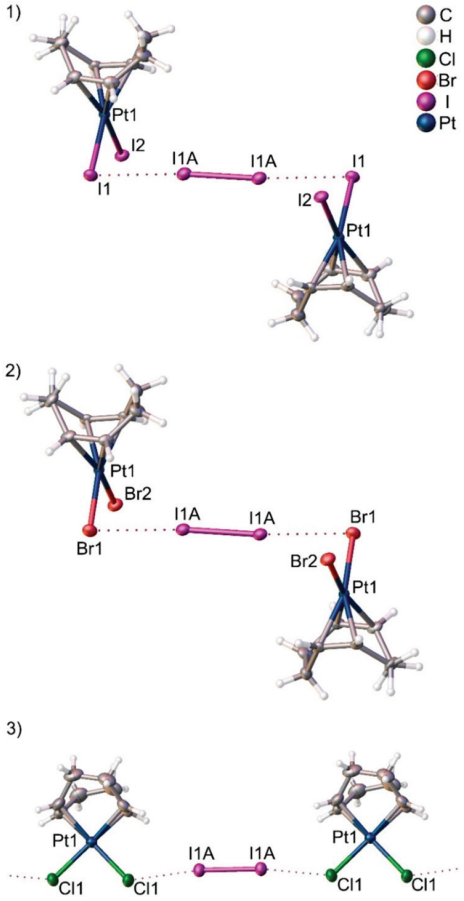

Figure 2. Adducts of PtX_2COD (X = I, Br, Cl) with I_2: (1, 2) **1**·0.5I_2 and **2**·0.5I_2 represent isomorphic heterotrimers; (3) **3**·I_2 represents a polymeric structure.

An elongation of a covalent bond (R−X, where RX is an XBD, X is any halogen atom with an electron-deficient region, R is the group covalently bound to X) in an XBD is a typical observation according to the IUPAC definition of halogen bonding (R−X···Y, where ··· is an XB and Y is an XBA with an electron-rich area).[11] The elongation indicates the strength and nature of the interaction between the XB donor and acceptor. In case of I_2 adducts the I−I bond length of the molecular iodine varies quite a bit (Table 2), increasing in the order **3**·I_2 < **2**·0.5I_2 < **1**·0.5I_2. In the solid-state structure of I_2 obtained by low-temperature SCXRD at 110 K, the I−I bond length is 2.7179(2) Å.[34] In comparison to that, the I−I bond length in the obtained adducts is elongated, except for the adduct **3**·I_2 (2.7002(6) Å), for which the shortest I−I distance is found. Also, in **3**·I_2 the XB was slightly stronger than in the other two adducts according to the R_{IX} value (0.84 for **3**·I_2, 0.86 for **1**·0.5I_2, and **2**·0.5I_2).

Table 2. I−I Distances in the Obtained Single Crystals of the $PtX_2COD\cdot I_2$ Adducts

	adduct		
	1·0.5I_2	**2**·0.5I_2	**3**·I_2
d(I−I), Å	2.7516(6)	2.7256(8)	2.7002(6)

Within the series of I_2 adducts no substitution of the halide coordinated to the Pt(II) complex takes place, although for transition-metal complexes substitution of the halide in a reaction with I_2 is known in the literature.[35,36] One of the rare examples with no halide substitution can be found in the work of Johnson et al.,[37] where the series of sterically crowded neutral pincer palladium complex eswith various halides (Cl, Br, I) interact with an I_2 molecule. However, the most probable explanation is steric hindrance preventing the substitution, yet in the I_2 adducts obtained in the current work steric availability does not result in halide substitution. It is worth mentioning that Pt(II) complexes are often oxidized to Pt(IV) in reactions with I_2.[38−41] However, neither oxidation of Pt(II) to Pt(IV) nor halide substitution occurs in the case of **2**·0.5I_2 or **3**·I_2. This was confirmed by a ^{195}Pt NMR analysis, which revealed only one ^{195}Pt peak in PtX_2COD + I_2 $CDCl_3$ solutions with no significant shift in comparison to the pure PtX_2COD in $CDCl_3$ (see the Pt NMR analysis section in the Supporting Information).

2.2.3. FIB Adducts. Inspired by the successful cocrystallizations of I_2 adducts, another popular halogen-bond donor, FIB, was tested. All of the adducts **1**·1.5FIB, **2**·2FIB, and **3**·2FIB have a 2D polymeric structure; however, only **2**·2FIB and **3**·2FIB represent isomorphs (Figures 3 and Figure 4). In the case of **1**·1.5FIB, the crystal structure contains two inequivalent Pt(II) complex units: first, where the metal complex forms four XBs with four molecules of FIB; second, where the metal complex forms two XBs with two molecules of FIB (Figure 3.1).

The strengths of the XBs estimated by the distance reduction ratio R_{IX} are rather similar in the case of **2**·2FIB (0.87 and 0.90) and **3**·2FIB (0.86 and 0.91) and tend to be slightly weaker in the case of **1**·1.5FIB (0.91−0.96). Moreover, other types of interactions were found among the adducts such as Pt···I (Table 3), F···π (Table 4), and exclusively for **1**·1.5FIB an I2···‖ interaction (COD double bond, with *d*(I1··· ‖) =

https://dx.doi.org/10.1021/acs.cgd.0c01314
Cryst. Growth Des. XXXX, XXX, XXX−XXX

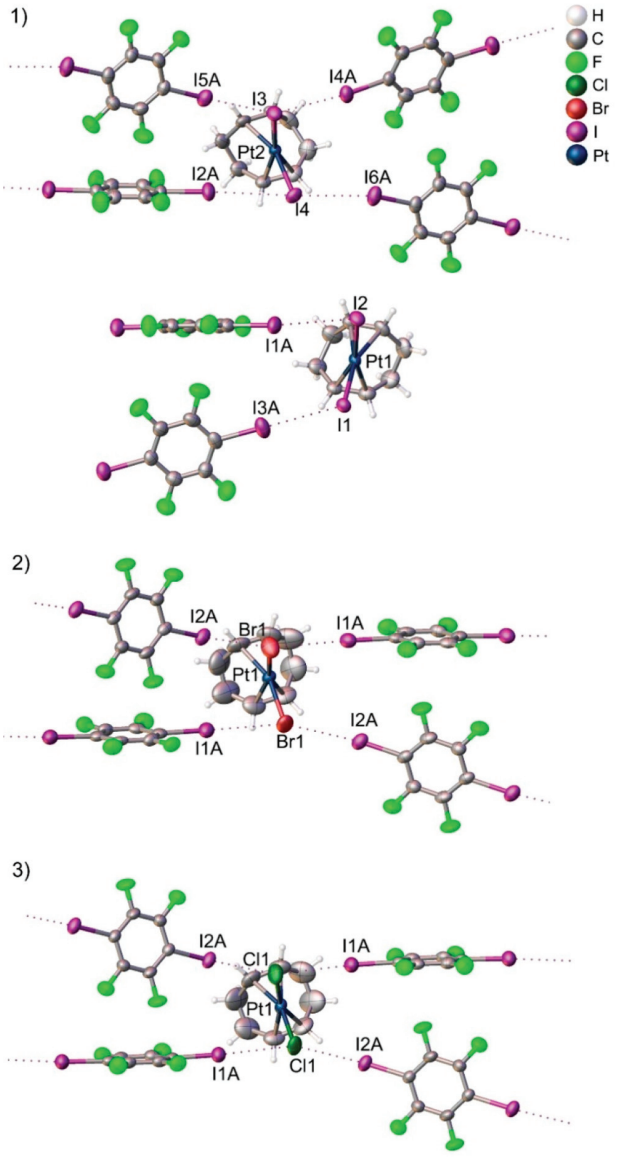

Figure 3. Polymeric adducts of PtX_2COD (X = I, Br, Cl) with FIB: (1) **1**·1.5FIB adduct contains two independent PtI_2COD units (upper and lower pictures) and **1** at the upper picture participates in four XBs, while **1** in the lower picture participates in only two XBs; (2, 3) structures **2**·2FIB and **3**·2FIB represent isomorphs.

Table 3. I···Pt Distances in the Obtained Single Crystals of the Adducts PtX_2COD·*n*FIB

cluster	contact, I···Pt	d(I···Pt), Å	R_{IPt}[a]
1·1.5FIB	I1A···Pt1	3.7990(6)	1.02
	I2A···Pt2	3.8127(4)	1.03
2·2FIB	I1A···Pt1	3.9821(8)	1.07
3·2FIB	I1A···Pt1	3.8732(6)	1.05

[a] $R_{IPt} = d(I\cdots Pt)/(R^{I}_{vdW} + R^{Pt}_{vdW})$, where R^{I}_{Pt} is a distance reduction ratio, I is an I atom, Pt is a Pt atom, d(I···Pt) is the distance between I and Pt in Å, and R^{I}_{vdW} and R^{Pt}_{vdW} are the van der Waals radii of I (1.98 Å) and Pt (1.72 Å), respectively, as determined by Bondi.[30]

Table 4. F···π Distances in the Obtained Single Crystals of the Adducts PtX_2COD·*n*FIB

cluster	contact, F···π	atoms involved in π-plane	d(F···π), Å
1·1.5FIB	F9A···π	I2A, F2A, F1A, I1A, F4A, F3A	2.846(5)
2·2FIB	F3A···π	I1A, F1A, F2A, I1A, F1A, F2A	2.701(6)
3·2FIB	F3A···π	I1A, F1A, F2A, I1A, F1A, F2A	2.719(5)

3.719(5) Å). These interactions were further studied with quantum-chemical methods in section 2.3.3.

In summary, isomorphic structures were found in both the I_2 and FIB series; however, the isomorphic pairs are different **1**·$0.5I_2$ is isomorphous to **2**·$0.5I_2$, and **2**·2FIB is isomorphous to **3**·2FIB. In all of the adducts in the case of the acute I···X−Pt angle the XB tends to be weaker than in the case of the obtuse angle (Table 1), which may be associated with the additional interaction with the Pt(II) center. Interestingly, the adducts of **2** are always involved in isomorphism.

On the basis of the average R_{IX} parameter among the CHI_3, I_2, and FIB series the strength of the XB increasing in the order CHI_3 (R_{IX} = 0.93) < FIB (R_{IX} = 0.91) < I_2 (R_{IX} = 0.85). This tendency is in agreement with computational data (based on the maximum of electrostatic potential (V_{max}) values, the distribution of electron pairs, and an analysis of NCI-plots, see section 2.3).

2.3. Theoretical Studies of Noncovalent Interactions.

With the help of computational chemistry the electrostatic nature and relative strength of noncovalent interactions discovered by SCXRD can be described. Due to computational efficiency and reasonable accuracy the Kohn−Sham (KS) density functional theory (DFT) method was used to calculate the electron density distribution.

A careful analysis of the calculated electron density distribution can reveal noncovalent interactions and their

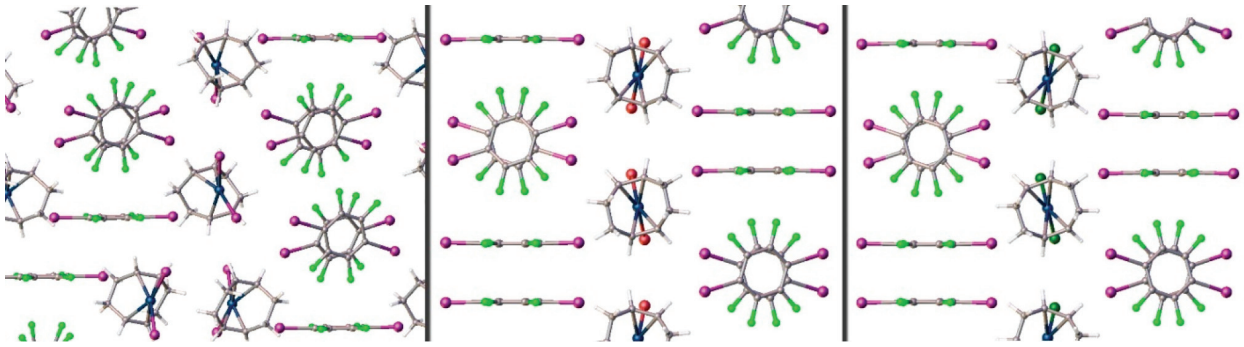

Figure 4. Grown view of the SCXRD structures of adducts with FIB (**1**·1.5FIB, **2**·2FIB, and **3**·2FIB; left, middle, and right pictures, respectively) along the *a* axes. **2**·2FIB and **3**·2FIB structures represent isomorphs.

https://dx.doi.org/10.1021/acs.cgd.0c01314
Cryst. Growth Des. XXXX, XXX, XXX−XXX

properties. Out of all of the computation methods, a combination of three approaches may give a broader picture of the noncovalent interactions: an analysis of electrostatic potential (ESP),[33,42] a noncovalent interaction (NCI) plot[20] analysis, and the electron localization function (ELF)[43] in combination with Bader's quantum theory of atoms in molecules (QTAIM).[44] Noncovalent interactions can be characterized and further visualized in real space with the NCI-plot[20] program. The great advantage of this program is insensitivity to the choice of computational method (same densities by different methods). The main function of the NCI-plot is to reveal whether the interaction is repulsive or attractive and to describe the strength of noncovalent bonding.[45,46] The map of electrostatic potential (MEP) visualizes the anisotropic charge distribution on the 0.001 au contour of a molecule's surface. That feature can be used to predict and interpret noncovalent interactions.[33,47,48] The electron localization function calculates and visualizes shared and unshared electron pairs. Previously this function has already been used in investigations of XBs and related interactions.[49−56] A combination of ELF and QTAIM analyses displays bond paths at the interaction areas, which helps to interpret the donor−acceptor nature of the interaction. A further analysis of the order of the ED (electron density) and ESP (electrostatic potential) minima along the bond paths[21,53−55,57−59] allows revealing the nucleophilic and electrophilic partners in the interactions.

While ESP and ELF + QTAIM analyses provide information about the donor−acceptor nature of interactions, an NCI-plot analysis reveals the strength and visualizes noncovalent interactions in real space.

The models for theoretical studies were directly cut from the corresponding experimental crystal structures, creating clusters: **1**·$(CHI_3)_4$; $(\mathbf{1})_2$·I_2, $(\mathbf{2})_2$·I_2, $(\mathbf{3})_2$·I_2; $(\mathbf{1})_2$·$(FIB)_{10}$, **2**·$(FIB)_{10}$, **3**·$(FIB)_{10}$.

2.3.1. Electrostatic Potential Surface (ESP) Analysis. An analysis of the anisotropic charge distribution visualized by a map of electrostatic potential (MEP) can explain observed noncovalent interactions.[14,60,61] In the case of halogen bonding an electron-deficient area (σ-hole located on the elongation of the covalent σ-bond) at the surface of the XB donor atom interacts with an electron-rich area at the surface of the XB acceptor atom. The directionality of the halogen bond is dependent on the σ-hole magnitude,[62] the value represented by the maximum of the ESP (V_{max}). Therefore, to estimate the geometry and strength of the noncovalent interaction V_{max} must be analyzed. As proposed by Bader et al., the electrostatic potential should be calculated at the 0.001 au contour of a molecule's surface since it illustrates 96% of the electronic charge of a molecule.[63]

All of the XBDs and XBAs were subjected to an analysis of anisotropic charge distribution. MEPs of XBAs (PtX_2COD, X = Cl, Br, I; Figure 5) visualized differences in the polarizability of halides in the Pt(II) complexes: polarizability increases in the order **3** < **2** < **1**. The least polarized chloride is least sensitive to the directionality of the halogen bond. In the case of XBDs almost similar V_{max} values were found for I_2 and FIB (Figure 6 and Table 5), and the smallest value was found for CHI_3. According to the V_{max} value both I_2 and FIB are more favorable XBDs than CHI_3 and therefore can form stronger XBs.

Although these values slightly differ from R_{IX} (CHI_3 ($\overline{R_{IX}}$ = 0.93), FIB ($\overline{R_{IX}}$ = 0.91), I_2 ($\overline{R_{IX}}$ = 0.85)) and the NCI-plot

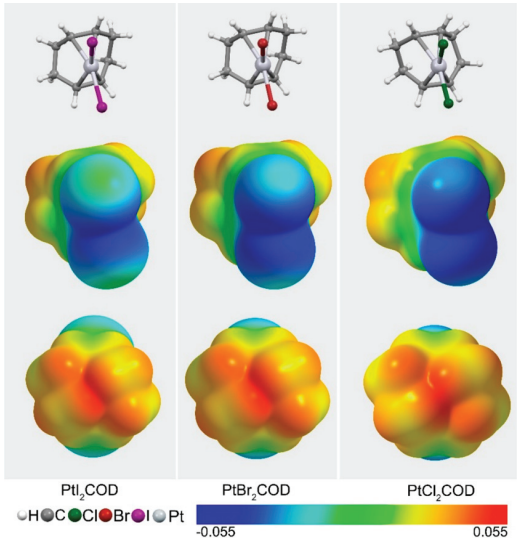

Figure 5. Electrostatic potential calculated at the PBE0-D3/def2-TZVP computational level on the 0.001 au molecular surface of PtX_2COD using the same color scale from −0.055 to +0.055 au.

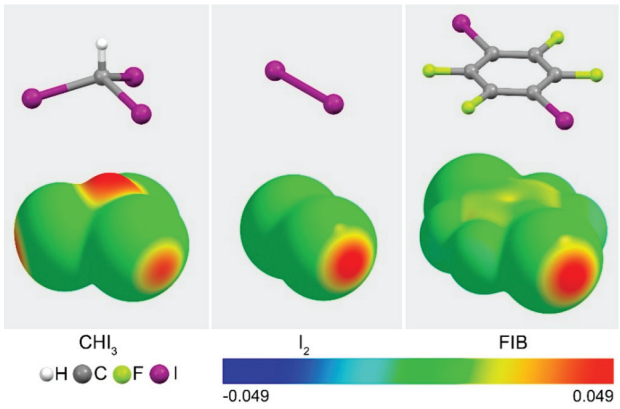

Figure 6. Electrostatic potential calculated at the PBE0-D3/def2-TZVP computational level on the 0.001 au molecular surface of CHI_3, I_2, and FIB using the same color scale from −0.049 to +0.049 au.

Table 5. Maximum ESP (V_{max}) Values of Selected Halogenated Molecules Calculated at the PBE0-D3/def2-TZVP Level

molecule	atom	V_{max}, au
CHI_3	I	0.042
	H	0.049
I_2	I	0.052
FIB	I	0.053

trend (see section 2.3.2) (CHI_3 ($\overline{\text{sign}(\lambda_2)\rho}$ = 0.0116), FIB ($\overline{\text{sign}(\lambda_2)\rho}$ = 0.0135), I_2 ($\overline{\text{sign}(\lambda_2)\rho}$ = 0.0196)), they give an estimation of the directionality and strength (the strongest possible is with I_2 and FIB) of the interaction.

2.3.2. NCI-Plot Analysis. To visualize noncovalent interactions in real space, the reduced electron density gradient (s) has to be plotted against $\text{sign}(\lambda_2)\rho$: interactions are visualized as spikes in the graph. Attractive interactions are located in the $-\text{sign}(\lambda_2)\rho$ area, and the stronger the interaction, the more negative $\text{sign}(\lambda_2)\rho$ is. To visualize noncovalent interactions in

https://dx.doi.org/10.1021/acs.cgd.0c01314
Cryst. Growth Des. XXXX, XXX, XXX−XXX

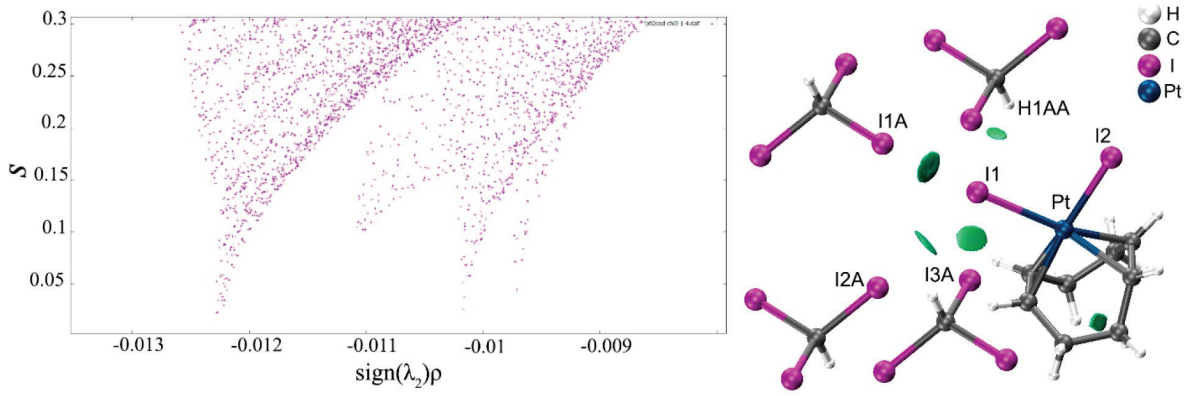

Figure 7. Plot of sign(λ_2)ρ vs s (left) and gradient isosurface (right, s = 0.3 au; in the [−0.013, − 0.008] au range of sign(λ_2)ρ) for the cluster **1**·$(CHI_3)_4$. Green isosurfaces on the 3D plot represent weak stabilizing interactions. All spikes in the 2D plot represent XBs, except the second spike, which represents a ring interaction in COD.

real space, an input of the 2D plot data is used to construct reduced density gradient isosurfaces. Obtained isosurfaces correspond to the spikes of the 2D plot, and the interaction strength is described by the color of the interaction. The plot is colored in the RGB (red−green−blue) scheme, where red represents strong destabilizing interactions, green delocalized medium to weak interactions, and blue strong stabilizing interactions. Low density value isosurfaces (i.e., −0.005 < sign(λ_2)ρ < 0.005 au) are associated with weaker dispersion interactions, while slightly higher density value isosurfaces (i.e., −0.05 < sign(λ_2)ρ < −0.005 au and 0.005 < sign(λ_2)ρ < 0.05 au) are associated with stronger noncovalent interactions.[64] To create a concise image, different cutoffs were applied, visualizing only the interactions in the region of interest. However, due to program limitations, the COD ring interaction was not cut out, although it is not considered relevant to the discussion.

To get an insight into the interactions in the obtained crystal structures, it was decided to use 2D NCI-plots for numerical descriptions and 3D plots for visualizations of interactions in real space.

2.3.2.1. CHI_3 Adduct. In the case of **1**·$(CHI_3)_4$ five relatively strong noncovalent interactions are located in the [−0.013, −0.008] au range of the sign(λ_2)ρ area (Figure 7 and Table 6).

Table 6. sign(λ_2)ρ Data on Noncovalent Interactions in the Adduct 1·$(CHI_3)_4$

interaction	sign(λ_2)ρ
I1A···I1−Pt1, I2A···I1−Pt1	−0.0123
COD ring	−0.0110
I3A···I1−Pt1	−0.0102
H1AA···I1−Pt1	−0.0097

According to the NCI-plot analysis the strength of interaction increases in the order H1AA···I1−Pt < I3A···I1−Pt < COD ring < I1A···I1−Pt ≈ I2A···I1−Pt; this correlates to the interaction strength deduced by SCXRD studies.

2.3.2.2. I_2 Adducts. In the case of I_2 clusters plots of s vs sign(λ_2)ρ have the same shape with slight differences (see Figure S6 in the Supporting Information). Two types of noncovalent interactions (XB and ring interaction in COD) were found in the [−0.022, 0.005] au range of sign(λ_2)ρ (Figure 8). In the 2D plots the leftmost spike represents an XB, the next spike represents a ring interaction in COD; sign(λ_2)ρ numerical values of the interactions are presented in Table 7.

According to an NCI-plot analysis the XB in the cluster $(\mathbf{2})_2$·I_2 is the weakest of the I_2 adduct series (sign(λ_2)ρ = −0.0191), while XB in $(\mathbf{1})_2$·I_2 and $(\mathbf{3})_2$·I_2 represent interactions of the same strength (sign(λ_2)ρ = −0.0198), although the difference among the three is quite small. On comparison of these results $(\mathbf{2})_2$·I_2 < $(\mathbf{1})_2$·I_2 ≈ $(\mathbf{3})_2$·I_2 with SCXRD deduced strengths **1**·$0.5I_2$ ≈ **2**·$0.5I_2$ < **3**·I_2, it can be seen in both cases the I_2 adduct with **3** is involved in the strongest XB interaction.

2.3.2.3. FIB Adducts. In the series of FIB adducts various noncovalent interactions were found in the [−0.018, −0.006] au range of sign(λ_2)ρ (Figure 9 and Table 8). The patterns of 2D plots appear similar for the isomorphic structures **2**·$(FIB)_{10}$ and **3**·$(FIB)_{10}$. The strength of the XB estimated with the distance reduction ratio R_{IX} increases in the order $(\mathbf{1})_2$·$(FIB)_{10}$ < **2**·$(FIB)_{10}$ ≈ **3**·$(FIB)_{10}$, which correlates with the strength trend by an NCI-plot analysis (Table 8). Moreover, an NCI-plot analysis revealed other types of stabilizing interactions among the adducts such as Pt···I, a F···π interaction, and an I2···‖ (COD double bond) interaction exclusively for $(\mathbf{1})_2$·$(FIB)_{10}$ (detailed information on F···π and I···‖ interactions can be found in Table S6 and Figure S7 in the Supporting Information). Although these types of interactions are weaker than XBs, they are still located in an area more negative than weaker dispersive interactions (−0.005 < sign(λ_2)ρ < 0.005 au), providing extra stabilization in the structure. Despite the presence of the sterically hindering COD ligand, a Pt···I contact was found in all of the FIB adducts. The strength of the Pt···I interaction increases in the order **2**·$(FIB)_{10}$ < **3**·$(FIB)_{10}$ < $(\mathbf{1})_2$·$(FIB)_{10}$. Possibly the strength of the XB becomes weaker due to a competition of the XB and an attractive Pt···I interaction between **1** and the FIB molecule. This correlates with the trend deduced by SCXRD analysis that for a wider Pt−X···I angle a stronger XB interaction is observed.

On the basis of the average sign(λ_2)ρ parameter among the CHI_3, I_2, and FIB series of adducts the strength of XB increases in the order CHI_3 ($\overline{\text{sign}(\lambda_2)\rho}$ = −0.0116) < FIB ($\overline{\text{sign}(\lambda_2)\rho}$= −0.0135) < I_2 ($\overline{\text{sign}(\lambda_2)\rho}$ = −0.0196). This estimation is in the agreement with the experimental evaluation based on the average R_{IX} parameter. Although NCI-plot analysis gives information about the topology and strength of interactions, it cannot determine the donor−acceptor nature of the

https://dx.doi.org/10.1021/acs.cgd.0c01314
Cryst. Growth Des. XXXX, XXX, XXX−XXX

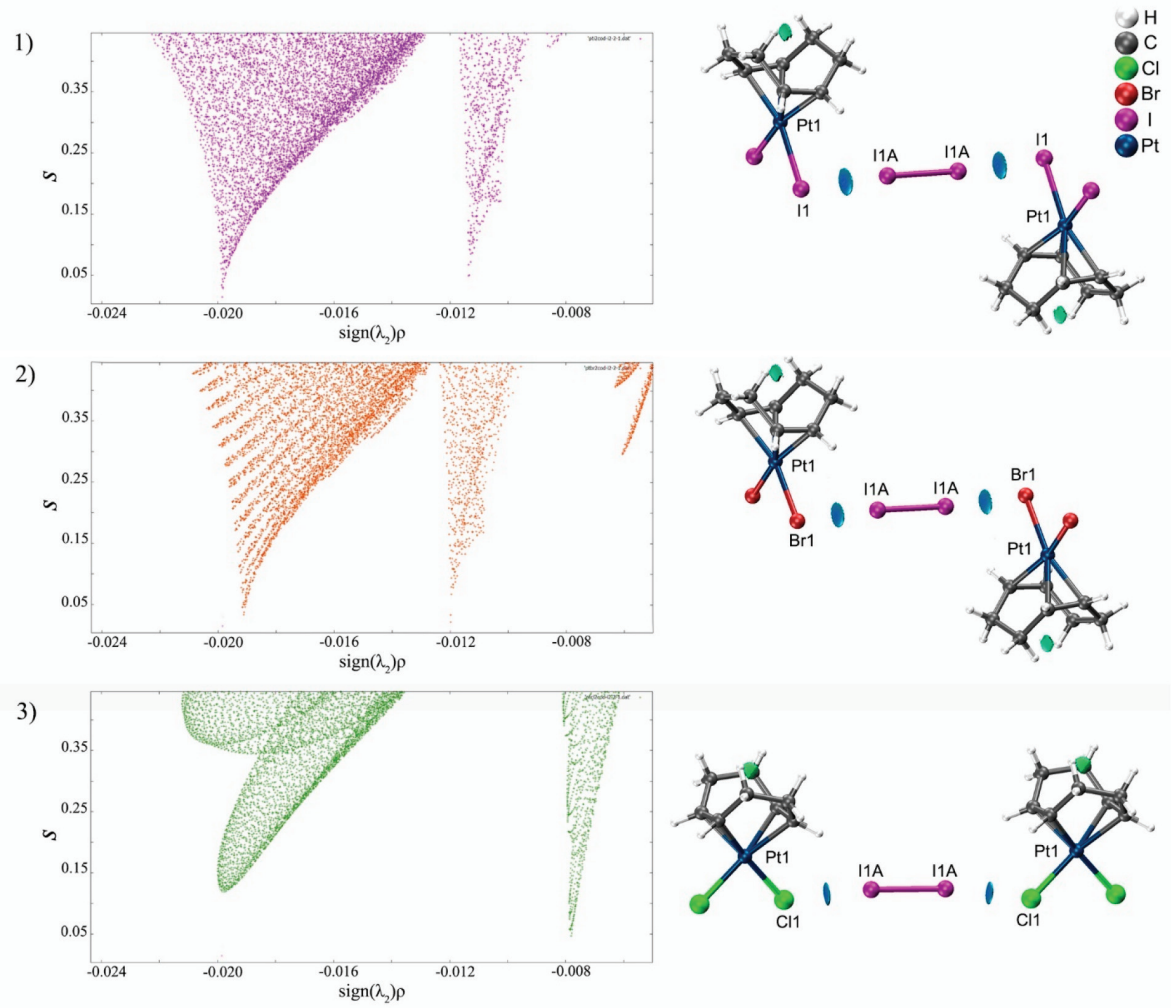

Figure 8. Plots of the sign(λ_2)ρ vs s (left) and gradient isosurfaces (right, s = 0.3 au; in the [−0.022, − 0.005] au. range of sign(λ_2)ρ) for (1) $(\mathbf{1})_2{\cdot}I_2$, (2) $(\mathbf{2})_2{\cdot}I_2$, and (3) $(\mathbf{3})_2{\cdot}I_2$. 2D plots are colored such that purple, orange, and green represent plots for **1**, **2**, and **3** clusters with I_2, respectively, The isosurfaces on the 3D plots are colored such that blue and green represent very strong and medium to weak stabilizing interactions, respectively. The leftmost spike in all 2D plots represents an XB, and the second spike from the left represents a ring interaction in COD.

Table 7. sign(λ_2)ρ Data on Noncovalent Interactions in PtX_2COD (X = Cl, Br, I) Adducts with I_2

	sign(λ_2)ρ		
interaction	$(\mathbf{1})_2{\cdot}I_2$	$(\mathbf{2})_2{\cdot}I_2$	$(\mathbf{3})_2{\cdot}I_2$
I1A···X−Pt1	−0.0198	−0.0191	−0.0198
COD ring	−0.0113	−0.0119	−0.0078

interactions. However, ELF + QTAIM and ED/ESP minima studies can give an insight into the nature of the interaction, and they are discussed in section 2.3.3.

2.3.3. Electron Localization Function (ELF) Analysis. In order to get more information about the weak interactions under study, a topological analysis of the electron density distribution (within the formalism of Bader's QTAIM method)[44] for the $\mathbf{1}{\cdot}(CHI_3)_4$, $(\mathbf{1})_2{\cdot}I_2$, $(\mathbf{2})_2{\cdot}I_2$, $(\mathbf{3})_2{\cdot}I_2$, $(\mathbf{1})_2{\cdot}(FIB)_{10}$, $\mathbf{2}{\cdot}(FIB)_{10}$, and $\mathbf{3}{\cdot}(FIB)_{10}$ clusters as model systems was performed, followed by a calculation and analysis of the electron localization function (ELF).[43,65−67] The ELF is a derivative of the electron density, which allows the location of areas of shared and unshared electron pairs. A combination of ELF and QTAIM methods is represented in Figures 10−Figure 14, where ELF projections were plotted together with bond (3, −1) critical points (blue), nuclear (3, −3) critical points (brown), ring (3, +1) critical points (orange), and bond paths (black lines).

In $\mathbf{1}{\cdot}(CHI_3)_4$, the I···I bond paths (Figure 10) go through the ELF > 0.75 areas on the iodine I atoms (i.e., through the lone pairs) and through depleted ELF regions on the iodoform I atoms corresponding to a reduced shielding of I nuclei in the σ-holes. These observations confirm the XB nature of the I···I interactions, where iodide ligands represent nucleophiles and iodoform molecules represent electrophiles.

The same observations were performed for $(\mathbf{1})_2{\cdot}I_2$ and $(\mathbf{2})_2{\cdot}I_2$ (Figure 11), $(\mathbf{3})_2{\cdot}I_2$ (Figure 12), $\mathbf{2}{\cdot}(FIB)_{10}$ and $\mathbf{3}{\cdot}(FIB)_{10}$ (Figure 13), and halogen-bonding bond paths go through lone pairs on the halide ligands and the σ-holes on I atoms in XB donors. It is notable that in the case of the $(\mathbf{1})_2{\cdot}I_2$ and $(\mathbf{2})_2{\cdot}I_2$ clusters (Figure 11) ELF areas, bond critical points, and bond path locations are the same for both clusters, revealing the similarity in nature of the noncovalent interactions. Supposedly, the similarity follows the isomorphism of the correspond-

https://dx.doi.org/10.1021/acs.cgd.0c01314
Cryst. Growth Des. XXXX, XXX, XXX−XXX

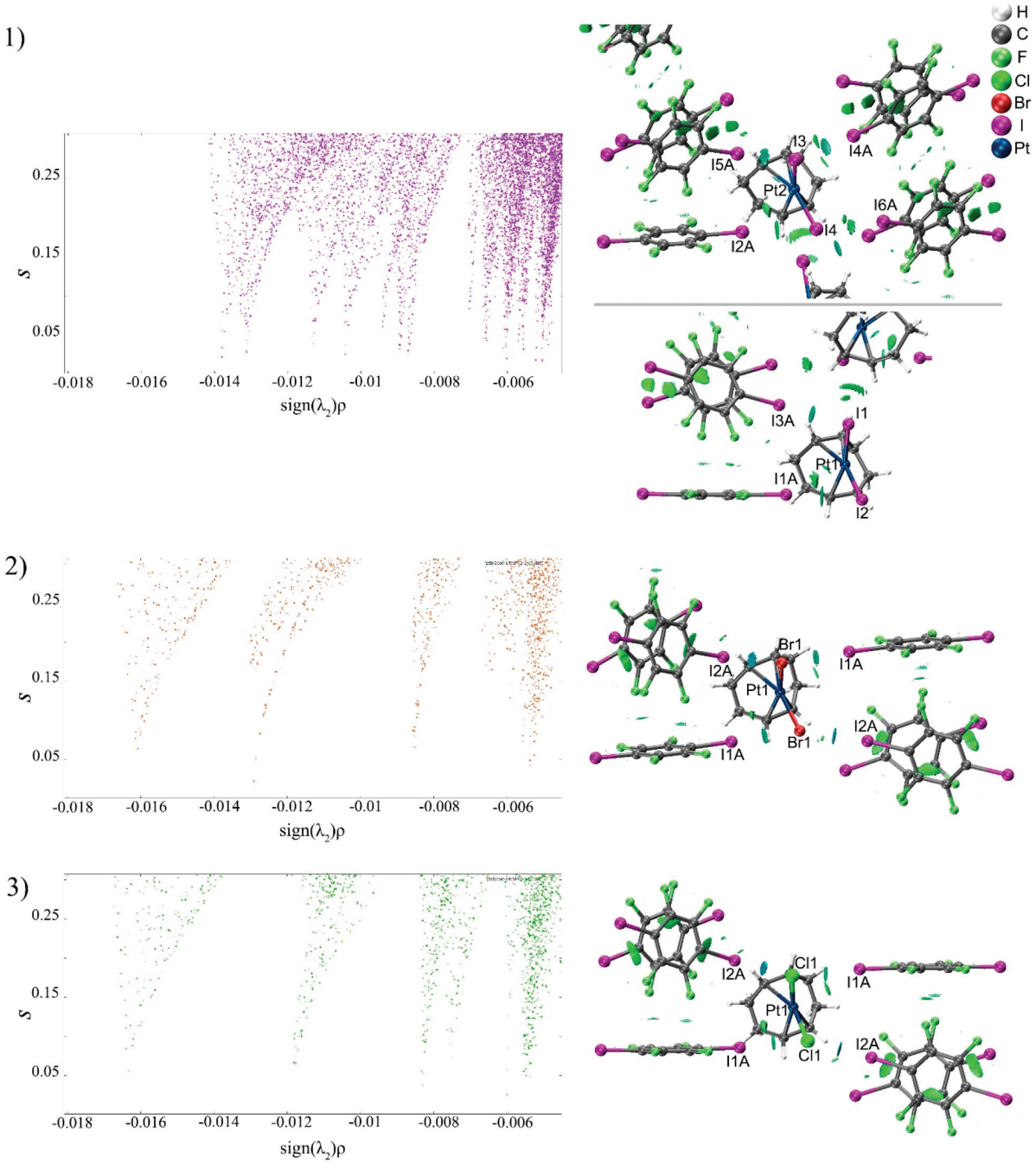

Figure 9. Plot of sign(λ_2)ρ vs s (left) and gradient isosurface (right, s = 0.3 au; in the [−0.018, −0.0045] au range of sign(λ_2)ρ) for (1) $(\mathbf{1})_2\cdot(\mathrm{FIB})_{10}$, (2) $\mathbf{2}\cdot(\mathrm{FIB})_{10}$, and (3) $\mathbf{3}\cdot(\mathrm{FIB})_{10}$. The isosurfaces on the 3D plots are colored such that blue and green represent strong and medium to weak stabilizing interactions, respectively. The leftmost spike in all 2D plots represents an XB, which is shown in blue.

ing crystals. The same trend is observed for $\mathbf{2}\cdot(\mathrm{FIB})_{10}$ and $\mathbf{3}\cdot(\mathrm{FIB})_{10}$ (Figure 13).

In the case of $(\mathbf{1})_2\cdot(\mathrm{FIB})_{10}$ (Figure 14), two of the C−I···I−Pt XBs are followed by the C−I···Pt interactions, as confirmed by bond paths and bond critical points. The nature of these interactions is not clear, because the I···Pt bond paths go through the ELF areas between the maximum and minimum on the I atoms. Platinum(II) centers can be both electrophiles[68,69] and nucleophiles[5,31,70] in I···Pt in the other systems.

More information about the philicity of interacting atoms in noncovalent interactions can be obtained by an analysis of the order of the ED (electron density) and ESP (electrostatic potential) minima along the bond path.[21,53−55,57−59] The minimum of ESP is shifted toward the nucleophilic atom, while the ED minimum is shifted toward the electrophilic atom. The 1D profiles of the ED and ESP functions along the I···X (X = Cl, Br, I) bond paths confirmed the nucleophilic nature of the halides toward diiodine and organoiodides due to a valuable

https://dx.doi.org/10.1021/acs.cgd.0c01314
Cryst. Growth Des. XXXX, XXX, XXX−XXX

Table 8. sign(λ_2)ρ Data on Noncovalent Interactions in $(\mathbf{1})_2\cdot(FIB)_{10}$, $\mathbf{2}\cdot(FIB)_{10}$, and $\mathbf{3}\cdot(FIB)_{10}$ in the [−0.018, − 0.006] au Range of sign(λ_2)ρ)

$(\mathbf{1})_2\cdot(FIB)_{10}$		$\mathbf{2}\cdot(FIB)_{10}$		$\mathbf{3}\cdot(FIB)_{10}$	
interaction	sign(λ_2)ρ	interaction	sign(λ_2)ρ	interaction	sign(λ_2)ρ
I1A···I2−Pt1	−0.0138				
I5A···I3−Pt2	−0.0131	I2A···Br1−Pt1	−0.0161	I2A···Cl1−Pt1	−0.0163
I4A···I3−Pt2	−0.0131				
I6A···I4−Pt2	−0.0094				
I3A···I1−Pt1	−0.0113	I1A···Br1−Pt1	−0.0129	I1A···Cl1−Pt1	−0.0118
I2A···I4−Pt2	−0.0104				
I4A···Pt2	−0.0066				
I1A···Pt1	−0.0089	I1A···Pt1	−0.0065	I1A···Pt1	−0.0075
I2A···Pt2	−0.0087				

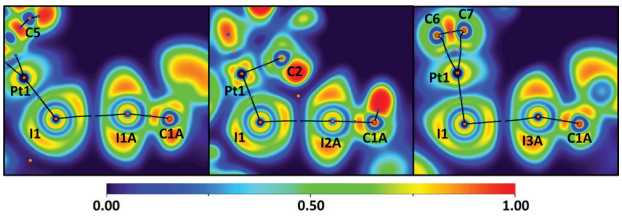

Figure 10. ELF projections and bond paths (black lines), BCPs (blue dots), NCPs (brown dots), and RCPs (orange dots) for the C−I···I−Pt XBs in $\mathbf{1}\cdot(CHI_3)_4$.

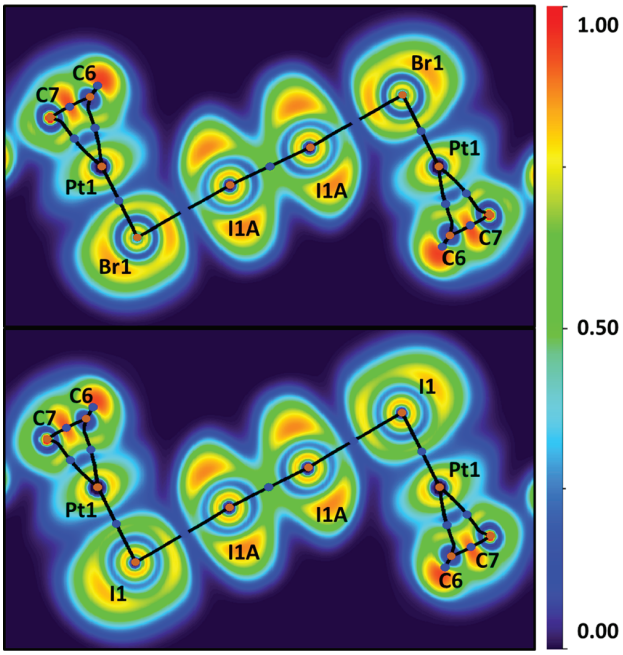

Figure 11. ELF projections for the I−I···X−Pt XBs in $(\mathbf{2})_2\cdot I_2$ (top, X = Br) and $(\mathbf{1})_2\cdot I_2$ (bottom, X = I).

shift of the ESP minima to the halide electron density basins in all cases (Figures S8−S12 in the Supporting Information).

The analogous 1D profiles of the ED and ESP functions along the I1A···Pt1 and I2A···Pt2 bond paths in $(\mathbf{1})_2\cdot(FIB)_{10}$ indicate (Figure 15) that the ESP minima in both cases are only slightly shifted to the Pt electron density basins.

This shift may be interpreted as the nucleophilicity of Pt toward I in both cases. It means that I1A···Pt1 and I2A···Pt2 can both be treated as metal-involving halogen bonding.

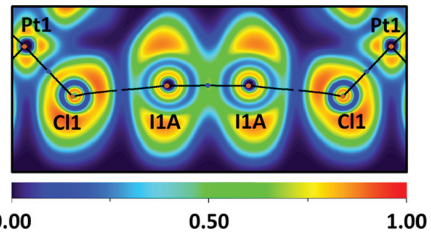

Figure 12. ELF projection and bond paths (black lines), BCPs (blue dots), NCPs (brown dots), and RCPs (orange dots) for the I−I···Cl−Pt XBs in $(\mathbf{3})_2\cdot I_2$.

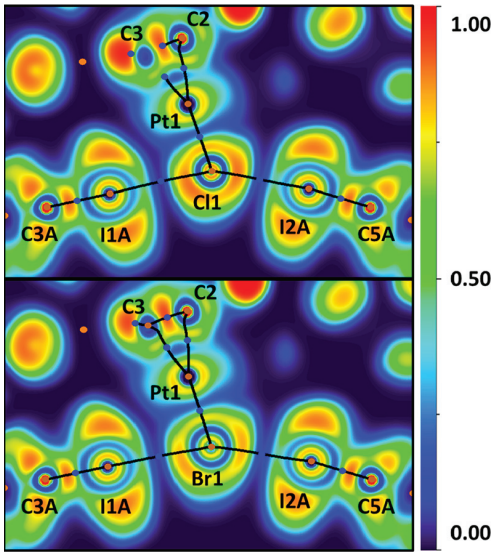

Figure 13. ELF projection and bond paths (black lines), BCPs (blue dots), NCPs (brown dots), and RCPs (orange dots) for the C−I···X−Pt XBs in $\mathbf{3}\cdot(FIB)_{10}$ (X = Cl, top) and $\mathbf{2}\cdot(FIB)_{10}$ (X = Br, bottom).

However, low values of the shifts, together with the geometrical parameters of the contacts ($\angle$(C1A−I1A···Pt1) = 142.14(18)° and $\angle$(C4A−I2A···Pt2) = 141.13(17)°; d(I1A···Pt1) = 3.7990(6) Å and d(I2A···Pt2) = 3.8127(4) Å, more than $R^{I}_{vdW} + R^{Pt}_{vdW}$ = 3.73 Å), still preserve the possibility of intermediate[68] or even invert[69] philicity in the I···Pt interactions.

3. CONCLUSIONS

Novel adducts of platinum(II) halide 1,5-cyclooctadiene (COD) complexes with classical XB donors were successfully

https://dx.doi.org/10.1021/acs.cgd.0c01314
Cryst. Growth Des. XXXX, XXX, XXX−XXX

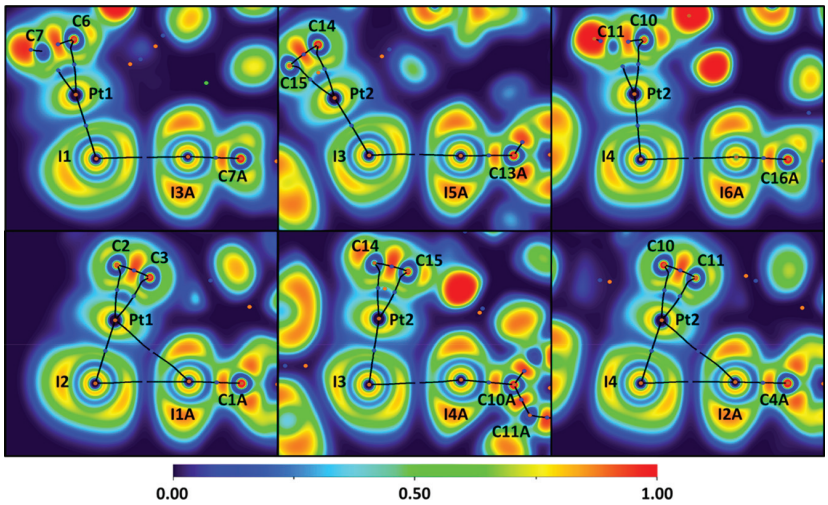

Figure 14. ELF projection and bond paths (black lines), BCPs (blue dots), NCPs (brown dots), and RCPs (orange dots) for the C–I···X–Pt XBs and the C–I···Pt interactions in $(\mathbf{1})_2 \cdot (FIB)_{10}$.

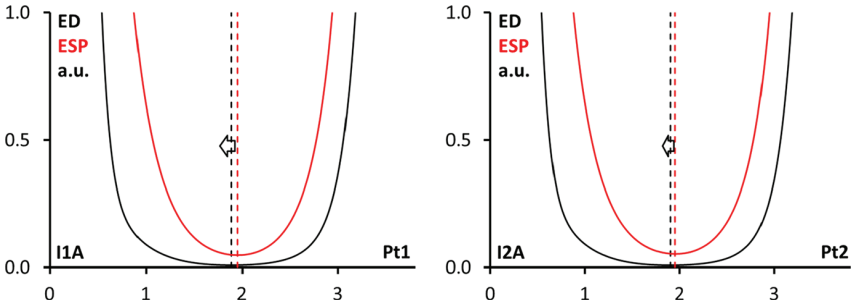

Figure 15. Criterion of ED minimum vs ESP minimum: the ED (black) and the ESP (red) for the I1A···Pt1 and I2A···Pt2 interactions in $(\mathbf{1})_2 \cdot (FIB)_{10}$. Interatomic distances are given in Å.

crystallized for the first time. When the halide in the complex was changed, various geometries in the adducts were achieved. Within the $PtX_2COD \cdot n$XBD series one pair of isomorphic cocrystals was always formed: $PtBr_2COD/PtI_2COD$ in cocrystals with I_2 and $PtCl_2COD/PtBr_2COD$ in cocrystals with FIB. Interestingly, the adducts of $PtBr_2COD$ are always involved in isomorphism. This shows the intermediate nature of Br in the row Cl–Br–I.

All of the structures have unique properties. The adduct $PtI_2COD \cdot CHI_3$ represents the first example of a transition-metal iodide complex with CHI_3. The fact that neither substitution of halide in the PtX_2 COD complex nor Pt(II) oxidation takes place in cocrystallizations with I_2 is a rare feature of these cocrystals, allowing the building of supramolecular systems containing Pt(II) centers. Moreover, in the case of $PtX_2COD \cdot nI_2$ complexes, small changes in the complex composition, such as a variation of the halide, gives a possibility of switching from an isolated cluster to a polymeric structure. $PtX_2COD \cdot n$FIB adducts contain such unusual noncovalent interactions as I···Pt, F···π, and I2···|| interactions, giving additional stabilization to the adduct together with classical halogen bonding.

Computational studies revealed that halogen bonds are the strongest noncovalent stabilizing interactions in all the obtained systems, confirming an important role of XB in crystal engineering. According to the NCI-plot studies strength of halogen bonding is increasing in the row CHI_3, FIB, I_2, and this trend agrees with SCXRD studies. Another type of weak interactions found in FIB adducts is possible I···Pt metal involving halogen bonding. This type of contact was studied with a novel combination of ELF + QTAIM analyses. The method has revealed the nucleophilicity of the Pt center toward I of the FIB molecule, deepening the understanding of the donor/acceptor pairing.

To summarize, in this work we have successfully applied noncovalent interactions, in particular halogen bonding, as an instrument to create various supramolecular clusters. When halides of the system are modified, it is possible to influence the strength of the interaction and cluster size. Understanding these trends allows the use of noncovalent interactions as a tool to build novel metallopolymers.

4. EXPERIMENTAL SECTION

4.1. General Computational Details. All of the obtained systems were analyzed within the scope of DFT theory. In the calculation of noncovalently bonded systems it is important to consider dispersion forces: for example, a the D3 dispersion correction of Grimme can be applied.[71] The PBE0-D3 dispersion corrected functional is a good option for systems containing noncovalent interactions.[71−75] While for most atoms the 6-31G* basis set will perform well, in case of the XB series with various halides one needs to consider adding basis set optimization for halides. For this purpose the def2-TZVP basis set[76] with a pseudopotential for the inner-core electrons can be used. This basis set can be obtained from the basis set exchange database.[77] The use of the def2-TZVP basis set

https://dx.doi.org/10.1021/acs.cgd.0c01314
Cryst. Growth Des. XXXX, XXX, XXX–XXX

with effective core potential (ECP) for heavy atoms is good for reducing computational cost in systems with many heavy elements (heavier than Kr) and describing relativistic effects in deep core electrons.[78] Wave function files were obtained in the Gaussian 09 (revision D.01) program package.[79] Complexes **1**−**3**, CHI_3, I_2, and FIB were subjected to full energy minimization using the PBE0-D3 dispersion corrected functional with a 6-31G* basis set for all atoms except for chlorine, bromine, iodine, and platinum, for which a def2-TZVP basis with a pseudopotential for the inner-core electrons was used. The models for the solid-state structures were directly cut from the corresponding experimental crystal structures (creating clusters **1**·$(CHI_3)_4$, $(\mathbf{1})_2{\cdot}I_2$, $(\mathbf{2})_2{\cdot}I_2$, $(\mathbf{3})_2{\cdot}I_2$, $(\mathbf{1})_2{\cdot}(FIB)_{10}$, **2**·$(FIB)_{10}$, and **3**·$(FIB)_{10}$) and analyzed without geometry optimization due to complexity. The strength and topology of the interactions were studied with the NCI-plot program[20] implemented in Critic2 software,[80] and 2D and 3D visualizations were performed with the Gnuplot[81] and VMD programs,[82] respectively. ESP surfaces of the PtX_2COD and XBD molecules were calculated and visualized with AIMALL.[83] ELF projections and QTAIM analyses were performed with Multiwfn 3.7.[84] Coordinates and numbering for single molecules and clusters can be found in Tables S7−S13 in the Supporting Information.

4.2. General Experimental Details. All chemicals and solvents such as $CHCl_3$ (VWR Chemicals BDH), EtOH (99.5%, Altia Industrial), diisopropyl ether (≥98.5%, Fluka Chemical Corp.), K_2PtCl_4 (99.9%, Alfa Aesar), KBr (99%, J.T. Baker), KI (≥99.0%, Fisher Scientific), COD (≥98.0%, Aldrich), $PtCl_2COD$ (99%, Strem Chemicals), I_2 (Mallinckrodt), CHI_3 (>99%, Fluka AG), and FIB (99%, Fluorochem) were used without additional purification.

The crystal data for all of the obtained adducts are summarized in Tables S3−S5 in the Supporting Information. For each experiment a single crystal was selected from the sample under a microscope in darkness (except for the light from the microscope itself), immersed in cryo-oil, and mounted in a MiTeGen loop SCXRD data for the measurement. Single crystals were measured on a Bruker-Nonius Kappa CCD diffractometer with an APEX-II CCD detector using graphite-monochromated Mo Kα (λ = 0.71073 Å) radiation at 170 K. The data collection and reduction for data processing was performed using the programs DENZO and SCALEPACK.[85] The intensities for data collected by the Bruker-Nonius Kappa diffractometer were corrected for absorption using SADABS[86] with the multiscan absorption correction type method. All structures were solved with direct methods (SHELXT-2015)[87] and refined by full-matrix least squares on F^2 using the OLEX2[88] software, which utilizes the SHELXL-2015[89] module. All H atoms were positioned geometrically and constrained to ride on their parent atoms: U_{iso} = 1.2U_{eq}(parent atom).

Caution! COD is hazardous to health and should be handled with care.

PtX_2COD complexes were synthesized according to the procedure reported by Rigamonti et al.[28] with slight modifications.

*4.2.1. Synthesis of PtI_2COD (**1**).* K_2PtCl_4 (1 mmol, 418.6 mg) was dissolved in 10 mL of distilled water, and then KI (5 mmol, 834 mg) was added to the mixture and it was stirred for 1 h; the solution turned brown. After that 10 mL of 100% glacial acetic acid and COD (4 mmol, 432.7 mg, 0.49 mL) were added sequentially. The mixture was stirred at 80 °C overnight to give was a transparent reddish solution with a yellow precipitate. The precipitate was filtered off with a Buchner funnel and successively washed with 25 mL of H_2O, 30 mL of EtOH, and 25 mL of diisopropyl ether. After that yellow precipitate was dissolved in $CHCl_3$ and left for recrystallization at RT by slow solvent evaporation. Yield: 439.4 mg (79%).

*4.2.2. Synthesis of $PtBr_2COD$ (**2**).* K_2PtCl_4 (0.5 mmol, 207.6 mg) was dissolved in 5 mL of distilled water, and then KBr (2.5 mmol, 297.5 mg) was added to the mixture and it was stirred for 1 h; and the solution turned reddish. After that 5 mL of 100% glacial acetic acid and COD (3 mmol, 216.4 mg, 0.25 mL) were added sequentially. The mixture was stirred at 80 °C overnight to give a yellow solution with a yellow precipitate. The precipitate was filtered off of the solution with a Buchner funnel and successively washed with 10 mL of H_2O, 15 mL of EtOH, and 10 mL of diisopropyl ether. After that the yellow precipitate was dissolved in $CHCl_3$ and left for recrystallization at RT by slow solvent evaporation. Yield: 187.8 mg (0.41 mmol, 81%).

4.2.3. Cocrystallizations of PtI_2COD with Halogen-Bond Donors. PtI_2COD (0.03 mmol, 16.7 mg) was dissolved in 2 mL of $CHCl_3$, and 0.06 mmol of the halogen-bond donor was added sequentially. The solution was stirred until the mixture became homogeneous and then left for crystallization at RT by slow solvent evaporation.

Anal. Found for $PtI_2COD{\cdot}I_2$: C, 14.47; H, 1.86; N, 0.00. Calcd: C, 14.05; H, 1.77; N, 0.00. Found for $PtI_2COD{\cdot}CHI_3$: C, 11.60; H, 1.6; N, 0.01. Calcd: C, 11.37; H, 1.38; N, 0.00. Found for $PtI_2COD{\cdot}1,4\text{-}C_6F_4I_2$: C, 17.48; H, 1.17; N, 0.00. Calcd: C, 17.60; H, 1.04; N, 0.00.

4.2.4. Cocrystallizations of $PtBr_2COD$ with Halogen-Bond Donors. $PtBr_2COD$ (0.02 mmol, 9.3 mg) was dissolved in 2 mL of $CHCl_3$, and 0.04 mmol of the halogen-bond donor was added sequentially. The solution was stirred until the mixture became homogeneous and then left for crystallization at RT by slow solvent evaporation.

Anal. Found for $PtBr_2COD{\cdot}I_2$: C, 16.59; H, 2.14; N, 0.00. Calcd: C, 16.29; H, 2.05; N, 0.00. Found for $PtBr_2COD{\cdot}1,4\text{-}C_6F_4I_2$: C, 19.45; H, 1.40; N, 0.00. Calcd: C, 18.96; H, 0.96; N, 0.00.

4.2.5. Cocrystallizations of $PtCl_2COD$ with Halogen-Bond Donors. $PtCl_2COD$ (0.03 mmol, 11.2 mg) was dissolved in 2 mL of $CHCl_3$, and 0.06 mmol of the halogen-bond donor was added sequentially. The solution was stirred until the mixture became homogeneous and then left for crystallization at RT by slow solvent evaporation.

Anal. Found for $PtCl_2COD{\cdot}I_2$: C, 19.14; H, 2.36; N, 0.00. Calcd: C, 19.18; H, 2.41; N, 0.00. Found for $PtCl_2COD{\cdot}1,4\text{-}C_6F_4I_2$: C, 21.38; H, 1.23; N, 0.00. Calcd: C, 20.39; H, 1.03; N, 0.00.

■ ASSOCIATED CONTENT

Supporting Information

The Supporting Information is available free of charge at https://pubs.acs.org/doi/10.1021/acs.cgd.0c01314.

Details of computational, crystallographic, and ^{195}Pt NMR studies (PDF)

Accession Codes

CCDC 2031113−2031119 contain the supplementary crystallographic data for this paper. These data can be obtained free of charge via www.ccdc.cam.ac.uk/data_request/cif, or by emailing data_request@ccdc.cam.ac.uk, or by contacting The Cambridge Crystallographic Data Centre, 12 Union Road, Cambridge CB2 1EZ, UK; fax: +44 1223 336033.

■ AUTHOR INFORMATION

Corresponding Author

Matti Haukka − *Department of Chemistry, University of Jyväskylä, FI-40014 Jyväskylä, Finland;* orcid.org/0000-0002-6744-7208; Email: matti.o.haukka@jyu.fi

Authors

Margarita Bulatova − *Department of Chemistry, University of Jyväskylä, FI-40014 Jyväskylä, Finland;* orcid.org/0000-0002-1904-5394

Daniil M. Ivanov − *Institute of Chemistry, Saint Petersburg State University, Saint Petersburg 199034, Russia;* orcid.org/0000-0002-0855-2251

Complete contact information is available at: https://pubs.acs.org/10.1021/acs.cgd.0c01314

Author Contributions

M.B. performed synthesis, crystallizations, SCXRD studies, computations of wave functions, and ESP and NCI-plot analysis, as well as manuscript preparation. D.M.I. performed

https://dx.doi.org/10.1021/acs.cgd.0c01314
Cryst. Growth Des. XXXX, XXX, XXX−XXX

ELF and QTAIM analysis. Both M.B. and D.M.I. contributed to data interpretation and analysis. M.H. guided the research and experimental design. The manuscript was written through contributions of all authors. All authors have given approval to the final version of the manuscript.

Funding

This work was supported by the Academy of Finland (Project No. 295581). Experimental and theoretical investigations of the adducts with [PtI_2(COD)] were supported by the Russian Science Foundation (Project No. 19-73-10016 for D.M.I.).

Notes

The authors declare no competing financial interest.

■ ACKNOWLEDGMENTS

We thank Elina Hautakangas for help in elemental analysis studies and Alberto Otero de la Roza for his consultations on the Critic2 program.

■ ABBREVIATIONS

BCP, bond critical point; COD, 1,5-cyclooctadiene; EA, elemental analysis; ELF, electron localization function; ESP, electrostatic potential; FIB, 1,4-diiodotetrafluorobenzene; MEP, map of electrostatic potential; NCI-plot, noncovalent interactions plot; NCP, nuclear critical point; QTAIM, quantum theory of atoms in molecules; RCP, ring critical point; SCXRD, single-crystal X-ray diffraction; XB, halogen bond; XBD, halogen-bond donor; XBA, halogen-bond acceptor

■ REFERENCES

(1) Williams, J. A. G. Photochemistry and Photophysics of Coordination Compounds. In *Platinum BT - Photochemistry and Photophysics of Coordination Compounds II*; Balzani, V., Campagna, S., Eds.; Springer Berlin Heidelberg: Berlin, Heidelberg, 2007; pp 205−268. DOI: 10.1007/128_2007_134.

(2) Eryazici, I.; Moorefield, C. N.; Newkome, G. R. Square-Planar Pd(II), Pt(II), and Au(III) Terpyridine Complexes: Their Syntheses, Physical Properties, Supramolecular Constructs, and Biomedical Activities. *Chem. Rev.* **2008**, *108*, 1834−1895.

(3) Gossage, R. A.; Ryabov, A. D.; Spek, A. L.; Stufkens, D. J.; van Beek, J. A. M.; van Eldik, R.; van Koten, G. Models for the Initial Stages of Oxidative Addition. Synthesis, Characterization, and Mechanistic Investigation of H1-I2 Organometallic "Pincer" Complexes of Platinum. X-Ray Crystal Structures of [PtI(C6H3-{CH2NMe2}2−2,6)(H1-I2)] and Exo-Meso-[Pt(H1-I3)(H1. *J. Am. Chem. Soc.* **1999**, *121*, 2488−2497.

(4) Ivanov, D. M.; Kirina, Y. V.; Novikov, A. S.; Starova, G. L.; Kukushkin, V. Y. Efficient π-Stacking with Benzene Provides 2D Assembly of Trans-[PtCl2(p-CF3C6H4CN)2]. *J. Mol. Struct.* **2016**, *1104*, 19−23.

(5) Baykov, S. V.; Dabranskaya, U.; Ivanov, D. M.; Novikov, A. S.; Boyarskiy, V. P. Pt/Pd and I/Br Isostructural Exchange Provides Formation of C-I···Pd, C-Br···Pt, and C-Br···Pd Metal-Involving Halogen Bonding. *Cryst. Growth Des.* **2018**, *18*, 5973−5980.

(6) Hildebrand, A.; Sarosi, I.; Lonnecke, P.; Silaghi-Dumitrescu, L.; Sarosi, M. B.; Silaghi-Dumitrescu, I.; Hey-Hawkins, E. Heteropolytopic Arsanylarylthiolato Ligands: Cis-Trans Isomerism of Nickel(II), Palladium(II), and Platinum(II) Complexes of 1-AsPh2−2-SHC6H4. *Inorg. Chem.* **2012**, *51*, 7125−7133.

(7) Petz, W.; Kutschera, C.; Neumuller, B. Reaction of the Carbodiphosphorane Ph3PCPPh3 with Platinum(II) and -(0) Compounds: Platinum Induced Activation of C-H Bonds. *Organometallics* **2005**, *24*, 5038−5043.

(8) Lachachi, M. B.; Benabdallah, T.; Aguiar, P. M.; Youcef, M. H.; Whitwood, A. C.; Lynam, J. M. Synthesis of a Series of New Platinum Organometallic Complexes Derived from Bidentate Schiff-Base Ligands and Their Catalytic Activity in the Hydrosilylation and Dehydrosilylation of Styrene. *Dalton Trans.* **2015**, *44*, 11919−11928.

(9) Bosch, E.; Kruse, S. J.; Krueger, H. R.; Groeneman, R. H. Role of π-π Stacking and Halogen Bonding by 1,4-Diiodoperchlorobenzene To Organize the Solid State To Achieve a [2 + 2] Cycloaddition Reaction. *Cryst. Growth Des.* **2019**, *19*, 3092−3096.

(10) Carreras, L.; Benet-Buchholz, J.; Franconetti, A.; Frontera, A.; van Leeuwen, P. W. N. M.; Vidal-Ferran, A. Halogen Bonding Effects on the Outcome of Reactions at Metal Centres. *Chem. Commun.* **2019**, *55*, 2380−2383.

(11) Desiraju, G. R.; Ho, S. P.; Kloo, L.; Legon, A. C.; Marquardt, R.; Metrangolo, P.; Politzer, P.; Resnati, G.; Rissanen, K. Definition of the Halogen Bond (IUPAC Recommendations 2013). *Pure Appl. Chem.* **2013**, *85*, 1711.

(12) Hassel, O. Structural Aspects of Interatomic Charge-Transfer Bonding. *Science* **1970**, *170*, 497−502.

(13) Politzer, P.; Murray, J. S. Halogen Bonding: An Interim Discussion. *ChemPhysChem* **2013**, *14*, 278.

(14) Cavallo, G.; Metrangolo, P.; Milani, R.; Pilati, T.; Priimagi, A.; Resnati, G.; Terraneo, G. The Halogen Bond. *Chem. Rev.* **2016**, *116*, 2478−2601.

(15) Teyssandier, J.; Mali, K. S.; De Feyter, S. Halogen Bonding in Two-Dimensional Crystal Engineering. *ChemistryOpen* **2020**, *9*, 225−241.

(16) Metrangolo, P.; Resnati, G.; Pilati, T.; Liantonio, R.; Meyer, F. Engineering Functional Materials by Halogen Bonding. *J. Polym. Sci., Part A: Polym. Chem.* **2007**, *45*, 1−15.

(17) Priimagi, A.; Cavallo, G.; Forni, A.; Gorynsztejn-Leben, M.; Kaivola, M.; Metrangolo, P.; Milani, R.; Shishido, A.; Pilati, T.; Resnati, G. Halogen Bonding versus Hydrogen Bonding in Driving Self-Assembly and Performance of Light-Responsive Supramolecular Polymers. *Adv. Funct. Mater.* **2012**, *22*, 2572.

(18) Berger, G.; Soubhye, J.; Meyer, F. Halogen Bonding in Polymer Science: From Crystal Engineering to Functional Supramolecular Polymers and Materials. *Polym. Chem.* **2015**, *6*, 3559−3580.

(19) Bentz, K. C.; Cohen, S. M. Supramolecular Metallopolymers: From Linear Materials to Infinite Networks. *Angew. Chem., Int. Ed.* **2018**, *57*, 14992−15001.

(20) Contreras-García, J.; Johnson, E. R.; Keinan, S.; Chaudret, R.; Piquemal, J.-P.; Beratan, D. N.; Yang, W. NCIPLOT: A Program for Plotting Non-Covalent Interaction Regions. *J. Chem. Theory Comput.* **2011**, *7*, 625−632.

(21) Mata, I.; Molins, E.; Alkorta, I.; Espinosa, E. Topological Properties of the Electrostatic Potential in Weak and Moderate N···H Hydrogen Bonds. *J. Phys. Chem. A* **2007**, *111*, 6425−6433.

(22) Huber, S. M.; Scanlon, J. D.; Jimenez-Izal, E.; Ugalde, J. M.; Infante, I. On the Directionality of Halogen Bonding. *Phys. Chem. Chem. Phys.* **2013**, *15*, 10350−10357.

(23) Wolters, L. P.; Schyman, P.; Pavan, M. J.; Jorgensen, W. L.; Bickelhaupt, F. M.; Kozuch, S. The Many Faces of Halogen Bonding: A Review of Theoretical Models and Methods. *Wiley Interdiscip. Rev. Comput. Mol. Sci.* **2014**, *4*, 523−540.

(24) Johnson, M. T.; Dzolic, Z.; Cetina, M.; Wendt, O. F.; Ohrstrom, L.; Rissanen, K. Neutral Organometallic Halogen Bond Acceptors: Halogen Bonding in Complexes of PCPPdX (X = Cl, Br, I) with Iodine (I2), 1,4-Diiodotetrafluorobenzene (F4DIBz), and 1,4-Diiodooctafluorobutane (F8DIBu). *Cryst. Growth Des.* **2011**, *12*, 362−368.

(25) Adonin, S. A.; Sokolov, M. N.; Fedin, V. P. Polyhalide-Bonded Metal Complexes: Structural Diversity in an Eclectic Class of Compounds. *Coord. Chem. Rev.* **2018**, *367*, 1−17.

(26) Novikov, A. S.; Ivanov, D. M.; Bikbaeva, Z. M.; Bokach, N. A.; Kukushkin, V. Y. Noncovalent Interactions Involving Iodofluorobenzenes: The Interplay of Halogen Bonding and Weak Lp(O)···π-Holearene Interactions. *Cryst. Growth Des.* **2018**, *18*, 7641−7654.

(27) Ding, X.; Tuikka, M.; Rissanen, K.; Haukka, M. Extended Assemblies of Ru(Bpy)(CO)2 × 2 (X = Cl, Br, I) Molecules Linked

https://dx.doi.org/10.1021/acs.cgd.0c01314
Cryst. Growth Des. XXXX, XXX, XXX−XXX

by 1,4-Diiodotetrafluoro-Benzene (DITFB) Halogen Bond Donors. *Crystals* **2019**, *9*, 319.
(28) Rigamonti, L.; Forni, A.; Manassero, M.; Manassero, C.; Pasini, A. Cooperation between Cis and Trans Influences in Cis-PtII(PPh3)2 Complexes: Structural, Spectroscopic, and Computational Studies. *Inorg. Chem.* **2010**, *49*, 123−135.
(29) Troff, R. W.; Makela, T.; Topic, F.; Valkonen, A.; Raatikainen, K.; Rissanen, K. Alternative Motifs for Halogen Bonding. *Eur. J. Org. Chem.* **2013**, *2013*, 1617−1637.
(30) Bondi, A. Van Der Waals Volumes and Radii. *J. Phys. Chem.* **1964**, *68*, 441−451.
(31) Ivanov, D. M.; Novikov, A. S.; Ananyev, I. V.; Kirina, Y. V.; Kukushkin, V. Y. Halogen Bonding between Metal Centers and Halocarbons. *Chem. Commun.* **2016**, *52*, 5565−5568.
(32) Fromm, K. M.; Bergougnant, R. D.; Robin, A. Y. Di-Benzo-18-Crown-6 and Its Derivatives as Ligands in the Search for Ion Channels. *Z. Anorg. Allg. Chem.* **2006**, *632*, 828−836.
(33) Politzer, P.; Murray, J. S.; Clark, T. Halogen Bonding: An Electrostatically-Driven Highly Directional Noncovalent Interaction. *Phys. Chem. Chem. Phys.* **2010**, *12*, 7748−7757.
(34) Bertolotti, F.; Shishkina, A. V.; Forni, A.; Gervasio, G.; Stash, A. I.; Tsirelson, V. G. Intermolecular Bonding Features in Solid Iodine. *Cryst. Growth Des.* **2014**, *14*, 3587−3595.
(35) Mosquera, M. E. G.; Gomez-Sal, P.; Diaz, I.; Aguirre, L. M.; Ienco, A.; Manca, G.; Mealli, C. Intriguing I2 Reduction in the Iodide for Chloride Ligand Substitution at a Ru(II) Complex: Role of Mixed Trihalides in the Redox Mechanism. *Inorg. Chem.* **2015**, *55*, 283−291.
(36) Bezzubov, S. I.; Kalle, P.; Bilyalova, A. A.; Tatarin, S. V.; Dolzhenko, V. D. Overcoming the Inertness of Iridium(III) in a Facile Single-Crystal to Single-Crystal Reaction of Iodine Vapor with a Cyclometalated Chloride Monomer. *Chem. - Eur. J.* **2018**, *24*, 12779−12783.
(37) Johnson, M. T.; Dzolic, Z.; Cetina, M.; Wendt, O. F.; Ohrstrom, L.; Rissanen, K. Neutral Organometallic Halogen Bond Acceptors: Halogen Bonding in Complexes of PCPPdX (X = Cl, Br, I) with Iodine (I 2), 1,4- Diiodotetrafluorobenzene (F4DIBz), and 1,4-Diiodooctafluorobutane (F8DIBu). *Cryst. Growth Des.* **2012**, *12*, 362−368.
(38) Clark, H. C.; Manzer, L. E. Reactions of (π-1,5-Cyclo-octadiene) Organoplatinum(II) Compounds and the Synthesis of Perfluoroalkylplatinum Complexes. *J. Organomet. Chem.* **1973**, *59*, 411−428.
(39) Crispini, A.; Aiello, I.; La Deda, M.; Godbert, N.; Ghedini, M.; Lelj, F.; Amati, M. Fluorine Interactions in the 3D Packing of "Pt(IV)I2" Organometallic Molecular Materials: Structural and Computational Approaches. *Cryst. Growth Des.* **2017**, *17*, 409−413.
(40) Fanizzi, F. P.; Natile, G.; Lanfranchi, M.; Tiripicchio, A.; Laschi, F.; Zanello, P. Steric Crowding and Redox Reactivity in Platinum(II) and Platinum(IV) Complexes Containing Substituted 1,10-Phenanthrolines. *Inorg. Chem.* **1996**, *35*, 3173−3182.
(41) Janse van Rensburg, J. M.; Oskarsson, A.; Roodt, A. Cis-Trans Isomers of PtX4 L2(X = Halogen and L = Neutral Ligand): Trans-Bis-(Dimethyl Sulfide)Tetra-Iodidoplatinum(IV). *Acta Crystallogr. Sect. C* **2008**, *64*, m40−m42.
(42) Politzer, P.; Lane, P.; Concha, M. C.; Ma, Y.; Murray, J. S. An Overview of Halogen Bonding. *J. Mol. Model.* **2007**, *13*, 305.
(43) Becke, A. D.; Edgecombe, K. E. A Simple Measure of Electron Localization in Atomic and Molecular Systems. *J. Chem. Phys.* **1990**, *92*, 5397−5403.
(44) Bader, R. F. W. *Atoms in Molecules: A Quantum Theory*; Clarendon Press: 1990.
(45) Lane, J. R.; Contreras-Garcia, J.; Piquemal, J.-P.; Miller, B. J.; Kjaergaard, H. G. Are Bond Critical Points Really Critical for Hydrogen Bonding? *J. Chem. Theory Comput.* **2013**, *9*, 3263−3266.
(46) Lefebvre, C.; Rubez, G.; Khartabil, H.; Boisson, J.-C.; Contreras-García, J.; Henon, E. Accurately Extracting the Signature of Intermolecular Interactions Present in the NCI Plot of the Reduced Density Gradient versus Electron Density. *Phys. Chem. Chem. Phys.* **2017**, *19*, 17928−17936.
(47) Ramasubbu, N.; Parthasarathy, R.; Murray-Rust, P. Angular Preferences of Intermolecular Forces around Halogen Centers: Preferred Directions of Approach of Electrophiles and Nucleophiles around Carbon-Halogen Bond. *J. Am. Chem. Soc.* **1986**, *108*, 4308.
(48) Cox, S. R.; Williams, D. E. Representation of the Molecular Electrostatic Potential by a Net Atomic Charge Model. *J. Comput. Chem.* **1981**, *2*, 304−323.
(49) Triguero, S.; Llusar, R.; Polo, V.; Fourmigue, M. Halogen Bonding Interactions of Sym-Triiodotrifluorobenzene with Halide Anions: A Combined Structural and Theoretical Study. *Cryst. Growth Des.* **2008**, *8*, 2241−2247.
(50) Cauliez, P.; Polo, V.; Roisnel, T.; Llusar, R.; Fourmigue, M. The Thiocyanate Anion as a Polydentate Halogen Bond Acceptor. *CrystEngComm* **2010**, *12*, 558.
(51) Juarez-Perez, E. J.; Aragoni, M. C.; Arca, M.; Blake, A. J.; Devillanova, F. A.; Garau, A.; Isaia, F.; Lippolis, V.; Nunez, R.; Pintus, A.; Wilson, C. A Unique Case of Oxidative Addition of Interhalogens IX (X = Cl, Br) to Organodiselone Ligands: Nature of the Chemical Bonding in Asymmetric I−Se−X Polarised Hypervalent Systems. *Chem. - Eur. J.* **2011**, *17*, 11497−11514.
(52) Xu, L.; Sang, P.; Zou, J.-W.; Xu, M.-B.; Li, X.-M.; Yu, Q.-S. Evaluation of Nucleotide C-Br···O-P Contacts from ONIOM Calculations: Theoretical Insight into Halogen Bonding in Nucleic Acids. *Chem. Phys. Lett.* **2011**, *509*, 175−180.
(53) Bartashevich, E. V.; Matveychuk, Y. V.; Troitskaya, E. A.; Tsirelson, V. G. Characterizing the Multiple Non-Covalent Interactions in N, S-Heterocycles-Diiodine Complexes with Focus on Halogen Bonding. *Comput. Theor. Chem.* **2014**, *1037*, 53−62.
(54) Bartashevich, E.; Yushina, I.; Kropotina, K.; Muhitdinova, S.; Tsirelson, V. Testing the Tools for Revealing and Characterizing the Iodine{−}iodine Halogen Bond in Crystals. *Acta Crystallogr., Sect. B: Struct. Sci., Cryst. Eng. Mater.* **2017**, *73*, 217−226.
(55) Dabranskaya, U.; Ivanov, D. M.; Novikov, A. S.; Matveychuk, Y. V.; Bokach, N. A.; Kukushkin, V. Y. Metal-Involving Bifurcated Halogen Bonding C-Br···η2(Cl-Pt). *Cryst. Growth Des.* **2018**, *19*, 1364−1376.
(56) Yushina, I. D.; Kolesov, B. A. Interplay of Intra- and Intermolecular Interactions in Solid Iodine at Low Temperatures: Experimental and Theoretic Spectroscopy Study. *J. Phys. Chem. A* **2019**, *123*, 4575−4580.
(57) Lamberts, K.; Handels, P.; Englert, U.; Aubert, E.; Espinosa, E. Stabilization of Polyiodide Chains via Anion···anion Interactions: Experiment and Theory. *CrystEngComm* **2016**, *18*, 3832−3841.
(58) Bartashevich, E.; Mukhitdinova, S.; Yushina, I.; Tsirelson, V. Electronic Criterion for Categorizing the Chalcogen and Halogen Bonds: Sulfur{−}iodine Interactions in Crystals. *Acta Crystallogr., Sect. B: Struct. Sci., Cryst. Eng. Mater.* **2019**, *75*, 117−126.
(59) Bartashevich, E.; Matveychuk, Y.; Tsirelson, V. Identification of the Tetrel Bonds between Halide Anions and Carbon Atom of Methyl Groups Using Electronic Criterion. *Molecules* **2019**, *24*, 1083.
(60) Aakeroy, C. B.; Baldrighi, M.; Desper, J.; Metrangolo, P.; Resnati, G. Supramolecular Hierarchy among Halogen-Bond Donors. *Chem. - Eur. J.* **2013**, *19*, 16240.
(61) Aakeroy, C. B.; Wijethunga, T. K.; Desper, J. Practical Crystal Engineering Using Halogen Bonding: A Hierarchy Based on Calculated Molecular Electrostatic Potential Surfaces. *J. Mol. Struct.* **2014**, *1072*, 20−27.
(62) Kolar, M.; Hostas, J.; Hobza, P. The Strength and Directionality of a Halogen Bond Are Co-Determined by the Magnitude and Size of the σ-Hole. *Phys. Chem. Chem. Phys.* **2014**, *16*, 9987−9996.
(63) Bader, R. F. W.; Carroll, M. T.; Cheeseman, J. R.; Chang, C. Properties of Atoms in Molecules: Atomic Volumes. *J. Am. Chem. Soc.* **1987**, *109*, 7968−7979.
(64) Johnson, E. R.; Keinan, S.; Mori-Sanchez, P.; Contreras-Garcia, J.; Cohen, A. J.; Yang, W. Revealing Noncovalent Interactions. *J. Am. Chem. Soc.* **2010**, *132*, 6498−6506.

https://dx.doi.org/10.1021/acs.cgd.0c01314
Cryst. Growth Des. XXXX, XXX, XXX−XXX

(65) Silvi, B.; Savin, A. Classification of Chemical Bonds Based on Topological Analysis of Electron Localization Functions. *Nature* **1994**, *371*, 683−686.
(66) Savin, A.; Nesper, R.; Wengert, S.; Fassler, T. F. ELF: The Electron Localization Function. *Angew. Chem., Int. Ed. Engl.* **1997**, *36*, 1808−1832.
(67) Fuentealba, P.; Chamorro, E.; Santos, J. C. Understanding and Using the Electron Localization Function. In *Theoretical Aspects of Chemical Reactivity*; Toro-Labbe, A. B. T.-T. C. C., Ed.; Elsevier: 2007; Vol. *19*, Chapter 5, pp 57−85. DOI: 10.1016/S1380-7323(07)80006-9.
(68) Bikbaeva, Z. M.; Ivanov, D. M.; Novikov, A. S.; Ananyev, I. V.; Bokach, N. A.; Kukushkin, V. Y. Electrophilic-Nucleophilic Dualism of Nickel(II) toward Ni···I Noncovalent Interactions: Semicoordination of Iodine Centers via Electron Belt and Halogen Bonding via σ-Hole. *Inorg. Chem.* **2017**, *56*, 13562−13578.
(69) Stephenson, N. C. The Crystal Structure of Di-Iododi-(o-Phenylenebisdimethylarsine) Platinum(II) Pt(C6H4[As(CH3)2]2)-2I2. *J. Inorg. Nucl. Chem.* **1962**, *24*, 791−795.
(70) Rozhkov, A. V.; Ivanov, D. M.; Novikov, A. S.; Ananyev, I. V.; Bokach, N. A.; Kukushkin, V. Y. Metal-Involving Halogen Bond Ar-I···[Dz2PtII] in a Platinum Acetylacetonate Complex. *CrystEngComm* **2020**, *22*, 554−563.
(71) Steinmetz, M.; Grimme, S. Benchmark Study of the Performance of Density Functional Theory for Bond Activations with (Ni,Pd)-Based Transition-Metal Catalysts. *ChemistryOpen* **2013**, *2*, 115−124.
(72) Tasinato, N.; Grimme, S. Unveiling the Non-Covalent Interactions of Molecular Homodimers by Dispersion-Corrected DFT Calculations and Collision-Induced Broadening of Ro-Vibrational Transitions: Application to (CH2F2)2 and (SO2)2. *Phys. Chem. Chem. Phys.* **2015**, *17*, 5659−5669.
(73) Niksic-Franjic, I.; Ljubic, I. Comparing the Performances of Various Density Functionals for Modelling the Mechanisms and Kinetics of Bimolecular Free Radical Reactions in Aqueous Solution. *Phys. Chem. Chem. Phys.* **2019**, *21*, 23425−23440.
(74) Tang, H.; Tao, J. Long-Range Dispersion-Corrected Density Functional for Noncovalent Interactions. *Int. J. Mod. Phys. B* **2019**, *33*, 1950300.
(75) Varadwaj, P.; Varadwaj, A.; Marques, H. Halogen Bonding: A Halogen-Centered Noncovalent Interaction Yet to Be Understood. *Inorganics* **2019**, *7*, 40.
(76) Weigend, F.; Ahlrichs, R. Balanced Basis Sets of Split Valence, Triple Zeta Valence and Quadruple Zeta Valence Quality for H to Rn: Design and Assessment of Accuracy. *Phys. Chem. Chem. Phys.* **2005**, *7*, 3297−3305.
(77) Pritchard, B. P.; Altarawy, D.; Didier, B.; Gibson, T. D.; Windus, T. L. New Basis Set Exchange: An Open, Up-to-Date Resource for the Molecular Sciences Community. *J. Chem. Inf. Model.* **2019**, *59*, 4814−4820.
(78) Dolg, M. Relativistic Effective Core Potentials. In *Relativistic Electronic Structure Theory*; Schwerdtfeger, P. B. T.-T. C., Ed.; Elsevier: 2002; Vol. *11*, Chapter 14, pp 793−862. DOI: 10.1016/S1380-7323(02)80040-1.
(79) Frisch, M. J.; Trucks, G. W.; Schlegel, H. B.; Scuseria, G. E.; Robb, M. A.; Cheeseman, J. R.; Scalmani, G.; Barone, V.; Mennucci, B.; Petersson, G. A.; Nakatsuji, H.; Caricato, M.; Li, X.; Hratchian, H. P.; Izmaylov, A. F.; Bloino, J.; Zheng, G.; Sonnenberg, J. L.; Hada, M.; Ehara, M.; Toyota, K.; Fukuda, R.; Hasegawa, J.; Ishida, M.; Nakajima, T.; Honda, Y.; Kitao, O.; Nakai, H.; Vreven, T.; Montgomery, J. A., Jr.; Peralta, J. E.; Ogliaro, F.; Bearpark, M.; Heyd, J. J.; Brothers, E.; Kudin, K. N.; Staroverov, V. N.; Keith, T.; Kobayashi, R.; Normand, J.; Raghavachari, K.; Rendell, A.; Burant, J. C.; Iyengar, S. S.; Tomasi, J.; Cossi, M.; Rega, N.; Millam, J. M.; Klene, M.; Knox, J. E.; Cross, J. B.; Bakken, V.; Adamo, C.; Jaramillo, J.; Gomperts, R.; Stratmann, R. E.; Yazyev, O.; Austin, A. J.; Cammi, R.; Pomelli, C.; Ochterski, J. W.; Martin, R. L.; Morokuma, K.; Zakrzewski, V. G.; Voth, G. A.; Salvador, P.; Dannenberg, J. J.; Dapprich, S.; Daniels, A. D.; Farkas, O.; Foresman, J. B.; Ortiz, J. V.; Cioslowski, J.; Fox, D. J. *Gaussian 09, Rev. D.01*; Gaussian Inc.: Wallingford, CT, 2013.
(80) Otero-De-La-Roza, A.; Johnson, E. R.; Luana, V. Critic2: A Program for Real-Space Analysis of Quantum Chemical Interactions in Solids. *Comput. Phys. Commun.* **2014**, *185*, 1007−1018.
(81) Williams, T.; Kelley, C. *Gnuplot 4.4: An Interactive Plotting Program*; http://Sourceforge.Net/Projects/Gnuplot, 2010
(82) Humphrey, W.; Dalke, A.; Schulten, K. VMD: Visual Molecular Dynamics. *J. Mol. Graphics* **1996**, *14*, 33−38.
(83) Keith, T. A. *AIMALL (Ver. 12.06.03)*; TK Gristmill Software: Overland Park, KS, USA. 2003.
(84) Lu, T.; Chen, F. Multiwfn: A Multifunctional Wavefunction Analyzer. *J. Comput. Chem.* **2012**, *33*, 580−592.
(85) Otwinowski, Z.; Minor, W. Processing of X-Ray Diffraction Data Collected in Oscillation Mode. *Methods Enzymol.* **1997**, *276*, 307−326.
(86) Blessing, R. H. Outlier Treatment in Data Merging. *J. Appl. Crystallogr.* **1997**, *30*, 421−426.
(87) Sheldrick, G. M. SHELXT - Integrated Space-Group and Crystal-Structure Determination. *Acta Crystallogr., Sect. A: Found. Adv.* **2015**, *71*, 3−8.
(88) Dolomanov, O. V.; Bourhis, L. J.; Gildea, R. J.; Howard, J. A. K.; Puschmann, H. OLEX2: A Complete Structure Solution, Refinement and Analysis Program. *J. Appl. Crystallogr.* **2009**, *42*, 339−341.
(89) Sheldrick, G. M. Crystal Structure Refinement with SHELXL. *Acta Crystallogr., Sect. C: Struct. Chem.* **2015**, *71*, 3−8.

https://dx.doi.org/10.1021/acs.cgd.0c01314
Cryst. Growth Des. XXXX, XXX, XXX−XXX

II

UNCOMMON I–I···(I–M) METAL-INVOLVING NONCOVALENT INTERACTION SUPPORTED BY CLASSICAL HALOGEN BOND IN PALLADIUM(II) AND PLATINUM(II) ISOCYANIDE COCRYSTALS

by

Margarita Bulatova, Daniil Ivanov, J. Mikko Rautiainen, Mikhail A. Kinzhalov, Khai-Nghi Truong, Manu Lahtinen, & Matti Haukka

Submitted manuscript.

Request a copy from author.

III

CONTROLLING THE CRYSTAL GROWTH OF POTASSIUM IODIDE WITH A 1,1′-BIS(PYRIDIN-4-YLMETHYL)-2,2′-BIIMIDAZOLE LIGAND (L) – FORMATION OF A LINEAR $[K_4I_4L_4]_N$ POLYMER WITH CUBIC $[K_4I_4]$ CORE UNITS

by

Margarita Bulatova, Rajendhraprasad Tatikonda, Pipsa Hirva, Evgeny Bulatov, Elina Sievänen & Matti Haukka

CrystEngComm, **2018**, 20, 3631-3633

DOI: 10.1039/c8ce00483h

CrystEngComm

COMMUNICATION

View Article Online
View Journal

Cite this: DOI: 10.1039/c8ce00483h

Received 29th March 2018,
Accepted 15th May 2018

DOI: 10.1039/c8ce00483h

rsc.li/crystengcomm

Controlling the crystal growth of potassium iodide with a 1,1′-bis(pyridin-4-ylmethyl)-2,2′-biimidazole ligand (L) – formation of a linear $[K_4I_4L_4]_n$ polymer with cubic $[K_4I_4]$ core units†

Margarita Bulatova,[a] Rajendhraprasad Tatikonda,[a] Pipsa Hirva,[b] Evgeny Bulatov,[a] Elina Sievänen[a] and Matti Haukka *[a]

The crystal growth of potassium iodide was controlled by using the neutral organic 1,1′-bis(pyridin-4-ylmethyl)-2,2′-biimidazole (L) ligand as a modifier. The selected modifier allows the preservation of original cubic $[K_4I_4]$ units and their arrangement into a linear ligand-supported 1D chain. The supported $[K_4I_4]$ cubes are only slightly distorted compared to the cubes found in pure KI salt. The N–K binding of the ligand to the KI salt, as well as weak I···H, N···H, and N···I interactions, stabilizes the structure to create a unique 1D polymer of neutral potassium iodide ionic salt inside the $[K_4I_4L_4]_n$ complex.

Controlled crystal growth is an important method for tuning the physicochemical properties of compounds in the solid state.[1] Various compounds can inhibit or promote crystal growth and, thus, have been used as crystal growth modifiers.[2–4] Interactions between a crystallizing solute and a modifier compound can range from covalent bonds to non-covalent interactions such as van der Waals interactions, electrostatic interactions, hydrogen bonding, π–π stacking, *etc.*[2] To obtain the desired impact on crystal growth, a modifier must be carefully designed with consideration of all possible forms of interactions.

The growth of an inorganic salt, such as KI, can be controlled physically by space limitation or chemically by using modifier molecules that limit the free 3D self-assembling growth of KI units. Sloan *et al.* have used the physical approach to limit the growth of KI within a single-walled carbon nanotube (SWCNT). It has been shown that it is possible to grow a 1D KI chain consisting of repeating cubic K_4I_4 units by using SWCNTs with a 1.2–1.6 nm median diameter. Although the cubic basic structures of the repeating $[K_4I_4]$ units resembled closely those found in pure KI, some distortions of K–I distances and K–I–K angles were observed.[5] Inside the restricted space of a SWCNT, only one-dimensional growth was possible and further modifications of KI were prevented. The chemical approach can be used to control and modify the growth of crystals containing potassium iodide. There have been several attempts to organize KI into continuous structures with organic and metalorganic molecules. Kruszynski *et al.* have synthesized a hybrid net compound using hexamethylenetetramine (htma) ligands that are bonded to K atoms through the nitrogen atoms of the ligands. The presence of htma molecules promotes the growth of nearly linear 1D chains of K–I–K–I. Furthermore, htma molecules link neighboring chains into parallel bundles. However, in this case, the cubic K_4I_4 units found in pure KI are lost and replaced with a simple chain.[6] Rhodium tetracarboxylates have also been inserted into the continuous KI structure giving more or less a planar arrangement of K and I, as shown by Amo-Ochoa *et al.*[7] Liu *et al.* have reported the structure of $[Cu_2K(Mtta)I_2]$ (where Mtta is deprotonated 5-methyl-1*H*-tetrazole). In this structure, the KI units can be seen as a chain of "opened potassium iodide cubes", where

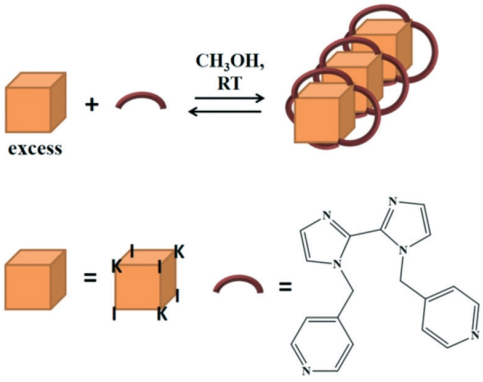

Fig. 1 Formation of a polymeric $[K_4I_4L_4]_n$ chain.

[a] *Department of Chemistry, University of Jyväskylä, P.O. Box 35, FI-40014, Jyväskylä, Finland. E-mail: matti.o.haukka@jyu.fi*
[b] *Department of Chemistry, University of Eastern Finland, P.O. Box 111, 80101, Joensuu, Finland. E-mail: pipsa.hirva@uef.fi*

† Electronic supplementary information (ESI) available. CCDC 1588805. For ESI and crystallographic data in CIF or other electronic format see DOI: 10.1039/c8ce00483h

Cu and the two nitrogen atoms of the Mtta ligand are inserted in one edge of the cubes.[8] Using 2,9-dimethyl-1,10-phenanthroline ligands, Buttery *et al.* have obtained an even more opened structure, where the length of the KI chain has been limited to six K and four I atoms.[9] However, in all of the chemically modified structures described above, the original cubic arrangement of pure KI is either heavily distorted or completely lost and the chemical additives used cannot really be seen as modifiers for crystal growth.

By using 1,1′-bis(pyridin-4-ylmethyl)-2,2′-biimidazole (L) as the chemical modifier, we succeeded in obtaining the first 1D polymeric structure that retains the original cubic K_4I_4 structure of KI (Fig. 1). In the ligand supported polymer of $[K_4I_4L_4]_n$, the K_4I_4 cubes are repeated only in one direction. The 1D polymeric compound was obtained in the reaction of KI with 1,1′-bis(pyridin-4-ylmethyl)-2,2′-biimidazole (L) in methanol under ambient conditions. To obtain the $[K_4I_4L_4]_n$ product with a reasonable yield, an excess of KI was needed in the reaction mixture. The X-ray quality crystals were obtained by allowing the solvent to evaporate slowly. The polymer growth was driven by self-assembly of the components; however, the detailed mechanism of the crystal growth is not clear (Fig. 1). According to the solid state studies (see the ESI,† solid state studies), the $[K_4I_4L_4]_n$ polymer is stable in air up to 200 °C. Liquid state studies (see ESI,† liquid state studies) of $[K_4I_4L_4]_n$ revealed that upon longer storage in a protic solvent, such as methanol, the coordination of the ligand to potassium iodide is lost, and the structure collapses back to the K^+ and I^- ions, releasing the neutral ligand.

According to the single crystal XRD data,‡ the nearly cubic $[K_4I_4]_n$ units in the structure are supported by the ligands (Fig. 2). Each distorted octahedral coordination sphere of K atoms consists of four I atoms and two pyridine nitrogen atoms of the ligands.

In the $[K_4I_4L_4]_n$ cube, the K–I distances range from 3.4759(4) Å to 3.5674(5) Å, and K–I–K and I–K–I angles within the cube range from 86.336(13)° to 89.198(11)° and from 90.397(10)° to 96.490(13)°, respectively. Additionally, the K–N distances vary slightly from 2.815(2) Å to 2.906(2) Å (Fig. 2), being the average K–N bond length according to the Cambridge Structural Database.[10] The K_4I_4 core units in the $K_4I_4L_4$ structure closely resemble the cubic structure of the crystalline pure KI salt, where the K–I distances are 3.525 Å and the K–I–K angles as well as the I–K–I angles are 90°.[11]

Two ligand-supported cubes are connected with direct K–I bonds (3.4712 Å, bond A in Fig. 2), which are slightly shorter than K–I bonds within the cubes (3.5674 Å, bond B in Fig. 2). The K–I–K and I–K–I angles between neighboring cubes in the polymer are 170.41(2)°, while in pure KI, the corresponding K–I–K or I–K–I angles are 180°. Despite the slight distortion of the K_4I_4 unit within the $[K_4I_4L_4]_n$ polymer, the basic cubic arrangement of the K_4I_4 core is retained compared to the pure KI.

However, the geometry of the ligands allows the $[K_4I_4L_4]$ units only to form a linear $[K_4I_4L_4]_n$ polymeric chain instead of a 3D structure. L was found to be extremely selective towards KI. No other alkali metal halide 1D polymers were obtained under the same crystallization conditions. Likewise, the use of a similar ligand (1,1′-bis(pyridin-3-ylmethyl)-2,2′-biimidazole) instead of 1,1′-bis(pyridin-4-ylmethyl)-2,2′-biimidazole failed to produce a polymeric structure due to the change in the location of the coordination sites.

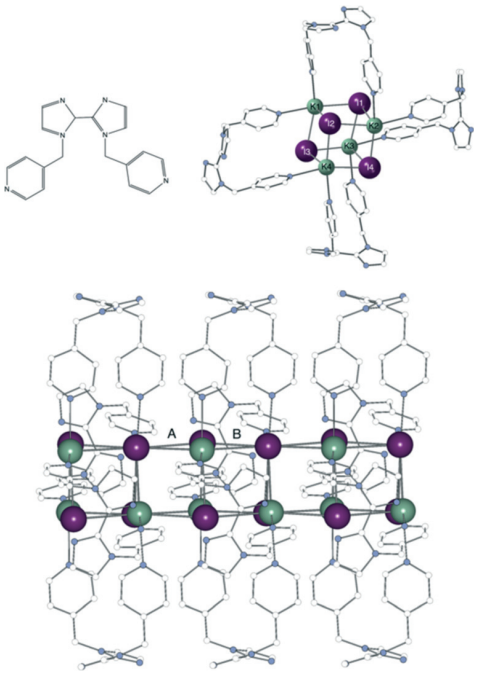

Fig. 2 Structure of the $[K_4I_4L_4]_n$ polymer [**]. Top: left – Ligand; right – $[K_4I_4L_4]$ unit. Selected bond lengths (Å) and angles (°): K1–I1 = K3–I3: 3.5037(5), K2–I2 = K4–I4 = K1–I3 = K3–I1: 3.5674(5), K4–I2 = K2–I4: 3.5037(5), K1–I2 = K2–I1 = K3–I4 = K4–I3: 3.4759(4), K–N: 2.815(2) and 2.906(2). The K–I–K angles of the supported unit range from 86.336(13) to 89.198(11) and the I–K–I angles from 90.397(10) to 96.490(13). Bottom: A chain of three $[K_4I_4L_4]$ units. K–I distance between the units (A): 3.4712(5) Å and within the unit (B): 3.4759(4) Å. K–I–K and I–K–I angles between the supported units along the chain: 170.41(2)°.

The impact of the supporting ligands on the stability of the $[K_4I_4]_n$ chain-like structure was studied computationally (for details see the ESI†).[12–16] Models comprising 1, 2, and 3 $K_4I_4L_4$ units were cut directly from the crystal structure and analyzed without geometry optimization. The energetics of the corresponding unsupported linear $[K_4I_4]_n$ models, obtained from the crystal structure of pure KI, were also analyzed and compared with the ligand supported models.

Single point energies of $[K_4I_4]_n$ and $[K_4I_4L_4]_n$ (n = 1–3) were calculated. In both series, the n = 1 case was set as the reference with zero energy, and the stabilization energies obtained by adding the second and the third cubes to the models (n = 2 and 3) were calculated. The two series were compared to see if the presence of ligands had any impact on the stability of the growing chain. The addition of new cubes ($[K_4I_4L_4]$ or $[K_4I_4]$) into the chains stabilizes the growing structure in both cases as expected. However, the stabilization effect is emphasized in the case of the ligand-substituted $[K_4I_4L_4]_n$ model.

According to the results, the growth of the ligand-supported 1D polymer is energetically favored over the growth of pure KI. The results are summarized in more detail in the ESI,† Computational studies and Results and discussion (Tables S2 and S3 and Fig. S6–S9†).

Selected properties of the electron density of $[K_4I_4]_n$, $[K_4I_4]_n[K_4I_4]_{2n}$ and $[K_4I_4L_4]_n$ models (for visualization of the models; see the ESI,† Fig. S6 and S8) were analyzed by quantum theory of atoms in molecules (QTAIM) to study the nature of the interactions. The calculations indicate that when the $[K_4I_4L_4]_n$ chain forms, the nature of the K···I interactions remains essentially the same as in the cubic $[K_4I_4]_n$ without supporting ligands. This is the case even though the interaction of the ligand nitrogen atoms with the potassium ions is fairly strong, 13–16 kJ mol^{-1}. All K···I and I···I interactions also remain clearly electrostatic. This is confirmed by the ratio between potential energy density and kinetic energy density, which is less than 1 in all cases. The electrostatic character of the interaction is further supported by the small value of the delocalization index indicating only a negligible amount of electron-sharing in these contacts. The ligands form additional weak hydrogen bonding interactions (I···H and N···H), as well as π–π and N···I interactions, which have a further role in the stabilization. Notably, the interactions remain the same even in the larger 3D models of the crystals.

Conclusions

The results show that it is possible to limit the growth of $[K_4I_4]$ units in only one dimension by choosing a suitable modifier ligand. According to computational studies, a one-dimensional extension of the ligand supported $[K_4I_4L_4]_n$ chain is energetically more favorable than the extension of the pure $[K_4I_4]_n$ chain, indicating the directing role of the ligand. In addition to the N–K bonds, weak interactions support the structure further. The key to the linear growth lies in the flexibility of the ligand, its steric properties, and its suitable bite distance. The bite distance also promotes its high selectivity towards KI salt. With careful design, it should be possible to obtain selective crystal growth modifiers for other ionic salts also.

Conflicts of interest

There are no conflicts to declare.

Acknowledgements

We thank the Academy of Finland (proj. No. 295581), Elina Hautakangas, and COST Action CM1302 and CM1402 for being inspiring cradles for new ideas. We acknowledge grants of computer capacity from the Finnish Grid and Cloud Infrastructure (persistent identifier urn:nbn: fi:research-infras-2016072533).

Notes and references

‡ Crystal data. $C_{18}H_{16}IKN_6$, M = 482.37, crystal dimensions: 0.083 mm × 0.159 mm × 0.283 mm, tetragonal, $P4_2/n$, a = 23.5606(2) Å, b = 23.5606(2) Å, c = 6.92267(8) Å, V = 3842.79(8) Å^3, Z = 8, ρ_{calc} = 1.668 Mg m^{-3}, μ(Kα) = 15.149 mm^{-1}, $2\theta_{max}$ = 76.940°, no. measured refln. = 18 332, no. unique refln. = 4035, R_{int} = 0.0336, R_1 ($I \geq 2\sigma$) = 0.0262, wR_2 ($I \geq 2\sigma$) = 0.0670, residual el. density min/max = 0.871 and −0.698 e Å^{-3}.

1 F. Jones and M. I. Ogden, *CrystEngComm*, 2010, **12**, 1016–1023.
2 K. N. Olafson, R. Li, B. G. Alamani and J. D. Rimer, *Chem. Mater.*, 2016, **28**, 8453–8465.
3 L. Wang and G. H. Nancollas, *Chem. Rev.*, 2008, **108**, 4628–4669.
4 F. C. Meldrum and H. Cölfen, *Chem. Rev.*, 2008, **108**, 4332–4432.
5 J. Sloan, M. C. Novotny, S. R. Bailey, G. Brown, C. Xu, V. C. Williams, S. Friedrichs, E. Flahaut, R. L. Callender, A. P. E. York, K. S. Coleman, M. L. H. Green, R. E. Dunin-Borkowski and J. L. Hutchison, *Chem. Phys. Lett.*, 2000, **329**, 61–65.
6 R. Kruszynski, T. Sieranski, A. Bilinska, T. Bernat and E. Czubacka, *Struct. Chem.*, 2012, **23**, 1643–1656.
7 P. Amo-Ochoa, R. Jiménez-Aparicio, J. Perles, M. R. Torres, M. Gennari and F. Zamora, *Cryst. Growth Des.*, 2013, **13**, 4977–4985.
8 B. Liu, Y.-C. Qiu, G. Peng and H. Deng, *CrystEngComm*, 2010, **12**, 270–276.
9 J. H. N. Buttery, Effendy, S. Mutrofin, N. C. Plackett, B. W. Skelton, C. R. Whitaker and A. H. White, *Z. Anorg. Allg. Chem.*, 2006, **6**, 1809–1828.
10 C. R. Groom, I. J. Bruno, M. P. Lightfoot and S. C. Ward, *Acta Crystallogr., Sect. B: Struct. Sci., Cryst. Eng. Mater.*, 2016, **72**, 171–179.
11 M. Ahtee, *Ann. Acad. Sci. Fenn., Ser. A6*, 1969, 1–11.
12 M. J. Frisch, G. W. Trucks, H. B. Schlegel, G. E. Scuseria, M. A. Robb, J. R. Cheeseman, G. Scalmani, V. Barone, B. Mennucci, G. A. Petersson, H. Nakatsuji, M. Caricato, X. Li, H. P. Hratchian, A. F. Izmaylov, J. Bloino, G. Zheng and J. L. Sonnenberg, *Gaussian 09, Revision C.01*, Inc. Wallingford, CT, 2009.
13 J. P. Perdew, K. Burke and M. Ernzerhof, *Phys. Rev. Lett.*, 1997, **78**, 1396.
14 D. Rappoport and F. Furche, *J. Chem. Phys.*, 2010, **133**, 134105.
15 R. F. W. Bader, *Atoms in Molecules: A Quantum Theory*, 1990.
16 T. A. Keith, *TK Gristmill Software*, Overl. Park KS, USA, 2003.

DEPARTMENT OF CHEMISTRY, UNIVERSITY OF JYVÄSKYLÄ
RESEARCH REPORT SERIES

1. Vuolle, Mikko: Electron paramagnetic resonance and molecular orbital study of radical ions generated from (2.2)metacyclophane, pyrene and its hydrogenated compounds by alkali metal reduction and by thallium(III)trifluoroacetate oxidation. (99 pp.) 1976
2. Pasanen, Kaija: Electron paramagnetic resonance study of cation radical generated from various chlorinated biphenyls. (66 pp.) 1977
3. Carbon-13 Workshop, September 6-8, 1977. (91 pp.) 1977
4. Laihia, Katri: On the structure determination of norbornane polyols by NMR spectroscopy. (111 pp.) 1979
5. Nyrönen, Timo: On the EPR, ENDOR and visible absorption spectra of some nitrogen containing heterocyclic compounds in liquid ammonia. (76 pp.) 1978
6. Talvitie, Antti: Structure determination of some sesquiterpenoids by shift reagent NMR. (54 pp.) 1979
7. Häkli, Harri: Structure analysis and molecular dynamics of cyclic compounds by shift reagent NMR. (48 pp.) 1979
8. Pitkänen, Ilkka: Thermodynamics of complexation of 1,2,4-triazole with divalent manganese, cobalt, nickel, copper, zinc, cadmium and lead ions in aqueous sodium perchlorate solutions. (89 pp.) 1980
9. Asunta, Tuula: Preparation and characterization of new organometallic compounds synthesized by using metal vapours. (91 pp.) 1980
10. Sattar, Mohammad Abdus: Analyses of MCPA and its metabolites in soil. (57 pp.) 1980
11. Bibliography 1980. (31 pp.) 1981
12. Knuuttila, Pekka: X-Ray structural studies on some divalent 3d metal compounds of picolinic and isonicotinic acid N-oxides. (77 pp.) 1981
13. Bibliography 1981. (33 pp.) 1982
14. 6^{th} National NMR Symposium, September 9-10, 1982, Abstracts. (49 pp.) 1982
15. Bibliography 1982. (38 pp.) 1983
16. Knuuttila, Hilkka: X-Ray structural studies on some Cu(II), Co(II) and Ni(II) complexes with nicotinic and isonicotinic acid N-oxides. (54 pp.) 1983
17. Symposium on inorganic and analytical chemistry May 18, 1984, Program and Abstracts. (100 pp.) 1984
18. Knuutinen, Juha: On the synthesis, structure verification and gas chromatographic determination of chlorinated catechols and guaiacols occuring in spent bleach liquors of kraft pulp mill. (30 pp.) 1984
19. Bibliography 1983. (47 pp.) 1984
20. Pitkänen, Maija: Addition of BrCl, B_2 and Cl_2 to methyl esters of propenoic and 2-butenoic acid derivatives and ^{13}C NMR studies on methyl esters of saturated aliphatic mono- and dichlorocarboxylic acids. (56 pp.) 1985
21. Bibliography 1984. (39 pp.) 1985
22. Salo, Esa: EPR, ENDOR and TRIPLE spectroscopy of some nitrogen heteroaromatics in liquid ammonia. (111 pp.) 1985

23. Humppi, Tarmo: Synthesis, identification and analysis of dimeric impurities of chlorophenols. (39 pp.) 1985
24. Aho, Martti: The ion exchange and adsorption properties of sphagnum peat under acid conditions. (90 pp.) 1985
25. Bibliography 1985 (61 pp.) 1986
26. Bibliography 1986. (23 pp.) 1987
27. Bibliography 1987. (26 pp.) 1988
28. Paasivirta, Jaakko (Ed.): Structures of organic environmental chemicals. (67 pp.) 1988
29. Paasivirta, Jaakko (Ed.): Chemistry and ecology of organo-element compounds. (93 pp.) 1989
30. Sinkkonen, Seija: Determination of crude oil alkylated dibenzothiophenes in environment. (35 pp.) 1989
31. Kolehmainen, Erkki (Ed.): XII National NMR Symposium Program and Abstracts. (75 pp.) 1989
32. Kuokkanen, Tauno: Chlorocymenes and Chlorocymenenes: Persistent chlorocompounds in spent bleach liquors of kraft pulp mills. (40 pp.) 1989
33. Mäkelä, Reijo: ESR, ENDOR and TRIPLE resonance study on substituted 9,10-anthraquinone radicals in solution. (35 pp.) 1990
34. Veijanen, Anja: An integrated sensory and analytical method for identification of off-flavour compounds. (70 pp.) 1990
35. Kasa, Seppo: EPR, ENDOR and TRIPLE resonance and molecular orbital studies on a substitution reaction of anthracene induced by thallium(III) in two fluorinated carboxylic acids. (114 pp.) 1990
36. Herve, Sirpa: Mussel incubation method for monitoring organochlorine compounds in freshwater recipients of pulp and paper industry. (145 pp.) 1991
37. Pohjola, Pekka: The electron paramagnetic resonance method for characterization of Finnish peat types and iron (III) complexes in the process of peat decomposition. (77 pp.) 1991
38. Paasivirta, Jaakko (Ed.): Organochlorines from pulp mills and other sources. Research methodology studies 1988-91. (120 pp.) 1992
39. Veijanen, Anja (Ed.): VI National Symposium on Mass Spectrometry, May 13-15, 1992, Abstracts. (55 pp.) 1992
40. Rissanen, Kari (Ed.): The 7. National Symposium on Inorganic and Analytical Chemistry, May 22, 1992, Abstracts and Program. (153 pp.) 1992
41. Paasivirta, Jaakko (Ed.): CEOEC'92, Second Finnish-Russian Seminar: Chemistry and Ecology of Organo-Element Compounds. (93 pp.) 1992
42. Koistinen, Jaana: Persistent polychloroaromatic compounds in the environment: structure-specific analyses. (50 pp.) 1993
43. Virkki, Liisa: Structural characterization of chlorolignins by spectroscopic and liquid chromatographic methods and a comparison with humic substances. (62 pp.) 1993
44. Helenius, Vesa: Electronic and vibrational excitations in some

biologically relevant molecules. (30 pp.) 1993

45. Leppä-aho, Jaakko: Thermal behaviour, infrared spectra and x-ray structures of some new rare earth chromates(VI). (64 pp.) 1994
46. Kotila, Sirpa: Synthesis, structure and thermal behavior of solid copper(II) complexes of 2-amino-2- hydroxymethyl-1,3-propanediol. (111 pp.) 1994
47. Mikkonen, Anneli: Retention of molybdenum(VI), vanadium(V) and tungsten(VI) by kaolin and three Finnish mineral soils. (90 pp.) 1995
48. Suontamo, Reijo: Molecular orbital studies of small molecules containing sulfur and selenium. (42 pp.) 1995
49. Hämäläinen, Jouni: Effect of fuel composition on the conversion of fuel-N to nitrogen oxides in the combustion of small single particles. (50 pp.) 1995
50. Nevalainen, Tapio: Polychlorinated diphenyl ethers: synthesis, NMR spectroscopy, structural properties, and estimated toxicity. (76 pp.) 1995
51. Aittola, Jussi-Pekka: Organochloro compounds in the stack emission. (35 pp.) 1995
52. Harju, Timo: Ultrafast polar molecular photophysics of (dibenzylmethine)borondifluoride and 4-aminophthalimide in solution. (61 pp.) 1995
53. Maatela, Paula: Determination of organically bound chlorine in industrial and environmental samples. (83 pp.) 1995
54. Paasivirta, Jaakko (Ed.): CEOEC'95, Third Finnish-Russian Seminar: Chemistry and Ecology of Organo-Element Compounds. (109 pp.) 1995
55. Huuskonen, Juhani: Synthesis and structural studies of some supramolecular compounds. (54 pp.) 1995
56. Palm, Helena: Fate of chlorophenols and their derivatives in sawmill soil and pulp mill recipient environments. (52 pp.) 1995
57. Rantio, Tiina: Chlorohydrocarbons in pulp mill effluents and their fate in the environment. (89 pp.) 1997
58. Ratilainen, Jari: Covalent and non-covalent interactions in molecular recognition. (37 pp.) 1997
59. Kolehmainen, Erkki (Ed.): XIX National NMR Symposium, June 4-6, 1997, Abstracts. (89 pp.) 1997
60. Matilainen, Rose: Development of methods for fertilizer analysis by inductively coupled plasma atomic emission spectrometry. (41 pp.) 1997
61. Koistinen, Jari (Ed.): Spring Meeting on the Division of Synthetic Chemistry, May 15-16, 1997, Program and Abstracts. (36 pp.) 1997
62. Lappalainen, Kari: Monomeric and cyclic bile acid derivatives: syntheses, NMR spectroscopy and molecular recognition properties. (50 pp.) 1997
63. Laitinen, Eira: Molecular dynamics of cyanine dyes and phthalimides in solution: picosecond laser studies. (62 pp.) 1997
64. Eloranta, Jussi: Experimental and theoretical studies on some

quinone and quinol radicals. (40 pp.) 1997

65. Oksanen, Jari: Spectroscopic characterization of some monomeric and aggregated chlorophylls. (43 pp.) 1998
66. Häkkänen, Heikki: Development of a method based on laser-induced plasma spectrometry for rapid spatial analysis of material distributions in paper coatings. (60 pp.) 1998
67. Virtapohja, Janne: Fate of chelating agents used in the pulp and paper industries. (58 pp.) 1998
68. Airola, Karri: X-ray structural studies of supramolecular and organic compounds. (39 pp.) 1998
69. Hyötyläinen, Juha: Transport of lignin–type compounds in the receiving waters of pulp mills. (40 pp.) 1999
70. Ristolainen, Matti: Analysis of the organic material dissolved during totally chlorine-free bleaching. (40 pp.) 1999
71. Eklin, Tero: Development of analytical procedures with industrial samples for atomic emission and atomic absorption spectrometry. (43 pp.) 1999
72. Välisaari, Jouni: Hygiene properties of resol-type phenolic resin laminates. (129 pp.) 1999
73. Hu, Jiwei: Persistent polyhalogenated diphenyl ethers: model compounds syntheses, characterization and molecular orbital studies. (59 pp.) 1999
74. Malkavaara, Petteri: Chemometric adaptations in wood processing chemistry. (56 pp.) 2000
75. Kujala Elena, Laihia Katri, Nieminen Kari (Eds.): NBC 2000, Symposium on Nuclear, Biological and Chemical Threats in the 21st Century. (299 pp.) 2000
76. Rantalainen, Anna-Lea: Semipermeable membrane devices in monitoring persistent organic pollutants in the environment. (58 pp.) 2000
77. Lahtinen, Manu: *In situ* X-ray powder diffraction studies of Pt/C, CuCl/C and Cu_2O/C catalysts at elevated temperatures in various reaction conditions. (92 pp.) 2000
78. Tamminen, Jari: Syntheses, empirical and theoretical characterization, and metal cation complexation of bile acid-based monomers and open/closed dimers. (54 pp.) 2000
79. Vatanen, Virpi: Experimental studies by EPR and theoretical studies by DFT calculations of α-amino-9,10-anthraquinone radical anions and cations in solution. (37 pp.) 2000
80. Kotilainen, Risto: Chemical changes in wood during heating at 150-260 °C. (57 pp.) 2000
81. Nissinen, Maija: X-ray structural studies on weak, non-covalent interactions in supramolecular compounds. (69 pp.) 2001
82. Wegelius, Elina: X-ray structural studies on self-assembled hydrogen-bonded networks and metallosupramolecular complexes. (84 pp.) 2001
83. Paasivirta, Jaakko (Ed.): CEOEC'2001, Fifth Finnish-Russian Seminar: Chemistry and Ecology of Organo-Element Compounds. (163 pp.) 2001
84. Kiljunen, Toni: Theoretical studies on spectroscopy and

atomic dynamics in rare gas solids. (56 pp.) 2001

85. Du, Jin: Derivatives of dextran: synthesis and applications in oncology. (48 pp.) 2001
86. Koivisto, Jari: Structural analysis of selected polychlorinated persistent organic pollutants (POPs) and related compounds. (88 pp.) 2001
87. Feng, Zhinan: Alkaline pulping of non-wood feedstocks and characterization of black liquors. (54 pp.) 2001
88. Halonen, Markku: Lahon havupuun käyttö sulfaattiprosessin raaka-aineena sekä havupuun lahontorjunta. (90 pp.) 2002
89. Falábu, Dezsö: Synthesis, conformational analysis and complexation studies of resorcarene derivatives. (212 pp.) 2001
90. Lehtovuori, Pekka: EMR spectroscopic studies on radicals of ubiquinones Q-*n*, vitamin K_3 and vitamine E in liquid solution. (40 pp.) 2002
91. Perkkalainen, Paula: Polymorphism of sugar alcohols and effect of grinding on thermal behavior on binary sugar alcohol mixtures. (53 pp.) 2002
92. Ihalainen, Janne: Spectroscopic studies on light-harvesting complexes of green plants and purple bacteria. (42 pp.) 2002
93. Kunttu, Henrik, Kiljunen, Toni (Eds.): 4th International Conference on Low Temperature Chemistry. (159 pp.) 2002
94. Väisänen, Ari: Development of methods for toxic element analysis in samples with environmental concern by ICP-AES and ETAAS. (54 pp.) 2002
95. Luostarinen, Minna: Synthesis and characterisation of novel resorcarene derivatives. (200 pp.) 2002
96. Louhelainen, Jarmo: Changes in the chemical composition and physical properties of wood and nonwood black liquors during heating. (68 pp.) 2003
97. Lahtinen, Tanja: Concave hydrocarbon cyclophane π-prismands. (65 pp.) 2003
98. Laihia, Katri (Ed.): NBC 2003, Symposium on Nuclear, Biological and Chemical Threats – A Crisis Management Challenge. (245 pp.) 2003
99. Oasmaa, Anja: Fuel oil quality properties of wood-based pyrolysis liquids. (32 pp.) 2003
100. Virtanen, Elina: Syntheses, structural characterisation, and cation/anion recognition properties of nano-sized bile acid-based host molecules and their precursors. (123 pp.) 2003
101. Nättinen, Kalle: Synthesis and X-ray structural studies of organic and metallo-organic supramolecular systems. (79 pp.) 2003
102. Lampiselkä, Jarkko: Demonstraatio lukion kemian opetuksessa. (285 pp.) 2003
103. Kallioinen, Jani: Photoinduced dynamics of $Ru(dcbpy)_2(NCS)_2$ – in solution and on nanocrystalline titanium dioxide thin films. (47 pp.) 2004
104. Valkonen, Arto (Ed.): VII Synthetic Chemistry Meeting and XXVI Finnish NMR Symposium. (103 pp.) 2004

105. Vaskonen, Kari: Spectroscopic studies on atoms and small molecules isolated in low temperature rare gas matrices. (65 pp.) 2004
106. Lehtovuori, Viivi: Ultrafast light induced dissociation of $Ru(dcbpy)(CO)_2I_2$ in solution. (49 pp.) 2004
107. Saarenketo, Pauli: Structural studies of metal complexing Schiff bases, Schiff base derived *N*-glycosides and cyclophane π-prismands. (95 pp.) 2004
108. Paasivirta, Jaakko (Ed.): CEOEC'2004, Sixth Finnish-Russian Seminar: Chemistry and Ecology of Organo-Element Compounds. (147 pp.) 2004
109. Suontamo, Tuula: Development of a test method for evaluating the cleaning efficiency of hard-surface cleaning agents. (96 pp.) 2004
110. Güneş, Minna: Studies of thiocyanates of silver for nonlinear optics. (48 pp.) 2004
111. Ropponen, Jarmo: Aliphatic polyester dendrimers and dendrons. (81 pp.) 2004
112. Vu, Mân Thi Hong: Alkaline pulping and the subsequent elemental chlorine-free bleaching of bamboo (*Bambusa procera*). (69 pp.) 2004
113. Mansikkamäki, Heidi: Self-assembly of resorcinarenes. (77 pp.) 2006
114. Tuononen, Heikki M.: EPR spectroscopic and quantum chemical studies of some inorganic main group radicals. (79 pp.) 2005
115. Kaski, Saara: Development of methods and applications of laser-induced plasma spectroscopy in vacuum ultraviolet. (44 pp.) 2005
116. Mäkinen, Riika-Mari: Synthesis, crystal structure and thermal decomposition of certain metal thiocyanates and organic thiocyanates. (119 pp.) 2006
117. Ahokas, Jussi: Spectroscopic studies of atoms and small molecules isolated in rare gas solids: photodissociation and thermal reactions. (53 pp.) 2006
118. Busi, Sara: Synthesis, characterization and thermal properties of new quaternary ammonium compounds: new materials for electrolytes, ionic liquids and complexation studies. (102 pp.) 2006
119. Mäntykoski, Keijo: PCBs in processes, products and environment of paper mills using wastepaper as their raw material. (73 pp.) 2006
120. Laamanen, Pirkko-Leena: Simultaneous determination of industrially and environmentally relevant aminopolycarboxylic and hydroxycarboxylic acids by capillary zone electrophoresis. (54 pp.) 2007
121. Salmela, Maria: Description of oxygen-alkali delignification of kraft pulp using analysis of dissolved material. (71 pp.) 2007
122. Lehtovaara, Lauri: Theoretical studies of atomic scale impurities in superfluid ^{4}He. (87 pp.) 2007
123. Rautiainen, J. Mikko: Quantum chemical calculations of structures, bonding, and spectroscopic properties of some sulphur and selenium iodine cations. (71 pp.) 2007
124. Nummelin, Sami: Synthesis, characterization, structural and

retrostructural analysis of self-assembling pore forming dendrimers. (286 pp.) 2008

125. Sopo, Harri: Uranyl(VI) ion complexes of some organic aminobisphenolate ligands: syntheses, structures and extraction studies. (57 pp.) 2008
126. Valkonen, Arto: Structural characteristics and properties of substituted cholanoates and *N*-substituted cholanamides. (80 pp.) 2008
127. Lähde, Anna: Production and surface modification of pharmaceutical nano- and microparticles with the aerosol flow reactor. (43 pp.) 2008
128. Beyeh, Ngong Kodiah: Resorcinarenes and their derivatives: synthesis, characterization and complexation in gas phase and in solution. (75 pp.) 2008
129. Välisaari, Jouni, Lundell, Jan (Eds.): Kemian opetuksen päivät 2008: uusia oppimisympäristöjä ja ongelmalähtöistä opetusta. (118 pp.) 2008
130. Myllyperkiö, Pasi: Ultrafast electron transfer from potential organic and metal containing solar cell sensitizers. (69 pp.) 2009
131. Käkölä, Jaana: Fast chromatographic methods for determining aliphatic carboxylic acids in black liquors. (82 pp.) 2009
132. Koivukorpi, Juha: Bile acid-arene conjugates: from photoswitchability to cancer cell detection. (67 pp.) 2009
133. Tuuttila, Tero: Functional dendritic polyester compounds: synthesis and characterization of small bifunctional dendrimers and dyes. (74 pp.) 2009
134. Salorinne, Kirsi: Tetramethoxy resorcinarene based cation and anion receptors: synthesis, characterization and binding properties. (79 pp.) 2009
135. Rautiainen, Riikka: The use of first-thinning Scots pine (*Pinus sylvestris*) as fiber raw material for the kraft pulp and paper industry. (73 pp.) 2010
136. Ilander, Laura: Uranyl salophens: synthesis and use as ditopic receptors. (199 pp.) 2010
137. Kiviniemi, Tiina: Vibrational dynamics of iodine molecule and its complexes in solid krypton - Towards coherent control of bimolecular reactions? (73 pp.) 2010
138. Ikonen, Satu: Synthesis, characterization and structural properties of various covalent and non-covalent bile acid derivatives of N/O-heterocycles and their precursors. (105 pp.) 2010
139. Siitonen, Anni: Spectroscopic studies of semiconducting single-walled carbon nanotubes. (56 pp.) 2010
140. Raatikainen, Kari: Synthesis and structural studies of piperazine cyclophanes – Supramolecular systems through Halogen and Hydrogen bonding and metal ion coordination. (69 pp.) 2010
141. Leivo, Kimmo: Gelation and gel properties of two- and three-component Pyrene based low molecular weight organogelators. (116 pp.) 2011
142. Martiskainen, Jari: Electronic energy transfer in light-harvesting complexes isolated from *Spinacia oleracea* and from three

photosynthetic green bacteria *Chloroflexus aurantiacus*, *Chlorobium tepidum*, and *Prosthecochloris aestuarii*. (55 pp.) 2011

143. Wichmann, Oula: Syntheses, characterization and structural properties of [O,N,O,X´] aminobisphenolate metal complexes. (101 pp.) 2011
144. Ilander, Aki: Development of ultrasound-assisted digestion methods for the determination of toxic element concentrations in ash samples by ICP-OES. (58 pp.) 2011
145. The Combined XII Spring Meeting of the Division of Synthetic Chemistry and XXXIII Finnish NMR Symposium. Book of Abstracts. (90 pp.) 2011
146. Valto, Piia: Development of fast analysis methods for extractives in papermaking process waters. (73 pp.) 2011
147. Andersin, Jenni: Catalytic activity of palladium-based nanostructures in the conversion of simple olefinic hydro- and chlorohydrocarbons from first principles. (78 pp.) 2011
148. Aumanen, Jukka: Photophysical properties of dansylated poly(propylene amine) dendrimers. (55 pp.) 2011
149. Kärnä, Minna: Ether-functionalized quaternary ammonium ionic liquids – synthesis, characterization and physicochemical properties. (76 pp.) 2011
150. Jurček, Ondřej: Steroid conjugates for applications in pharmacology and biology. (57 pp.) 2011
151. Nauha, Elisa: Crystalline forms of selected Agrochemical actives: design and synthesis of cocrystals. (77 pp.) 2012
152. Ahkola, Heidi: Passive sampling in monitoring of nonylphenol ethoxylates and nonylphenol in aquatic environments. (92 pp.) 2012
153. Helttunen, Kaisa: Exploring the self-assembly of resorcinarenes: from molecular level interactions to mesoscopic structures. (78 pp.) 2012
154. Linnanto, Juha: Light excitation transfer in photosynthesis revealed by quantum chemical calculations and exiton theory. (179 pp.) 2012
155. Roiko-Jokela, Veikko: Digital imaging and infrared measurements of soil adhesion and cleanability of semihard and hard surfaces. (122 pp.) 2012
156. Noponen, Virpi: Amides of bile acids and biologically important small molecules: properties and applications. (85 pp.) 2012
157. Hulkko, Eero: Spectroscopic signatures as a probe of structure and dynamics in condensed-phase systems – studies of iodine and gold ranging from isolated molecules to nanoclusters. (69 pp.) 2012
158. Lappi, Hanna: Production of Hydrocarbon-rich biofuels from extractives-derived materials. (95 pp.) 2012
159. Nykänen, Lauri: Computational studies of Carbon chemistry on transition metal surfaces. (76 pp.) 2012
160. Ahonen, Kari: Solid state studies of pharmaceutically important molecules and their derivatives. (65 pp.) 2012

161. Pakkanen, Hannu: Characterization of organic material dissolved during alkaline pulping of wood and non-wood feedstocks. (76 pp.) 2012
162. Moilanen, Jani: Theoretical and experimental studies of some main group compounds: from closed shell interactions to singlet diradicals and stable radicals. (80 pp.) 2012
163. Himanen, Jatta: Stereoselective synthesis of Oligosaccharides by *De Novo* Saccharide welding. (133 pp.) 2012
164. Bunzen, Hana: Steroidal derivatives of nitrogen containing compounds as potential gelators. (76 pp.) 2013
165. Seppälä, Petri: Structural diversity of copper(II) amino alcohol complexes. Syntheses, structural and magnetic properties of bidentate amino alcohol copper(II) complexes. (67 pp.) 2013
166. Lindgren, Johan: Computational investigations on rotational and vibrational spectroscopies of some diatomics in solid environment. (77 pp.) 2013
167. Giri, Chandan: Sub-component self-assembly of linear and non-linear diamines and diacylhydrazines, formulpyridine and transition metal cations. (145 pp.) 2013
168. Riisiö, Antti: Synthesis, Characterization and Properties of Cu(II)-, Mo(VI)- and U(VI) Complexes With Diaminotetraphenolate Ligands. (51 pp.) 2013
169. Kiljunen, Toni (Ed.): Chemistry and Physics at Low Temperatures. Book of Abstracts. (103 pp.) 2013
170. Hänninen, Mikko: Experimental and Computational Studies of Transition Metal Complexes with Polydentate Amino- and Aminophenolate Ligands: Synthesis, Structure, Reactivity and Magnetic Properties. (66 pp.) 2013
171. Antila, Liisa: Spectroscopic studies of electron transfer reactions at the photoactive electrode of dye-sensitized solar cells. (53 pp.) 2013
172. Kemppainen, Eeva: Mukaiyama-Michael reactions with α-substituted acroleins – a useful tool for the synthesis of the pectenotoxins and other natural product targets. (190 pp.) 2013
173. Virtanen, Suvi: Structural Studies of Dielectric Polymer Nanocomposites. (49 pp.) 2013
174. Yliniemelä-Sipari, Sanna: Understanding The Structural Requirements for Optimal Hydrogen Bond Catalyzed Enolization – A Biomimetic Approach.(160 pp.) 2013
175. Leskinen, Mikko V: Remote β-functionalization of β'-keto esters. (105 pp.) 2014
176. 12th European Conference on Research in Chemistry Education (ECRICE2014). Book of Abstracts. (166 pp.) 2014
177. Peuronen, Anssi: N-Monoalkylated DABCO-Based N-Donors as Versatile Building Blocks in Crystal Engineering and Supramolecular Chemistry. (54 pp.) 2014
178. Perämäki, Siiri: Method development for determination and recovery of rare earth elements from industrial fly ash. (88 pp.) 2014

179. Chernyshev, Alexander, N.: Nitrogen-containing ligands and their platinum(IV) and gold(III) complexes: investigation and basicity and nucleophilicity, luminescence, and aurophilic interactions. (64 pp.) 2014
180. Lehto, Joni: Advanced Biorefinery Concepts Integrated to Chemical Pulping. (142 pp.) 2015
181. Tero, Tiia-Riikka: Tetramethoxy resorcinarenes as platforms for fluorescent and halogen bonding systems. (61 pp.) 2015
182. Löfman, Miika: Bile acid amides as components of microcrystalline organogels. (62 pp.) 2015
183. Selin, Jukka: Adsorption of softwood-derived organic material onto various fillers during papermaking. (169 pp.) 2015
184. Piisola, Antti: Challenges in the stereoselective synthesis of allylic alcohols. (210 pp.) 2015
185. Bonakdarzadeh, Pia: Supramolecular coordination polyhedra based on achiral and chiral pyridyl ligands: design, preparation, and characterization. (65 pp.) 2015
186. Vasko, Petra: Synthesis, characterization, and reactivity of heavier group 13 and 14 metallylenes and metalloid clusters: small molecule activation and more. (66 pp.) 2015
187. Topić, Filip: Structural Studies of Nano-sized Supramolecular Assemblies. (79 pp.) 2015
188. Mustalahti, Satu: Photodynamics Studies of Ligand-Protected Gold Nanoclusters by using Ultrafast Transient Infrared Spectroscopy. (58 pp.) 2015
189. Koivisto, Jaakko: Electronic and vibrational spectroscopic studies of gold-nanoclusters. (63 pp.) 2015
190. Suhonen, Aku: Solid state conformational behavior and interactions of series of aromatis oligoamide foldamers. (68 pp.) 2016
191. Soikkeli, Ville: Hydrometallurgical recovery and leaching studies for selected valuable metals from fly ash samples by ultrasound-assisted extraction followed by ICP-OES determination. (107 pp.) 2016
192. XXXVIII Finnish NMR Symposium. Book of Abstracts. (51 pp.) 2016
193. Mäkelä, Toni: Ion Pair Recognition by Ditopic Crown Ether Based bis-Urea and Uranyl Salophen Receptors. (75 pp.) 2016
194. Lindholm-Lehto, Petra: Occurrence of pharmaceuticals in municipal wastewater treatment plants and receiving surface waters in Central and Southern Finland. (98 pp.) 2016
195. Härkönen, Ville: Computational and Theoretical studies on Lattice Thermal conductivity and Thermal properties of Silicon Clathrates. (89 pp.) 2016
196. Tuokko, Sakari: Understanding selective reduction reactions with heterogeneous Pd and Pt: climbing out of the black box. (85 pp.) 2016
197. Nuora, Piia: Monitapaustutkimus LUMA-Toimintaan liittyvissä oppimisympäristöissä tapahtuvista kemian oppimiskokemuksista. (171 pp.) 2016

198. Kumar, Hemanathan: Novel Concepts on The Recovery of By-Products from Alkaline Pulping. (61 pp.) 2016
199. Arnedo-Sánchez, Leticia: Lanthanide and Transition Metal Complexes as Building Blocks for Supramolecular Functional Materials. (227 pp.) 2016
200. Gell, Lars: Theoretical Investigations of Ligand Protected Silver Nanoclusters. (134 pp.) 2016
201. Vaskuri, Juhani: Oppiennätyksistä opetussuunnitelman perusteisiin - lukion kemian kansallisen opetussuunnitelman kehittyminen Suomessa vuosina 1918-2016. (314 pp.) 2017
202. Lundell Jan, Kiljunen Toni (Eds.): 22nd Horizons in Hydrogen Bond Research. Book of Abstracts. 2017
203. Turunen, Lotta: Design and construction of halogen-bonded capsules and cages. (61 pp.) 2017
204. Hurmalainen, Juha: Experimental and computational studies of unconventional main group compounds: stable radicals and reactive intermediates. (88 pp.) 2017
205. Koivistoinen Juha: Non-linear interactions of femtosecond laser pulses with graphene: photo-oxidation, imaging and photodynamics. (68 pp.) 2017
206. Chen, Chengcong: Combustion behavior of black liquors: droplet swelling and influence of liquor composition. (39 pp.) 2017
207. Mansikkamäki, Akseli: Theoretical and Computational Studies of Magnetic Anisotropy and Exchange Coupling in Molecular Systems. (190 p. + included articles) 2018.
208. Tatikonda, Rajendhraprasad: Multivalent N-donor ligands for the construction of coordination polymers and coordination polymer gels. (62 pp.) 2018
209. Budhathoki, Roshan: Beneficiation, desilication and selective precipitation techniques for phosphorus refining from biomass derived fly ash. (64 pp.) 2018
210. Siitonen, Juha: Synthetic Studies on 1-azabicyclo[5.3.0]decane Alkaloids. (140 pp.) 2018
211. Ullah, Saleem: Advanced Biorefinery Concepts Related to Non-wood Feedstocks. (57 pp.) 2018
212. Ghalibaf, Maryam: Analytical Pyrolysis of Wood and Non-Wood Materials from Integrated Biorefinery Concepts. (106 pp.) 2018

DEPARTMENT OF CHEMISTRY, UNIVERSITY OF JYVÄSKYLÄ
DISSERTATIONS PUBLISHED IN THE JYU DISSERTATIONS RESEARCH SERIES

1. Bulatov, Evgeny: Synthetic and structural studies of covalent and non-covalent interactions of ligands and metal center in platinum(II) complexes containing 2,2′-dipyridylamine or oxime ligands. (58 pp.) 2019. JYU Dissertations 70.
2. Annala, Riia: Conformational Properties and Anion Complexes of Aromatic Oligoamide Foldamers. (80 pp.) 2019. JYU Dissertations 84.
3. Isoaho, Jukka Pekka: Dithionite Bleaching of Thermomechanical Pulp - Chemistry and Optimal Conditions. (73 pp.) 2019. JYU Dissertations 85.
4. Nygrén, Enni: Recovery of rubidium from power plant fly ash. (98 pp.) 2019. JYU Dissertations 136.
5. Kiesilä, Anniina: Supramolecular chemistry of anion-binding receptors based on concave macromolecules. (68 pp.) 2019. JYU Dissertations 137.
6. Sokolowska, Karolina: Study of water-soluble p-MBA-protected gold nanoclusters and their superstructures. (60 pp.) 2019. JYU Dissertations 167.
7. Lahtinen, Elmeri: Chemically Functional 3D Printing: Selective Laser Sintering of Customizable Metal Scavengers. (71 pp.) 2019. JYU Dissertations 175.
8. Larijani, Amir: Oxidative reactions of cellulose under alkaline conditions. (102 pp.) 2020. JYU Dissertations 217.
9. Kolari, Kalle: Metal-metal contacts in late transition metal polymers. (60 pp.) 2020. JYU Dissertations 220.
10. Kauppinen, Minttu: Multiscale computational investigation of catalytic properties of zirconia supported noble metals. (87 pp.) 2020. JYU Dissertations 231.
11. Ding, Xin: Halogen Bond in Crystal Engineering: Structural Studies on Crystals with Ruthenium Centered Complexes and 1-(4-Pyridyl)-4-thiopyridine Zwitterion as Halogen Bond Acceptors. (59 pp.) 2020. JYU Dissertations 323.
12. Neuvonen, Antti: Toward an Understanding of Hydrogen-Bonding Bifunctional Organocatalyst Conformations and Their Activity in Asymmetric Mannich Reactions. (77 pp.) 2020. JYU Dissertations 336.
13. Kortet, Sami: 2,5-Diarylpyrrolidines and Pyroglutamic-Acid-Derived 2-Diarylmethyl-5-Aryl-Pyrrolidines: Their Synthesis and Use in Asymmetric Synthesis. (221 pp.) 2020. JYU Dissertations 337.
14. Saarnio, Ville: Fluorescent probes, noble metal nanoparticles and their nanocomposites: detection of nucleic acids and other biological targets. (80 pp.) 2021. JYU Dissertations 361.
15. Chernysheva, Maria: σ-hole interactions: the effect of the donors and acceptors nature in selenoureas, thioureas, halogenated species, substituted benzenes, and their adducts. (72 pp.) 2021. JYU Dissertations 370.